Aalborg Universitet

AALBORG UNIVERSITY
DENMARK

Modeling and Analysis of Stochastic Radio Channels

An Application of the Theory of Spatial Point Processes

Jakobsen, Morten Lomholt

Modeling and Analysis of Stochastic Radio Channels

-

An Application of the Theory of Spatial Point Processes

PhD Thesis

Morten Lomholt Jakobsen

Aalborg University
Department of Electronic Systems
Fredrik Bajers Vej 7B
DK-9220 Aalborg

Abstract

Several of today's most popular and widely used stochastic radio channel models rely in their construction on one-dimensional point processes. The first use of point processes as a tool for stochastic modeling of *time-invariant* radio channels can be traced back nearly half a century to the seminal work by Turin, with follow-up developments by Suzuki and Hashemi. Subsequently entered the popular contribution by Saleh and Valenzuela as well as the more recent extension by Spencer. Similarly, and originally proposed by Papantoniou, the use of one-dimensional point processes has also repeatedly been suggested as a modeling tool for *time-variant* stochastic radio channels.

Despite a pronounced use for *modeling purposes*, neither point processes nor their underlying theoretical framework have been favored in the literature as tools for the subsequent *analysis*. For example, the classical channel model by Saleh and Valenzuela has been widely used for simulation purposes such as performance assessments of communication systems. However, due to the models' heuristic construction the resulting channel properties and characteristics are not well-understood or not well-known (e.g. the shape of the *power-delay profile*).

In this work we view a representative selection of popular radio channel models from a new and highly facilitating perspective. We naturally exploit the fact that the original constructions of these channel models rely on point processes. By use of the theory of *spatial point processes* we obtain novel insight on the different channel models, their underlying structures and properties. The theoretical key to our achievements is the application of *Campbell's Theorem*.

In one of our main contributions we revisit the classical multipath channel model by Saleh and Valenzuela. We show that the model is comprised by the union of two dependent point processes, namely a *Poisson* point process and a *Cox* point process. We exploit this conceptual view to re-derive the intensity of path components and the channel's power-delay profile in a much simpler and more insightful way compared to previous derivations (the intensity rises linearly with propagation delay and the power-delay profile is *not* exponentially decaying). In essence, our conclusions arise as a direct result of the point process perspective and in particular due to the wide applicability and straightforward use of Campbell's Theorem.

Our main contribution is a thorough analysis of a particular class of time-variant stochastic radio channel models. Common to all models in this class is that individual multipath components are emerging and vanishing in a temporal birth-death like manner. The stochastic mechanism used to generate the birth-death behavior is governed by two facilitating assumptions. By aid of our spatial point process perspective and Campbell's Theorem we provide a novel analytical characterization of this stochastic mechanism. Additionally, we derive the general structure of the *time-frequency correlation function* for this type of time-variant channel models. Despite their birth-death behavior, we show under suitable assumptions that these channels become wide-sense stationary in both time and frequency. The engineering relevance of being able to analytically characterize this class of time-variant channel models is evident as key parameters enter explicit in practically measurable quantities (power-delay profile, large- and small-scale correlation functions, etc.). For instance, the power-delay profile can be estimated from channel sounding measurements and so we have a rigorous way of calibrating the model. So far, these practically measurable quantities have not been reported in the literature.

Finally, we illustrate also how the point process framework proves particularly beneficial in terms of computer simulation. In essence, the theoretical knowledge gained from the point process perspective enables new and alternative simulation methods to be applied. Furthermore, the theoretical insight allows for a variety of difficulties encountered in literature to be elegantly circumvented.

Dansk Resumé

Adskillige vellidte og almindeligt anvendte stokastiske radiokanalmodeller er baseret på én-dimensionale punktprocesser. Brugen af punktprocesser som et led i modelleringen af *tidsinvariante* stokastiske radiokanaler kan spores tilbage omtrent et halvt århundrede, til Turins skelsættende arbejde og til Suzuki og Hashemis opfølgende bidrag. Senere fulgte Saleh & Valenzuela op med deres populære model, og efterfølgende kom Spencers relativt nyere udvidelse heraf. Brugen af én-dimensionale punktprocesser er også gentagne gange blevet foreslået i forbindelse med modelleringen af *tidsvarierende* stokastiske radiokanaler, første gang af Papantoniou.

Til trods for de udbredte anvendelser til *modelleringsformål*, så er brugen af hverken punktprocesser eller den bagvedliggende teori blevet foretrukket i faglitteraturen til de efterfølgende *analyseformål*. Eksempelvis har Saleh & Valenzuelas populære radiokanalmodel været almindeligt brugt til simulationsformål, f.eks. til evaluering af forskellige kommunikationssystemers ydeevne. Imidlertid er flere af radiokanalmodellens vigtige egenskaber (f.eks. formen på *power-delay profilen*) helt eller delvist ukendte pga. modellens umiddelbare heuristiske opbygning.

I denne afhandling beskæftiger vi os med et repræsentativt udsnit af populære radiokanalmodeller, og vi anskuer dem fra et nyt og yderst fremmende synspunkt. Vi drager naturligt fordel af, at radiokanalmodellerne alle beror sig på punktprocesser. Ved anvendelse af teorien for *rumlige punktprocesser* tilegner vi os ny viden om de forskellige modeller, deres underliggende strukturer og deres egenskaber. *Campbells Sætning* udgør det altoverskyggende teoretiske redskab i denne sammenhæng.

Et af afhandlingens hovedbidrag udgøres af et tilbageblik på Saleh & Valenzuelas klassiske flervejskanalmodel. Vi viser, at modellen består af foreningsmængden mellem to afhængige punktprocesser; nemlig en *Poisson* punktproces og en *Cox* punktproces. Dette konceptuelle synspunkt udnyttes til, på ny, at udlede intensiteten for flervejskomponenterne samt til at udlede kanalens power-delay profil. Udledningen er væsentligt simplere, og den giver større indsigt end tidligere udledninger af de samme resultater (intensiteten vokser lineært med udbredelsesforsinkelsen, og power-delay profilen aftager *ikke* eksponentielt). Vores konklusioner udspringer, som et direkte resultat, af den alsidige og ukomplicerede brug af Campbells Sætning.

Afhandlingens hovedbidrag består af en tilbundsgående analyse af en særlig klasse af tidsvarierende stokastiske radiokanalmodeller. Fælles for alle modellerne i denne klasse er, at de individuelle flervejskomponenter opstår og forsvinder i et tidsmæssigt fødsels-døds lignende mønster. Den stokastiske anordning, som skaber fødsels-døds adfærden, reguleres af to fleksible men forenklende præmisser. Anvendelsen af rumlige punktprocesser og Campbells Sætning giver samlet anledning til en ny analytisk karakterisering af den stokastiske fødsels-døds anordning. Vi udleder derudover den generelle struktur af *tids-frekvens korrelationsfunktionen* for denne type af tidsvarierende radiokanalmodeller. Til trods for fødsels-døds adfærden er det, under passende antagelser, muligt for modellerne, at udvise svag stationaritet i både tid og frekvens. Fra et ingeniørmæssigt synspunkt, er de ovennævnte analytiske karakteriseringer åbenlyst relevante, fordi radiokanalmodellens nøgleparametre eksplicit kommer til udtryk i egentlige målbare størrelser (power-delay profilen, korrelationsfunktioner, osv.). Eksempelvis kan power-delay profilen estimeres udfra måledata, og således har man en velfunderet metode til at kalibrere modellen med. Radiokanalmodellens egentlige målbare størrelser har ikke tidligere været rapporteret i faglitteraturen.

Slutteligt illustrerer vi også, hvordan punktprocesserne og de medfølgende teoretiske perspektiver viser sig fordelagtige i forbindelse med computersimulering. Teorien viser sig nemlig at kunne bidrage med indsigt til nye og alternative simuleringsmetoder. Ydermere afhjælper de teoretiske aspekter også på elegant vis en række besværligheder, som tidligere er blevet påpeget i faglitteraturen.

Contents

Thesis Details

Thesis Title: Modeling and Analysis of Stochastic Radio Channels
- An Application of the Theory of Spatial Point Processes

PhD Student: Morten Lomholt Jakobsen

Supervisors: Prof. Dr. Sc. Techn. Bernard Henri Fleury, Aalborg University
Assoc. Prof. Troels Pedersen, Aalborg University

The main body of this PhD thesis consist of the following four papers together with a study note on point processes (Appendices A-E):

A   M. L. Jakobsen, T. Pedersen and B. H. Fleury, "Analysis of stochastic radio chan-
    nels with temporal birth-death dynamics: A marked spatial point process per-
    spective", (**submitted**), *IEEE Transactions on Antennas and Propagation*, Jul.,
    2013.

B   M. L. Jakobsen, T. Pedersen and B. H. Fleury, "Analysis of the stochastic channel
    model by Saleh & Valenzuela via the theory of point processes", *Proc. Interna-
    tional Zurich Seminar on Communications (IZS 2012)*, pp. 115-118, Feb. 2012.

C   M. L. Jakobsen, K. Laugesen, C. N. Manchón, G. E. Kirkelund, C. Rom and
    B. H. Fleury, "Parametric modeling and pilot-aided estimation of the wireless
    multipath channel in OFDM systems", *Proc. IEEE International Conference on
    Communications (ICC 2010)*, pp. 1-6, May 2010.

D   F. M. Schubert, M. L. Jakobsen and B. H. Fleury, "Non-stationary propagation
    model for scattering volumes with an application to the rural LMS channel", *IEEE
    Transactions on Antennas and Propagation*, Vol. 61, No. 5, pp. 2817-2828, May
    2013.

E   M. L. Jakobsen, "Point Processes in 2D", Study note used in the Master's course
    "Stochastic Processes" at Department of Electronic Systems, Aalborg University.

Additionally, the following two papers were co-authored by Morten Lomholt Jakobsen during his PhD studies at Aalborg University:

- S. Begusic, D. N. Urup, J. Kolonic, H. H. Pedersen, W. Wang, R. Raulefs, M. L. Jakobsen, G. Steinböck and T. Pedersen, "Wireless indoor positioning relying on observations of received power and mean delay", *Proc. IEEE International Conference on Communications (ICC 2013)*, Jun. 2013.

- N. L. Pedersen, M. L. Jakobsen, C. Rom and B. H. Fleury, "Analysis of smoothing techniques for subspace estimation with application to channel estimation", *Proc. IEEE International Conference on Communications (ICC 2011)*, pp. 1-6, Jun. 2011.

This thesis has been submitted for assessment in partial fulfillment of the PhD degree. The thesis is based on the submitted or published scientific papers which are listed above. Parts of the papers are used directly or indirectly in the extended summary of the thesis. As part of the assessment, co-author statements have been made available to the assessment committee and are also available at the Faculty. The thesis is not in its present form acceptable for open publication but only in limited and closed circulation as copyright may not be ensured.

Preface

This thesis is based on work which has been carried out during a period of approximately three and a half years. I graduated in June 2009 from the Department of Mathematical Sciences, Aalborg University, and since then I have been a staff member within the Section Navigation and Communications, Department of Electronic Systems, Aalborg University. The work has been co-funded by the Danish Agency for Science, Technology and Innovation while being partially performed within the ICT-216715 FP7 Network of Excellence in Wireless Communications (NEWCOM++), the project ICT-217033 Wireless Hybrid Enhanced Mobile Radio Estimators (WHERE), the project ICT-248894 Wireless Hybrid Enhanced Mobile Radio Estimators 2 (WHERE2), the 4GMCT cooperative research project co-financed by Intel Mobile Communications, Agilent Technologies, Aalborg University and the Danish National Advanced Technology Foundation, as well the European Commission in the framework of the FP7 Network of Excellence in Wireless Communications NEWCOM# (grant agreement no. 318306).

I would like to express my sincere appreciation to my supervisors, Professor Bernard Henri Fleury and Associate Professor Troels Pedersen. Thank you Bernard for being immensely patient with me and thank you for always taking the time when needed the most. Thank you Troels for all your guidance, comments, and thank you for persistently driving me towards even simpler justifications, explanations, and examples. Additionally, I would like to thank Frank M. Schubert for inspiring me and letting me discover the practical dimensions of our particular area of engineering. I can only admire the benefits emerging when people with different technical backgrounds are joining forces. I would also like to express my unconditional gratitude to the persons who accepted to enter as members of my PhD assessment committee, Associate Professor Massimo Franceschetti, Associate Professor Gerald Matz, and Associate Professor Troels Bundgaard Sørensen. Finally, I would like to thank our secretary Nina as well as all of my other colleagues and friends within the section.

Morten Lomholt Jakobsen
Aalborg University, July 26, 2013

Part I

Stochastic Radio Channels: Modeling and Analysis

Introduction to Channel Modeling and Selected Fundamentals

What is *radio channel modeling* and why is it needed? This question seems natural and relevant to ask. Especially if questioned by someone completely unfamiliar with *communications engineering* and *mathematics.* The answer should be straightforward for me to provide! If matters are kept simple enough, in the sense of omitting irrelevant technicalities, then it may even be that the person who originally asked the question is not entirely lost once I stop explaining. This chapter is deliberately formed with an intention to appear comprehensible (at least conceptually) for readers who are not familiar with the engineering discipline of radio channel modeling.

Communication systems engineering is all about enabling entities to communicate. Indeed, the ability to conveniently and reliably communicate is truly indispensable nowadays. *Radio communications* is most often applied when wired connections are not among the realistic options. The first wireless transmission based on radio waves took place more than a century ago when G. Marconi got the ingenious idea of using a flashlight to communicate from a boat to the shore. More precisely, he used a *spark-gap* transmitter and a *coherer* receiver to essentially make up a Morse code communication system. Nowadays, a multitude of radio communication systems are deployed all over and they operate across a wide range of physical distances and across even wider ranges of applications and purposes. Anything from a wireless optical mouse to deep-space communications, with GPS and cell phone applications as intermediate examples.

In its simplest form, a radio communication system consists of one transmitter (one transmit antenna) and one receiver (one receive antenna). The transmitter emits electromagnetic waves which propagate throughout the physical environment. The receiver senses the electromagnetic waves which were launched by the transmitter. The electromagnetic waves sensed by the receiver depend on the emitted waves (think of the Morse example). Hence, information can be inserted into the electromagnetic waves intended

for transmission. If propagation conditions of sufficiently good quality exist, it means that the originally inserted information can be recovered at the receiver. Conceptually, this is the key idea of any (radio) communication system.

Radio channel modeling has to do with the dependencies between the electromagnetic waves being transmitted and received. Knowledge of these dependencies is of paramount importance for the design and engineering of modern radio communication systems. When engineers speak of the wireless *radio channel* they essentially refer to the entire physical environment in which the electromagnetic waves propagate. Hence, the radio channel includes the atmosphere, buildings, vegetation, cars, humans and everything else which impact the propagation conditions of electromagnetic waves, including the transmit and receive antennas. From a conceptual point of view, one may think of the radio channel as a "black box" that we cannot control but only adapt to. Since we cannot control the wireless radio channel it inherently becomes an engineering challenge to build and design a communication system relying so fundamentally on it. The challenge becomes even more demanding when certain constraints and requirements are imposed on the communication system. A typical system requirement nowadays could be based on the ability to support steady connectivity at vehicular-speeds, with high-rate data transfers ongoing, and for a large number of users operating simultaneously. Yet, a radio communication system does not by default comply with three such conflicting demands. The key to make it all work initially relies on profound knowledge and understanding of the mechanisms of the wireless radio channel. In a nutshell, radio channel modeling consists of creating and studying *representations* of the real-world radio channel. As engineers, we use these representations to devise comprehension which enables us to *design*, *optimize* and *implement* wireless communication systems in practice.

A radio channel model consists most often of a *mathematical* representation. The language of mathematics allows for stringency in the formulation of such a model and provides at the same time a natural environment for several key optimization aspects. A radio channel model can be based on theoretical considerations, e.g. elements from physics, but it can also be inspired from intuition and empirical observations, i.e. measurements. As a naive starting point we could say that the task in radio channel modeling is to formulate a mathematical model which *efficiently*, *accurately* and *exhaustively* reproduces all relevant characteristics of the real propagation environment (although it may not be too clear what this really means!). Yet, research activities in radio channel modeling are naturally driven by today's communication systems as well as those intended for the near future. Current technological advancements play a key role as well. Hence, the research activities emerging as a result of the constraints and requirements imposed on today's 4G systems are rather different from the research activities taking place around the development of 1G systems. Several of the engineering challenges faced today were simply not relevant at that time. Accordingly, the "reproducing" capabilities of a radio channel model is to be understood relative to the effects and mechanisms which impact the performance and operability of current communication systems.

Before digging into concrete mathematical representations of the radio channel we stress here the fact that every model, be it of the radio channel or not, is created for a specific *purpose*. Accordingly, it makes sense to compare different models only if they are intended for the same purpose [1]. A radio channel model intended for *aircraft positioning* should really not be put in the context of, nor compared to, a channel model intended for *standardized throughput comparisons* among different cell phone architectures. Two models created for the very same purpose are perfectly comparable. However, it may not always be straightforward how to compare them, and which one of the models to utilize in the end depends most often on context. Nonetheless, an important concept to always keep in mind when dealing with models is the *principle of parsimony* (Occam's razor). The simplest explanation is the better! And, as Albert Einstein is often quoted for having said: "*things should be made as simple as possible, but not simpler*". This statement explains why the radio channel models developed for 1G communication systems did not account for what is needed today.

1 First View Upon the Radio Channel

To comprehend a complicated system it typically offers adequate conceptual simplicity to make drawings and to put things into boxes. As engineers we do that all the time, namely breaking matters into smaller confined pieces. Consider for that reason the communication system depicted in Fig. 1. The wireless radio channel, which for the
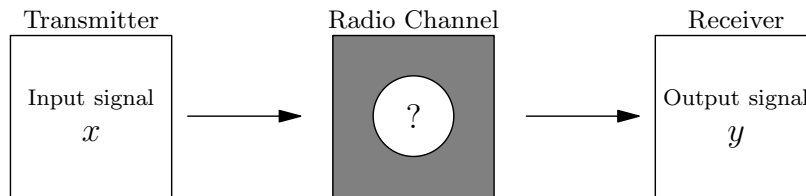
Fig. 1: A communication system with one transmitter, a "black box" radio channel, and one receiver.

moment is being perceived as a "black box", is connecting a transmitter and a receiver. At time t_1 the transmitter launches a signal x into the radio channel and at some time a bit later than t_1, the receiver captures a signal y. *Channel modeling is all about providing a characterization of the link between x and y.* At time t_2 the transmitter launches the exact same signal x into the radio channel and at some time later than t_2, the receiver captures a new signal. Yet, the latter signal being captured is not the same as the former (the signal we denoted as y). Maybe the receiver moved in between the two transmissions or maybe the propagation environment changed for some other

reason. A similar phenomenon occurs if signals are transmitted at different frequencies. *That is, the wireless radio channel alters its characteristics with time and frequency.* This is not all there is to say, but it's a sound and adequate point of departure. It is by all means nontrivial to enter the engineering world of radio channel modeling. There exist an excessive amount of concepts and just to get familiar with the common technical language requires a notable effort.

Personally, I have found great inspiration and comprehension from consulting R. S. Kennedy's book from 1969 entitled "Fading Dispersive Communication Channels" [2]. One of Kennedy's preliminary statements is that *"fading dispersive radio channels are adequately described as random linear time-varying filters".* (Accept for the moment that we do not know exactly what this means.) Kennedy also immediately highlights that parts of a channel model can most often be generalized at will. However, it also frequently appears that such attempts do not appreciably affect the applicability of the model to the problem of interest, whereas it does complicate the analysis (I'm using his choice of words without quoting minutely). In the end, the utility of a channel model is determined by the extent to which results deduced therefrom coincide with analogous results obtained by experiment (his words as well). In the channel modeling literature I have not yet found a modeling philosophy and the principle of parsimony conveyed as early, as explicit, and as concise as in Kennedy's book from 1969. However, Kennedy's experimentally driven utility aspect of the channel model should be supplemented by additional requirements such as tractability, accuracy and complexity. Of course, validation techniques such as *Monte Carlo simulation* were not among the standard options in 1969.

2 Linear Systems and Filters

This paragraph is highly inspired from an elegant and ultra short section in the book [3] by K. Gröchenig. The purpose is not to bore and stall the qualified reader with "ancient" fundamentals but merely to introduce a piece of engineering language leading to the concept of a random linear time-varying filter.

A *linear system* is a "black box" A which modifies an *input* element x into an *output* element $y = Ax$. The system being linear means that

$$A(c_1 x_1 + c_2 x_2) = c_1 A x_1 + c_2 A x_2$$

for all scalars c_1 and c_2 and for all input elements x_1 and x_2. Linearity is one of the most fundamental concepts in mathematics. For mathematicians, dealing with a *linear system* means dealing with a *linear operator*. What is not yet clear, no matter if we call it a system or an operator, is how x, y and A really look like. Mathematicians would most likely start talking about *Hilbert spaces*[1] and *bounded/continuos operators*

---

[1]The interested reader may consult, for instance [4] or [5].

while engineers would start talking about *bandwidth-limited finite-energy signals*[2]. Two different worlds are potentially joining forces and getting to know both languages is greatly advantageous but does not come over night, unfortunately. In any case, what is meant is that the action of the system cannot be arbitrarily powerful if it has to represent a real-world mechanism such as the wireless radio channel. If a finite portion of energy is released into the air we do not expect to be able to retrieve again unlimited amounts of energy. Here, we act mainly as engineers and for that reason, the input x and the output y will now be referred to as a *signals*. This means that x and y are scalar functions defined on the entire real line (interpreted as time). According to engineering tradition we then write $x(t)$ and $y(t)$ to indicate that the signals under consideration are evolving in time. Mathematicians would still write only x and y or maybe $x(\cdot)$ and $y(\cdot)$.

In *signal processing* the restriction of linear systems to the *time-invariant* case is of fundamental importance. A time-invariant linear system does not care if an input signal x is applied today or tomorrow. It simply shifts the output signal y from today till tomorrow without changing its shape. Hence, such systems are not appropriate as representations for mechanisms which, in fact, do alter their characteristics with time. Nonetheless, time-invariant linear systems are crucial in electrical engineering and the technical language originally proposed and used for these systems is found all over in literature. In signal processing the linear operator A is referred to as a linear *filter*. A filter is a mechanism that preserves and discards, like a coffee filter where water and taste should sustain or like a *low-pass* filter which removes high-frequency components. Time-invariant linear systems act as *convolution* operators in time and equivalently, as *multiplication* operators in frequency. In the written language of mathematics this means that

$$y(t) = \{Ax\}(t)$$

$$= \{h * x\}(t) = \int h(\tau)x(t - \tau)\mathrm{d}\tau \tag{1}$$

$$= \mathcal{F}^{-1}\{HX\}(t) = \int H(f)X(f)\mathrm{e}^{j2\pi ft}\mathrm{d}f. \tag{2}$$

The action in (1) is the *time-domain* convolution while the action in (2) is the *frequency-domain* multiplication followed by conversion back into the time-domain. In (2) we have $H = \mathcal{F}h$ as well as $X = \mathcal{F}x$, where $\mathcal{F}$ is yet another linear operator, namely the *Fourier transform* and $\mathcal{F}^{-1}$ is its inverse. Hence, the relationship in (2) renders itself much simpler in the frequency-domain since there it reads

$$Y = HX.$$

The quantity h in (1) is referred to as the *impulse response* of the linear time-invariant system and H is called the *transfer function*. These names are adequate since h reveals

_____

[2]For this matter the interested reader should definitely consult [6].

how the system (or filter) responds when excited by an *impulse*[3] and H explains how *pure frequencies* are transferred through the system.

To be able to capture a variety of real mechanisms we need to consider linear *time-varying* systems as well. In contrast to the time-invariant ones, these systems do indeed care whether an input signal x is applied today or tomorrow. In working with linear time-varying systems we wish to preserve our technical formalism from earlier. Essentially, this means that we wish to keep the notion of an impulse response and the associated transfer function (even though we end up abusing terminology a bit). The brute-force way of preserve our technical formalism is to simply add the necessary time-dependence to each of the functions h and H in (1) and (2). Accordingly, we now get the input-output relationship

$$y(t) = \{Ax\}(t)$$

$$= \int h(t,\tau)x(t-\tau)\mathrm{d}\tau \tag{3}$$

$$= \int H(t,f)X(f)\mathrm{e}^{j2\pi ft}\mathrm{d}f. \tag{4}$$

The function $h(t,\tau)$ in (3) has two variables and is referred to as the *time-variant impulse response* of the linear system[4]. It can be seen as a time-dependent (or time-indexed) family of impulse responses. Similarly, the function $H(t,f)$ in (4) is called the *time-variant transfer function*.

In practical applications the goal is often to learn the characteristics of a linear system, be it time-invariant or time-variant. Essentially, that is to describe the "black box" A using a small number of comprehensible parameters, preferably related to physically meaningful or observable quantities. Knowledge of these parameters enables to predict the future behavior of the system, at least for a limited period and to some reasonable degree of accuracy (like in weather forecasting). Yet, numerous practical systems are best captured, mimicked or represented if we add another layer of flexibility, namely *randomness*[5].

The mathematical theories of *probability* and *stochastic processes* [9, 10] are often employed in engineering contexts. This has to do with the fact that many real mechanisms are behaving in ways which we can conveniently/adequately perceive as being random, e.g. the weather, internet traffic flow or stock markets just to name a few. That

---

[3]Namely, the *Dirac delta* which belongs to an advanced mathematical discipline called *the theory of distributions*. The Dirac delta can be seen as a mathematical representation of the temporally infinitesimal interaction taking place when a hammer is smashed with great force onto an anvil. This conceptual view has been borrowed from [7], a recommendable introduction to the theory of distributions.

[4]An alternative name for $h(t,\tau)$ is the *input delay-spread function* [8] which, similar to the "impulse response" terminology, may appear somewhat misleading.

[5]Which can also frequently be viewed as ignorance or lack of detailed knowledge, but we do not find it appropriate to enter such a discussion here.

some mechanism behaves at random does not necessarily imply that it is completely irregular and disorderly. Systematic tendencies and recurring patterns are often in play but we cannot say with absolute certainty what to come next. Hence, when parameterizing a linear system A, we can for example decide upon certain candidate shapes for its impulse response or its transfer function. From measurements and experience we may know grossly or qualitatively how these functions behave. This is exactly the case for the wireless radio channel. In Sec. 8 and Sec. 9 we elaborate on a few popular approaches within *stochastic radio channel modeling*.

3 Fading Dispersive Radio Channels

Recall Kennedy's statement saying that fading dispersive radio channels are adequately described as random linear time-varying filters. In this section we set out to elaborate on his statement. In particular, we set out to conceptually elaborate on the two terms *fading* and *dispersion*. Both belong to the engineering vocabularies and dictionaries in use when dealing with radio channel modeling. And we may as well warn the reader immediately. The terminology in use within this area of engineering is not always consistent! This can be seen from a pessimistic perspective as well as from a rather positive perspective. The downside is that it can and does often lead to great confusion and frustration. On the other hand, it repeatedly forces one to stop-and-think and to wear sceptic but eventually rewarding glasses.

Conceptually, Kennedy tells us that the wireless radio channel acts like a filter. When a certain signal is launched into the channel, then a filtered version of the input comes out. Certain signal components are weakened or entirely removed while others are passed through undistorted. Since the channel is time-variant it does not consistently filter away the same signal features all the time. Which frequency components being distorted, how and when, is described by the time-variant (channel) transfer function $H(t,f)$. Fig. 2 illustrates a "frequency-slice" and a "time-slice" of some fictitious time-variant transfer function. In the left-hand side of the figure the time-variable t is kept fixed whereas in the right-hand side the frequency-variable f is fixed.

The above figure comprises all we need in order to grasp what communication engineers mean when they speak about fading. Fading is a common term used to emphasize the chasms in the two curves in Fig. 2. The degree of attenuation affecting the input signal is *not* constant and the channel recurrently exhibits a fade. Some fades are deep while others are not as can be seen from inspection of the different "valleys", e.g. in the left-hand side of the figure. Certain frequency components are experiencing levels of attenuation which are orders of magnitude stronger compared to other components. Essentially, this is the filtering nature of the wireless radio channel. Fading is caused by effects detrimental to propagation and signal reception. It is common to classify fading into different groups according to the underlying causes for it. Hence, in literature one frequently encounters keywords like *multipath*-fading and *shadow*-fading, *fast*-fading and
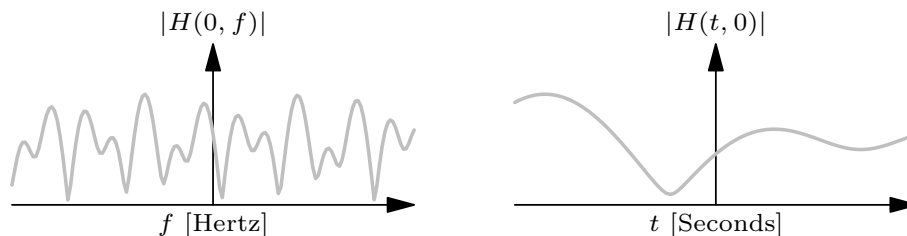
Fig. 2: Two slices of a time-variant channel transfer function $H(t, f)$. (Left) Magnitude of $H(0, f)$ versus frequency. (Right) Magnitude of $H(t, 0)$ versus time.

slow-fading or maybe *small-scale* fading and *large-scale* fading. We intentionally avoid entering a tedious discussion with the objective to define, justify, relate and compare the diverse terminology in use. Most academic textbooks on *wireless communications* or *radio channels* contain dedicated paragraphs with exactly such a discussion. Notes, warnings and remarks on terminology-wise misconceptions are often found too, e.g. as in [11, Sec. 2.2] where G. D. Durgin demystifies and clarifies why fast-fading is sometimes *not-so-fast* after all.

Dispersion and *selectivity* are two additional concepts from the world of channel modeling and both are intimately related to fading, yet, also intimately related to each other. The fictitious channel represented in Fig. 2 is said to be *selective* in both *time* and *frequency*. Such a channel is also often referred to as being *doubly-selective* with a default understanding of the selectivity to be with respect to time and frequency.

The wireless radio channel's selectivity in time is triggered via *motion* in the surrounding physical environment. Everything is essentially in an ever-changing mode since the receiver is often moving or changing its orientation, leaves on trees are rustling in the wind [11], cars are moving, etc. Unless everything in the propagation environment remains entirely static the resulting radio channel will exhibit selectivity in time, albeit the variations need not always be noteworthy.

Selectivity in frequency enters since the transmit signal propagates along multiple different physical routes or *paths* on its way to the receiver. This phenomenon is called *multipath propagation*. When the individual signal contributions eventually show up at the receiving antenna they superimpose and combine. As most individual signal contributions have traveled distinct physical routes it naturally means that some arrive later than others. Hence, individually delayed and individually attenuated copies of the original signal arrive and superimpose at the receiving antenna. When some signal copies arrive considerably later than the earliest ones it leads to severe signal distortion – especially if the time span allocated to transmit consecutive pieces of information is

smaller than the delays introduced in the channel[6]. Essentially, time-shifted copies of dissimilar pieces of information fall on top of each other and so the overall received signal is highly distorted from *interference* with itself. Engineers refer to this type of signal distortion as *inter-symbol-interference*.

As a rule of thumb, the radio channel's selectivity in time has to do with *motion* whereas the selectivity in frequency has to do with *multipath propagation*. Although this is a simplified view it still conceptually offers all we need to keep in mind. The last tricky fact we remain to comprehend is that *dispersion* is equivalent to *selectivity* (via Fourier transform duality). The radio channel being selective in frequency is nothing but to say that the channel is *dispersive in delay*. The radio channel being selective in time is to say that the channel is *dispersive in Doppler*[7]. Hence, the term dispersion is used to emphasize that the wireless radio channel essentially spreads out the input signal (in delay and Doppler).

We summarize shortly by recalling once more Kennedy's statement saying that fading dispersive radio channels are adequately described as random linear time-varying filters. And this time we have a fairly good conceptual idea on what his statement is all about.

4   System Functions

In radio channel modeling we seek to establish the link between an arbitrary input signal x and the corresponding output signal y. From (3) and (4) we know already two input-output relationships. Yet, we have also just got to know that the wireless radio channel is dispersive in *delay* and *Doppler*. That is, the radio channel takes the input signal x and spreads/smears it in delay and Doppler and brings it to the receiver antenna where the dispersed signal contributions superimpose, forming the output signal y. Neither (3) nor (4) directly provide this interpretation of the action of the wireless radio channel. A partial transform of the time-variant impulse response $h(t, \tau)$ brings forward this view,

---

[6]This is indeed the case for modern communications system which are required to support high-rate data transfers, achieved essentially by transmitting consecutive pieces of information very closely separated in time (i.e. the so-called *signaling period* is very short).

[7]The Doppler effect is a phenomenon which is well-known from acoustics. Most people have experienced it upon witnessing an ambulance approaching fast from behind, after which it passes straight by. The sound of the siren changes quite remarkably as the ambulance passes. When it approaches the sound waves are being squeezed due to the motion of the vehicle. On the other hand, when departing, the sound waves are being stretched. At the very intersection everything records completely irregular. It sounds like the siren is altering its frequency and this is all caused by the motion of the vehicle. Exactly the same enters in the wireless radio channel, namely that the electromagnetic waves are being squeezed and stretched due to physical motion in the propagation environment. As seen from the receiver, the incoming electromagnetic waves have all been individually shifted in frequency (in Doppler).

namely by introducing

$$s(\nu, \tau) := \int h(t, \tau) \mathrm{e}^{-j2\pi\nu t} \mathrm{d}t. \tag{5}$$

The function in (5) has two variables ν and τ which represent Doppler and delay, respectively. By rearranging the relationship in (5) and by inserting it in (3) we get immediately a new input-output equation reading

$$y(t) = \{Ax\}(t) = \iint s(\nu, \tau) x(t - \tau) \mathrm{e}^{j2\pi\nu t} \mathrm{d}\nu \mathrm{d}\tau. \tag{6}$$

The mathematical relationship in (6) reveals that the output signal y is a *superposition* of *translated* (delayed) and *modulated* (Doppler shifted) versions of the input signal x. Each delay-Doppler shifted version of the input signal is weighted by the corresponding value of the function $s(\nu, \tau)$ and all such contributions are combined. For this reason, the quantity $s(\nu, \tau)$ is called the *Doppler-delay spreading function* of the (doubly-dispersive/doubly-selective) radio channel. Essentially, we now have three different but equivalent input-output relationships at our disposal, namely (3), (4) and (6). Each relationship provides its own interpretation of the wireless radio channel and each of the quantities

$$\begin{aligned} h(t, \tau) : &\quad \text{the time-variant impulse response,} \\ H(t, f) : &\quad \text{the time-variant transfer function,} \\ s(\nu, \tau) : &\quad \text{the spreading function,} \end{aligned}$$

possesses its own properties and characteristics. The impulse response, the transfer function and the spreading function are in literature often referred to as *(channel) system functions*[8]. In the forthcoming chapter we provide a detailed overview of the relevant state-of-the-art modeling and characterization of these system functions.

5   Modeling Paradigms

Channel modeling paradigms and categorization of radio channel models. As mentioned earlier, we often seek to put things into adequate boxes in order to conveniently maintain an overview. For radio channel models relying explicitly on electromagnetic wave propagation it has been suggested to distinguish three overall paradigms, see [12, Sec. 2] for an overview. These paradigms are coined *deterministic* channel modeling, *geometric-stochastic* channel modeling and finally just *stochastic* channel modeling. The latter approach is sometimes encountered with prefixes such as "purely" or "non-geometrical"

---

[8] A fourth system function exists as well [8]. It has two frequency variables, namely ν and f. However, this particular system function has not received much attention in the channel modeling literature.

to emphasize that aspects related to geometry are not considered or incorporated in any way[9].

As a rule of thumb, deterministic channel models rely on geometry as well as considerations from physics, e.g. *optics* and *diffraction* theory. Deterministic models seek to accurately mimic how the electromagnetic waves propagate and interact with obstacles in the surrounding environment, ultimately seeking to approximate solutions of *Maxwell's equations*. Overall, deterministic approaches (such as *ray-tracing* [16, Sec. 3.4]) require a detailed description of the propagation environment, materials, surfaces, physical point-to-point distances, and so on. Deterministic models are often computationally demanding but potentially also very accurate.

To the contrary, purely stochastic channel models rely on partial ignorance. That is, the physical wave propagation phenomenon is still being mimicked but is now characterized by statistical means only. Essentially, certain stochastic mechanisms are proposed, probability distributions selected, and their parameters calibrated. Stochastic models are often flexible with respect to changes in the propagation environment, such as being applicable for both indoor and outdoor communications if the underlying parameters are adjusted accordingly.

The approach of geometric-stochastic channel modeling can be seen as an intermediate between deterministic modeling and purely stochastic modeling. Specifically, a geometric-stochastic channel model is incorporating certain assumptions about geometrical aspects in the propagation environment [12, Sec. 2.2]. Typical and popular examples of such assumptions are related to the actual physical positions of transmitter, receiver and obstacles. Yet, a geometric-stochastic channel model is also based on certain degrees of ignorance, e.g. such that the interactions between electromagnetic waves and physical objects are treated stochastically. One of the most dominant advantages of a geometric-stochastic modeling approach is its accurate relationship to the physical environment, e.g. in terms of the steady change in the propagation constellation caused by receiver movements.

The fundamental differences among the three paradigms described above do not render one particular paradigm more attractive or proper than another. It is crucial to notice that channel models belonging to different paradigms are typically used for *distinct purposes*. Ray-tracing models are in general not attractive for Monte Carlo simulations due to their computationally demanding nature. However, ray-tracing models are favorable for coverage prediction, something the stochastic models are usually not. Accordingly, a categorization of radio channel models does not necessarily enable an option for model comparison but merely it helps to maintain an overview.

---

[9]In [12], channel models relying explicitly on electromagnetic wave propagation are called *physical models*. We stress that numerous channel and propagation models proposed in the literature do not belong to this category, see e.g. [13, 14] and [12, Sec. 3] for examples of so-called *analytical models* [12]. Furthermore, other paradigms/categorizations exist in the channel modeling literature as well [15].

14

6 Outlook

We now possess conceptual knowledge as well as general insight on the engineering terminology in use within the area of stochastic radio channel modeling. In the forthcoming chapter we highlight a selection of landmark contributions which have entered since the earliest days of radio channel modeling. We indicate and discuss existing and emerging trends. In particular, we emphasize a selection of stochastic radio channel models which rely in their construction on point processes. These radio channel models serve as a natural starting point for the contributions of this thesis. Specifically, point processes comprise a convenient and adequate tool for stochastic modeling of linear time-invariant radio channels. This has been known for nearly half a century by now. However, point processes and the associated theoretical framework have not been adopted in a similar fashion when it comes to the important task of analyzing the variety of channel models proposed in the literature. The last decade has offered a few contributions in this direction [17–19] but seemingly without much recognition[10]. The ultimate goal with this thesis is to explore the powerful tools of the theory of spatial point processes in the context of stochastic radio channel modeling and analysis. Specifically, we seek to refine our understanding of the inherent structures and properties of stochastic radio channels and their impact on current and future communication systems and networks.

Throughout the work presented in this thesis it remains a standing assumption that the action of the wireless radio channel can be described via the integral equations (3), (4) and (6). Obviously, these three input-output relationships are disregarding the additive effect of noise as well as interference from other users of the wireless radio channel. Mitigation of noise and interference comprises another important topic in communications engineering which nonetheless is beyond the scope of this thesis. Although not directly emphasized in our main contributions, the point process tools developed can be naturally applied in extensions of the considered models and their use cases. This could for example be communication systems making use of multiple transmit and receive antennas (so-called *MIMO* systems) or radio channel models embedding additional propagation effects such as dispersion in *direction* and *polarization*. Finally, as we shall see, our main contributions are related only to two of the modeling paradigms mentioned in the previous section, namely the purely stochastic approaches (Papers A, B, and C) and the geometric-stochastic approaches (Paper D).

---

[10]Despite the fact that the theory of spatial point processes has already been successfully employed in related areas of research, namely, for the design and analysis of wireless networks [20].

A Subjective View Upon Trends and Seminal Contributions

The overview and exposition to be established in this chapter is non-exhaustive indeed, as well as biased from subjective preferences, thoughts, and impressions. The messages conveyed are better perceived if the reader has prior knowledge beyond that of the mere basics of stochastic radio channel modeling.

The earliest days of radio channel modeling were primarily influenced by S. O. Rice [21, 22] and L. Zadeh [23, 24]. *Shot-noise* random processes and *Campbell's Theorem* played dominant roles in Rice's work on a mathematical characterization of random noise. Zadeh introduced the *time-variant transfer function* and the notion of *system functions* in his analytical treatment of time-variant linear filters. The time-variant transfer function and Campbell's Theorem are both fundamental concepts within the contributions of this thesis, and hence, the combined work of Rice and Zadeh is naturally highlighted.

7   The Bello–Clarke–Kennedy Decade

Three seminal and very popular contributions concerning the modeling and characterization of stochastic radio channels are:

- P. A. Bello's *"Characterization of Randomly Time-Variant Linear Channels"* [8],

- R. H. Clarke's *"A Statistical Theory of Mobile-Radio Reception"* [25], and

- R. S. Kennedy's *"Fading Dispersive Communication Channels"* [2].

These contributions, all from the nineteen sixties, have been cited over and over and the trend is ongoing. Their ideas and expositions are so fundamental that these "classics"

still highly impact today's literature on radio channel modeling. Below we briefly highlight the key aspects of the work by Bello and Clarke. Since Kennedy's contribution was already mentioned in the previous chapter we omit bringing further details on his work at this point.

Bello characterizes, among others, the so-called *wide-sense stationary uncorrelated scattering* (WSSUS) channel. In this setup the system functions are modeled as random processes. The time-variant impulse response $h(t, \tau)$ is *wide-sense stationary* (WSS) in the time variable t and exhibits *uncorrelated scattering* (US) in the delay variable τ. The spreading function $s(\nu, \tau)$ is *white* in both variables whereas the time-variant transfer function $H(t, f)$ is WSS in both of its variables. Bello emphasizes that this doubly-selective channel is the simplest one to characterize in terms of correlation functions while fortunately also being a channel of practical interest. This fact most likely explains the overwhelming dominance of the use of this type of channel model in literature and practice. That $H(t, f)$ is doubly WSS means that its autocorrelation function

$$\mathbb{E}\big[H^*(t, f)H(t', f')\big] = R_H(\Delta t, \Delta f) \tag{7}$$

depends on two variables only, namely the lags $\Delta t := t' - t$ and $\Delta f := f' - f$. The quantity in the right-hand side of (7) is often referred to as the channel's *time-frequency correlation function*. The power spectral density of the random process $H(t, f)$ is the Fourier transform of the time-frequency correlation function, namely

$$P(\nu, \tau) := \iint R_H(\Delta t, \Delta f) \mathrm{e}^{-j2\pi(\nu\Delta t + \tau\Delta f)} \mathrm{d}\Delta t \mathrm{d}\Delta f. \tag{8}$$

This non-negative quantity, referred to as the channel's *scattering function*, reveals how the channel's average power is distributed jointly in Doppler and delay. In general, when the time-variant transfer function is non-stationary, the time-frequency correlation function depends on all four variables (t, t', f, f') in the left-hand side of (7) and *the* scattering function as above is not defined[11]. Major parts of Bello's landmark paper have reentered in literature multiple times, especially in modern academic textbooks [28, Chap. 6], [29, Chap. 7], [30, Chap. 3]. This is true, in particular for those graphs Bello used for demonstrating the relationship between different correlation functions (via duality and Fourier transforms).

Clarke originally derived the well-known bathtub-shaped *power-Doppler profile*

$$P_{\mathrm{Doppler}}(\nu; \nu_{\max}) := \int P(\nu, \tau) \mathrm{d}\tau \propto \frac{\mathbb{1}\big[|\nu| < \nu_{\max}\big]}{\sqrt{1 - (\nu/\nu_{\max})^2}}, \tag{9}$$

which frequently serves as a default choice when modeling the individual path gains in the widely used *Rayleigh-fading multipath channel*. The positive parameter $\nu_{\max}$

---

[11] A rigorous theoretical framework for handling, analyzing, and characterizing non-WSSUS channel models can be found in [26, 27]

controls the largest possible Doppler shift in the channel and is typically determined from assumptions on receiver and scatterer velocities. Larger Doppler shifts means more rapid channel selectivity in time in the sense of shorter intervals between consecutive fades, recall Fig. 2. Clarke's ideas were further developed by W. C. Jakes [31] and the bathtub-shaped Doppler spectrum is from time to time referred to as *Jakes' spectrum.* Doppler spectra more realistic compared to (9), in the sense of not only supposing horizontal wave propagation and consequently being less peaky at the support boundaries, were suggested by T. Aulin [32] some ten years after Clarke's pioneering contribution.

Having the above second-order characterizations of Bello and Clarke in mind, we now proceed to elaborate on a selection of concrete modeling suggestions.

8   A Class of Time-Invariant Stochastic Models

A simple, flexible, and widely used class of time-invariant stochastic channel impulse responses is given by [33, 34]

$$h(\tau) = \sum_{\ell=1}^{L} \alpha_\ell \delta(\tau - \tau_\ell), \tag{10}$$

where $\delta(\cdot)$ is the Dirac delta mentioned in the footnote on page 7. The parameters of the generic model in (10) are:

- L, the number of (multi)path components, which may be infinite,

- $(\alpha_1, \alpha_2, \ldots, \alpha_L)$, a collection of complex-valued[12] path gains, and

- $(\tau_1, \tau_2, \ldots, \tau_L)$, a collection of non-negative propagation delays.

Each term in the sum in (10) is called a *path component*, and each *integer-indexed* pair $(\alpha_\ell, \tau_\ell) \in \mathbb{C} \times \mathbb{R}_+$ is referred to as the corresponding *path parameter(s)*. Alternative channel models can include path components with additional or different path parameters, e.g. directions. We often abuse terminology and refer to the pair (α_ℓ, τ_ℓ) as a path component since this should not be able to cause any confusion.

Some of the parameters in (10) may enter the model in a deterministic fashion while others are randomly generated from realization to realization. For example, the parameter L and the collection $(\tau_1, \tau_2, \ldots, \tau_L)$ may be fixed in advance such that only the path gains $(\alpha_1, \alpha_2, \ldots, \alpha_L)$ are randomly assigned. Another example is where all parameters are generated at random, and so calling them "parameters" may seem a bit misleading. One can also imagine more peculiar constructions where deterministic infinite sequences $(\tau_1, \tau_2, \ldots)$ and $(\alpha_1, \alpha_2, \ldots)$ are predefined[13] and where each realization is formed using

---

[12] Incorporating both *magnitude* and *phase* such that $\alpha_\ell = |\alpha_\ell| \exp(j\theta_\ell)$, in contrast to [34, Sec. II].
[13] Basically resembling Durgin's *SLAC model* construction in [11, Sec. 4.4].

a random number L of randomly selected integer-indices $\big(\ell_{(1)}, \ell_{(2)}, \ldots, \ell_{(L)}\big) \in \mathbb{N}^L$, i.e. not necessarily those indices running from 1 to L. In principle, the "only" limiting factor at this stage is a combination of creativity, sanity, purpose, relevance, and simplicity (the principle of parsimony). Another limiting factor enters only later, namely *analytical tractability*. This key element appears now and then to be entirely forgotten when certain channel models are designed.

A variety of different radio channel models emerge in (10) upon specifying different joint distributions of all path components [34, Sec. IV]. An attractive way of doing so is to initially fix L or to select a suitable probability distribution (binomial, geometric, Poisson, etc.). Next step is to specify the joint distribution of the propagation delays $(\tau_1, \tau_2, \ldots, \tau_L)$ for any given value of L. Finally, the conditional joint distribution of $(\alpha_1, \alpha_2, \ldots, \alpha_L)$ is to be specified, for example such that

$$\mathbb{E}[\alpha_\ell|\tau_\ell] = 0 \qquad \text{and} \qquad \mathbb{E}\big[|\alpha_\ell|^2|\tau_\ell\big] = \sigma_\alpha^2(\tau_\ell), \qquad \ell = 1, 2, \ldots, L, \tag{11}$$

where the function $\sigma_\alpha^2(\cdot)$ is assigning conditional average power to each path gain as a function of its associated propagation delay. Motivated by physical arguments, the function $\sigma_\alpha^2(\tau)$ is usually selected to exercise a decaying trend versus increasing delay τ. More generally, the conditional joint distribution of $(\alpha_1, \alpha_2, \ldots, \alpha_L)$ can also be specified with correlated components, for example such that

$$\mathbb{E}[\boldsymbol{\alpha}|\boldsymbol{\tau}] = \mathbf{0} \qquad \text{and} \qquad \mathbb{E}\big[\boldsymbol{\alpha}\boldsymbol{\alpha}^H|\boldsymbol{\tau}\big] = \boldsymbol{\Sigma}_\alpha(\boldsymbol{\tau}), \tag{12}$$

where we have introduced a compact vector notation with $\boldsymbol{\tau} := (\tau_1, \tau_2, \ldots, \tau_L)^\top$ and $\boldsymbol{\alpha} := (\alpha_1, \alpha_2, \ldots, \alpha_L)^\top$. Notice that (11) is a special-case of (12), but notice also that entirely different choices could have been made as well. Yet, no matter how the conditional joint distribution of the path gains is selected it should in all cases remain feasible to calculate and normalize the channel's average power gain

$$P_{\text{total}} := \mathbb{E}\bigg[\bigg|\sum_{\ell=1}^{L} \alpha_\ell\bigg|^2\bigg]. \tag{13}$$

Obviously, the gain in (13) should be finite in order for the proposed model to make physical sense. Furthermore, without the ability to calculate (13) the suggested channel model renders itself of only very limited interest (even for simulation purposes).

Example 1. Consider the following construction of a model of type (10). Let L be any random variable with non-negative integer range. In each realization, conditioned on L, suppose that all path components (α_ℓ, τ_ℓ) are mutually i.i.d. and independent of L such that

$$f(\boldsymbol{\alpha}, \boldsymbol{\tau}|L) = \prod_{\ell=1}^{L} f(\alpha_\ell|\tau_\ell) f(\tau_\ell),$$

where f is used in a generic manner to represent several different probability density functions, being distinguishable only by their arguments. We assume that $f(\alpha_\ell|\tau_\ell)$ is such that $\mathbb{E}[\alpha_\ell|\tau_\ell] = 0$, i.e. (11) applies and we need to specify the function $\sigma_\alpha^2(\cdot)$ at some point. However, we can directly calculate the channel's average power gain as

$$
P_{\text{total}} = \mathbb{E}\bigg[\bigg(\sum_{\ell=1}^{L}\alpha_\ell\bigg)^*\bigg(\sum_{k=1}^{L}\alpha_k\bigg)\bigg] = \mathbb{E}\bigg[\sum_{\ell=1}^{L}\mathbb{E}\big[|\alpha_\ell|^2|L\big]\bigg] = \mathbb{E}\bigg[\sum_{\ell=1}^{L}\mathbb{E}\big[\mathbb{E}\big[|\alpha_\ell|^2|\tau_\ell\big]\big]\bigg]
$$
$$
= \mathbb{E}\bigg[\sum_{\ell=1}^{L}\mathbb{E}\big[\sigma_\alpha^2(\tau_\ell)\big]\bigg]
$$
$$
= \mathbb{E}\bigg[L\mathbb{E}\big[\sigma_\alpha^2(\tau_\star)\big]\bigg]
$$
$$
= \mathbb{E}[L]\mathbb{E}\big[\sigma_\alpha^2(\tau_\star)\big], \qquad (14)
$$

where $\tau_\star$ denotes an arbitrary propagation delay drawn from the marginal density $f(\tau)$.

We can now make explicit choices such as drawing the propagation delays uniformly on a suitably chosen interval $[0, \tau_{\max}]$ and letting $\sigma_\alpha^2(\tau) = Q\mathrm{e}^{-\rho\tau}$ for some positive constants Q and ρ. Entering these choices in (14) yields

$$
P_{\text{total}} = \mathbb{E}[L]\frac{Q}{\rho\tau_{\max}}(1 - \mathrm{e}^{-\rho\tau_{\max}}),
$$

which can be normalized via Q upon specifying the remaining three parameters. Such a normalization would be needed, e.g. in simulation studies regarding performance assessments of communication systems (to control the average signal-to-noise ratio).

More involved examples can be straightforwardly constructed by applying (12) with a non-diagonal conditional covariance structure $\boldsymbol{\Sigma}_\alpha$. The conditional joint density $f(\boldsymbol{\alpha}, \boldsymbol{\tau}|L)$ may also depend more crucially on L compared to just letting this integer assign the vector dimension of $\boldsymbol{\alpha}$ and $\boldsymbol{\tau}$. However, most calculations immediately turn tedious as a consequence of any such changes and assessment of the channel's average power gain P_{total} becomes non-trivial. This is exactly where the analytical tractability enters as a limiting factor.

Channel models of type (10) appear in numerous places in the literature [33, 34]. Some are quite simplistic while others are more sophisticated in their setup depending on the context. Some proposed models rely in their constructions on one-dimensional *point processes* (see Appendix E for an introduction) and these are particularly relevant for the scope of this thesis. Specific examples of such channel models are:

- G. L. Turin et al. [35], 1972, a model intended for urban radio communications. The collection of propagation delays $\{\tau_\ell\}$ forms a (possibly inhomogeneous) *Poisson point process* [36, 37]. The distribution of each path gain's magnitude $|\alpha_\ell|$ is log-normal with parameters depending on the corresponding propagation delay τ_ℓ.

- H. Suzuki [38], 1977, a PhD student of Turin treating the so-called Δ-K model, a follow-up development outlined already in Turin's original paper [35]. The collection of propagation delays $\{\tau_\ell\}$ now forms a *self-exciting* point process [39, Chap. 6], while in a special-case forming a *renewal* type point process as Suzuki also remarked in his PhD thesis [40, pp. 149]. The proposed construction, which aimed at triggering the propagation delays to form groups, was unfortunately found difficult to analyze. An important remark is that Suzuki appears to be the first to use the notion of "*local*" scattering, local clusters, local objects and so on. Such terminology is now frequently being used in the channel modeling literature.

- A. A. M. Saleh & R. A. Valenzuela [41], 1987, a model intended for indoor radio communications. This construction involves two layers of homogeneous Poisson point processes, designed specifically to enforce the propagation delays to form so-called *clusters*. Path gain magnitudes are Rayleigh distributed with a peculiar two-layered exponentially decaying structure for the conditional average powers.

From an analytical point of view the computational aspects are not getting any lighter upon introducing point processes in the generic channel model description (10). This is also clearly evidenced when consulting the original references [35, 38, 41] since only confined fragments of analytical characterizations are provided. However, by relatively obscure arguments, Saleh & Valenzuela do in fact obtain a closed-form expression of the average power gain (13) for their proposed two-layer model [41, Eq. (27)+(31)].

Apart from the average power gain of a certain channel model, we are similarly interested in being able to characterize its frequency domain correlation properties and its power-delay profile. This knowledge allows to calculate key parameters such as coherence bandwidth, delay spread, mean excess delay, maximum excess delay, and so on. These parameters are essential to the design and operability of modern communication and positioning systems.

Example 2. We proceed with a further analysis of the channel model from Example 1. Recall that L, the number of path components, is a random variable. The transfer function corresponding to the impulse response in (10) reads

$$H(f) = \sum_{\ell=1}^{L} \alpha_\ell e^{-j2\pi f \tau_\ell}, \tag{15}$$

which is an ordinary complex-valued random process in the frequency variable f. Under the same assumptions as in Example 1 we readily find that

$$\mathbb{E}\big[H(f)\big] = \mathbb{E}\bigg[\sum_{\ell=1}^{L} \mathbb{E}\Big[\underbrace{\mathbb{E}\big[\alpha_\ell|\tau_\ell\big]}_{=0}\,\mathrm{e}^{-j2\pi f\tau_\ell}\Big]\bigg] = 0,$$

i.e. the transfer function is a zero-mean process. The autocorrelation function of $H(f)$ is obtained by manipulations matching those leading to (14), and so

$$R_H(f,f') := \mathbb{E}\big[H^*(f)H(f')\big] = \mathbb{E}\bigg[\sum_{\ell=1}^{L}\alpha_\ell^* \mathrm{e}^{j2\pi f\tau_\ell}\sum_{k=1}^{L}\alpha_k \mathrm{e}^{-j2\pi f'\tau_k}\bigg], \qquad (16)$$

$$= \mathbb{E}[L]\mathbb{E}\big[\sigma_\alpha^2(\tau_\star)\mathrm{e}^{-j2\pi\Delta f\tau_\star}\big], \qquad (17)$$

$$= \widetilde{R}_H(\Delta f)$$

where all cross-terms vanish in (16), and where $\tau_\star$ denotes an arbitrary propagation delay drawn from the marginal density $f(\tau)$ as in Example 1. Thus, the transfer function $H(f)$ is found to be WSS and we notice how (17) differs from (14) only by the complex exponential term inside the expectation. Obviously, (17) coincides with (14) when evaluated at $\Delta f = 0$. By inspection of (17) we identify that the correlation function $\widetilde{R}_H(\Delta f)$ is in fact a scaled Fourier transform. Specifically, we have that

$$\widetilde{R}_H(\Delta f) = \mathbb{E}[L]\mathcal{F}\big\{f(\tau)\sigma_\alpha^2(\tau)\big\}(\Delta f),$$

and so we immediately find that the power-delay profile of this channel is given by

$$P_{\mathrm{delay}}(\tau) = \mathbb{E}[L]f(\tau)\sigma_\alpha^2(\tau) \qquad \text{with} \qquad \int_0^\infty P_{\mathrm{delay}}(\tau)\mathrm{d}\tau = P_{\mathrm{total}}.$$

Hence, a channel of type (10) with i.i.d. path components and conditionally uncorrelated zero-mean path gains is WSS in the frequency domain and has a power-delay profile given by the three-term product:

average number of path components

$\times$

marginal density of propagation delays

$\times$

conditional second-moment of path gains.

In case of L not being random we can simply replace $\mathbb{E}[L]$ by the constant L itself.

A key feature of the correlation function $\widetilde{R}_H(\Delta f)$ in Example 2 is that it contains the information necessary to form linear estimators of $H(f)$ which are optimal in minimum mean squared error sense, e.g. for OFDM applications. Furthermore, the main lobe of $\widetilde{R}_H(\Delta f)$ is used to extract knowledge about the pace at which the transfer function $H(f)$ decorrelates, i.e. the correlation function $\widetilde{R}_H(\Delta f)$ provides information about the coherence bandwidth of the channel [42].

For a point process construction such as the one by Saleh & Valenzuela [41], the frequency domain correlation function and the power-delay profile are not as easily assessed as in Example 2. In fact, these second-order characteristics have only recently been reported in literature [19]. Unfortunately, the results in [19] are obscured from a pronounced notational overhead in combination with the fact that most derivations rely on relatively advanced mathematical tools (measure-theoretical counting integrals, moment generating functionals for Poisson-driven shot-noise, etc.). Yet, the crucial analytical properties of Saleh & Valenzuela's model can be re-derived in a simpler and more insightful way (Paper B), essentially by application of point process related tools no more advanced than *Campbell's Theorem* [37, Sec. 3.2], [43, Prop. 4.1], [44, Thm. 2.2].

9 Time-Variant Stochastic Modeling

Despite the generic channel impulse response in (10) being time-invariant, this very model is frequently used for time-variant scenarios as well. The time axis is then sliced into appropriate slots and individual realizations of (10) are placed in each individual time slot. Such discretized time-variant constructions are often referred to as *block-fading channels*. However, there are also numerous other ways to design a stochastic model of the time-variant radio channel. A straightforward procedure is as follows. Start from the model in (10) and incorporate time-dependency into some or all of its parameters. One particular outcome of this strategy would lead to a sequence of models reading

$$a) \qquad h(\tau) = \sum_{\ell=1}^{L} \alpha_\ell \delta(\tau - \tau_\ell) \qquad (18)$$

$$b) \qquad h(t,\tau) = \sum_{\ell=1}^{L} \alpha_\ell(t) \delta(\tau - \tau_\ell) \qquad (19)$$

$$c) \qquad h(t,\tau) = \sum_{\ell=1}^{L(t)} \alpha_\ell(t) \delta(\tau - \tau_\ell) \qquad (20)$$

$$d) \qquad h(t,\tau) = \sum_{\ell=1}^{L(t)} \alpha_\ell(t) \delta\big(\tau - \tau_\ell(t)\big), \qquad (21)$$

with the model class in (18)/(21) incorporating the smallest/largest number of time-variant quantities. In fact, class a) in (18) is just copied from (10) and so not being time-variant at all. Furthermore, not all configurations are displayed above as $2\cdot2\cdot2 = 8$ different scenarios are possible:

L time-variant?	$\{\alpha_\ell\}$ time-variant?	$\{\tau_\ell\}$ time-variant?
yes or no	yes or no	yes or no

The course through the sequence a) $\rightarrow$ b) $\rightarrow$ c) $\rightarrow$ d) is deliberate and the reason for disregarding four alternative configurations is not that these are practically or theoretically irrelevant. The sequence a) $\rightarrow$ b) $\rightarrow$ c) $\rightarrow$ d) is chosen to represent a steady increase of "complexity" in the sense of time-variability. Within class d) we seek essentially to incorporate as many time-dynamic features as possible without breaching the scope of the original multipath channel model in (10). A conceptual illustration of a realization of some fictitious class d) model is provided in Fig. 3.
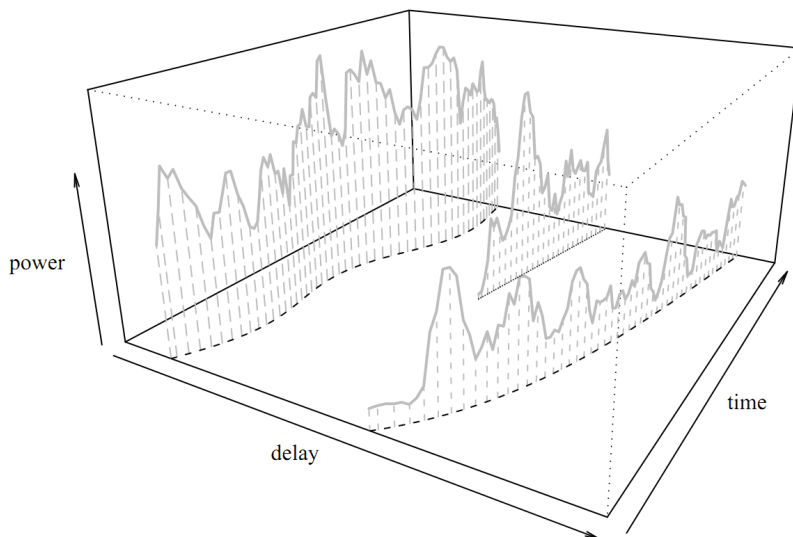
Fig. 3: (21) depicted in conceptual terms to highlight its time-variant multipath behavior. Initially, only two path components are present but as time progresses a new path component emerges. Propagation delays and path gain magnitudes are fluctuating with time.

Channel models belonging to class a) were discussed already in the previous section. Models from class b) are often found in literature [45], [46, Sec. II-C], [47, Chap. 6], [16, Chap. 6], and these appear to comprise the easiest type of time-variant radio channels

to "handle" and analyze. A known fact is that Bello's WSSUS characterization applies for all type b) models with conditionally uncorrelated zero-mean WSS path gain processes, see e.g. [45]. This fact renders merely what to be expected, especially with the conclusions from Example 2 in mind.

Channel models belonging to the classes c) and d) appear frequently in literature as well [34, Eq. (1)], [30, Chap. 3], [48]. Yet, the ability to analytically characterize these models seems to become more and more challenging with the increased degree of time-variability, as also emphasized by Hashemi in [34, Sec. V-A]. It is not immediately clear if a type c) model has the ability to enter as a member of the analytically attractive WSSUS class[14]. And if a type c) model can in fact be a WSSUS channel, under what specific conditions then? Intuitively, one expects at least that the integer-valued random process $L(t)$ in (20) has to be WSS. Yet, is this condition sufficient? Obviously, the same and even further speculations apply to the models of type d).

A few of the time-invariant channel constructions mentioned in the previous section employed point processes to incorporate dispersion in the delay-domain. However, point processes can similarly be used to incorporate dispersion in Doppler, direction, and so on. Some time-variant channel models of classes c) and d) rely on point processes. A popular setup used to generate the temporal random process $L(t)$ in (20)/(21) is based on a stochastic birth-death mechanism. Specifically, the birth-death mechanism is designed using a homogenous Poisson point process (birth times) in combination with a sequence of i.i.d. exponentially distributed random variables (lifetimes). This particular construction has entered in the literature several times [49–51] while being originally proposed in the context of radio channel modeling by S. J. Papantoniou [52]. Only few analytical properties of this particular type d) model have been reported in the channel modeling literature. This fact seems to confirm Hashemi's statement regarding the difficulties emerging due to increased time-variability. However, a wide range of analytical properties can be extracted by naturally exploiting the fact that the underlying construction relies on a point process (Paper A).

10 Analysis of Stochastic Radio Channels Via Point Processes and Campbell's Theorem

Two examples are provided in the following to indicate and hint towards the potential arising when employing the theory of spatial point processes to facilitate the analytical characterization of stochastic radio channel models. Concise and targeted introductions to the theory of spatial point processes can be found in Sec. 2 in Paper B or Sec. 3 in

---

[14]Being a member of the WSSUS class is to be understood here as a question of whether the associated time-variant channel transfer function $H(t, f)$ is doubly WSS. Essentially, the impulse response models considered in this section do not belong/fit within Bello's original work since these are not ordinary two-dimensional random processes. They are random generalized functions.

Paper A. Alternatively, Appendix E takes the form of a study note which provides a highly accessible introduction to spatial point processes. The examples below presuppose familiarity with several concepts from the theory of spatial point processes.

Example 3. Recall Example 2 where we derived a three-term product-structured power-delay profile for a simple time-invariant channel model of type (10). In this example we generalize the result and assess a similar product structure using a point process approach.

We start by reformulating the impulse response model in (10) using a one-dimensional point process Y (propagation delays) and a collection of conditionally uncorrelated zero-mean *marks* $\{\alpha_y : y \in Y\}$ (path gains). The exact reformulation reads

$$h(\tau) = \sum_{\ell=1}^{L} \alpha_\ell \delta(\tau - \tau_\ell) \qquad \longrightarrow \qquad h(\tau) = \sum_{y \in Y} \alpha_y \delta(\tau - y),$$

which for the moment looks as nothing but a shift in notation. The point process Y is defined on the non-negative reals $\mathbb{R}_+ := [0, \infty)$ and it has a non-negative intensity function $\varrho_Y(y)$. We assume that the complex-valued random marks are drawn such that

$$\mathbb{E}[\alpha_y|Y] = \mathbb{E}[\alpha_y|y] = 0, \qquad y \in Y,$$

and such that

$$\mathbb{E}\left[\alpha_y^* \alpha_{\tilde{y}}|Y\right] = \mathbb{E}\left[\alpha_y^* \alpha_{\tilde{y}}|y, \tilde{y}\right] = \sigma_\alpha^2(y)\mathbb{1}[y = \tilde{y}], \qquad y, \tilde{y} \in Y,$$

which is the assumption of conditionally uncorrelated zero-mean path gains. With our new notation the associated channel transfer function reads

$$H(f) = \sum_{y \in Y} \alpha_y \mathrm{e}^{-j2\pi f y}.$$

We can immediately proceed by computing its correlation function:

$$R_H(f, f') = \mathbb{E}[H^*(f)H(f')] = \mathbb{E}\left[\mathbb{E}[H^*(f)H(f')|Y]\right] \tag{22}$$

$$= \mathbb{E}\left[\sum_{y \in Y} \sum_{\tilde{y} \in Y} \mathbb{E}\left[\alpha_y^* \alpha_{\tilde{y}}|Y\right] \mathrm{e}^{j2\pi f y} \mathrm{e}^{-j2\pi f' \tilde{y}}\right],$$

$$= \mathbb{E}\left[\sum_{y \in Y} \underbrace{\sigma_\alpha^2(y)\mathrm{e}^{-j2\pi \Delta f y}}_{g(y;\Delta f)}\right], \tag{23}$$

$$= \int_0^\infty \varrho_Y(y)\sigma_\alpha^2(y)\mathrm{e}^{-j2\pi \Delta f y}\mathrm{d}y, \tag{24}$$

$$= \mathcal{F}\{\underbrace{\varrho_Y(\cdot)\sigma_\alpha^2(\cdot)}_{P_{\mathrm{delay}}(\cdot)}\}(\Delta f), \tag{25}$$

26

where the step in (22) amounts to standard conditioning, (23) follows by conditional uncorrelatedness, and the step from (23) to (24) follows by application of Campbell's Theorem.

In conclusion, we end up with a product-structured power-delay profile which generalizes the result from Example 2 (for a suitable choice of the point process Y). Conditioned on L, the collection in Y forms a binomial point process since the propagation delays are i.i.d. by assumption. Obviously, for the channel to make physical sense we should have

$$\int_0^\infty P_{\text{delay}}(y)\mathrm{d}y = \int_0^\infty \varrho_Y(y)\sigma_\alpha^2(y)\mathrm{d}y < \infty,$$

and so enforcing a natural decay-condition on the product $\varrho_Y(y)\sigma_\alpha^2(y)$. The result in (25) applies to any linear time-invariant channel model for which the propagation delays can be formulated as a point process and which holds conditionally uncorrelated zero-mean path gains as specified in the beginning of this example. In particular, the result holds for special-cases of the models proposed by Turin and Suzuki as well as the one by Saleh & Valenzuela (Paper B).

Assume that a channel model has been cast within the scope of Example 3. The frequency-domain correlation function and the associated power-delay profile are thus both offered without the need for tedious calculations. Casting a model within the scope of the above example amounts to specifying the desired type of point process for Y (binomial, Poisson, self-exciting, Cox, etc.), its intensity function $\varrho_Y(y)$, as well as the function $\sigma_\alpha^2(\cdot)$ which assigns conditional average power to the individual path gains.

Example 4. In the last paragraph of the previous section it was mentioned how the temporal random process $L(t)$ in (21) has been generated in the literature so far. Specifically, the suggested design is based on a homogenous Poisson point process (birth times) in combination with a sequence of i.i.d. exponentially distributed random variables (lifetimes). This construction can be naturally viewed as a marked Poisson point process X or equivalently, as a two-dimensional point process X (which is in fact a spatial Poisson point process with known intensity function since the marks are mutually independent).

From this two-dimensional point process perspective the analytical characterization of the random process $L(t)$ renders suddenly quite feasible. Specifically, the random process can be readily defined as

$$L(t) = \sum_{\boldsymbol{x} \in X} g(\boldsymbol{x}; t),$$

for a suitable choice of the function $g(\boldsymbol{x}; t)$, where the points are now displayed in boldface notation to stress that X is a two-dimensional point process. The mean

$\mathbb{E}[L(t)]$ can be computed using Campbell's Theorem and the time-varying impulse response in (20) or (21) can be reformulated into a sum indexed by a point process, essentially as in Example 3. Overall, the two-dimensional point process perspective briefly described in this example enables novel analytical characterization of the time-variant channel models in (20) and (21). In particular, it allows to partially answer some of our previous questions regarding potential WSSUS properties (Paper A).

From the above two examples the curiosity of the potential reader has hopefully been triggered. At least, we are now adequately prepared to take a closer look at the main contributions of this thesis as well as their implications.

28

Contributions, Conclusions, and Outlook

This chapter outlines and summarizes the key contributions of this PhD thesis, namely Papers A, B, C, and D, as well as the study note in Appendix E. The particular labeling of the papers is deliberately chosen to reflect subjective priorities. Yet, the true chronological order

Paper C (2010) $\rightarrow$ Paper B (2012) $\rightarrow$ Paper D (2013) $\rightarrow$ Paper A (submitted 2013),

indirectly tells a story about the progress of my work. In particular, it reveals how my personal view upon radio channel modeling has slowly but steadily changed, matured, and settled. Paper C is the earliest one, my first "real" publication. Ironically, this contribution does not at all rely on the theory of point processes. However, the curiosity, technical outcomes, and ideas spawned from this paper happened to establish the foundation for the subsequent direction of my work. My research activities are now notably influenced by the theory of point processes and this is partly the reason why the study note in Appendix E was put together almost two years ago.

11 Paper Contributions and Findings

In this section, all four papers are presented in a format which resembles an extended abstract. Table 1 provides an ultra short summary of each paper (see next page). The table essentially indicates the exact channel models being considered as well as the roles played by the point processes introduced in each paper.

Paper A:

Channel models:	Purely stochastic, mainly type c) but also type d)
Point processes:	Creates a temporal birth-death mechanism
	Used for indexing of path components
Main findings:	Novel and thorough analysis of birth-death mechanism
	Type c) models can be WSSUS
	Product-structured time-frequency correlation function

Paper B:

Channel model:	Purely stochastic, type a)
Point processes:	Creates delay dispersion
Main findings:	Model formed by dependent Poisson and Cox point processes
	Power-delay profile not exponentially decaying

Paper C:

Channel models:	Purely stochastic, types b) and d)
Point processes:	Not used
Main findings:	Appropriate channel model selection is crucial

Paper D:

Channel model:	Geometric-stochastic, type d) but such that $L(t) = L$
Point processes:	Creates dispersion (delay, Doppler, space)
Main findings:	Non-stationary but analytically tractable channel model

Table 1: Sparse overview of Papers A, B, C, and D.

$$
\text{a)} \qquad h(\tau) = \sum_{\ell=1}^{L} \alpha_\ell \delta(\tau - \tau_\ell)
$$

$$
\text{b)} \qquad h(t, \tau) = \sum_{\ell=1}^{L} \alpha_\ell(t) \delta(\tau - \tau_\ell)
$$

$$
\text{c)} \qquad h(t, \tau) = \sum_{\ell=1}^{L(t)} \alpha_\ell(t) \delta(\tau - \tau_\ell)
$$

$$
\text{d)} \qquad h(t, \tau) = \sum_{\ell=1}^{L(t)} \alpha_\ell(t) \delta\big(\tau - \tau_\ell(t)\big)
$$

The impulse response models from page 22.

Paper A – The topic of this paper is purely stochastic modeling and subsequent analysis of time-variant radio channels. Specifically, channel models of type (20) and (21) are considered with an underlying point process construction used to generate a temporal birth-death behavior of individual path components.

The approach in the paper is based on analytically tractable reformulations of (20) and (21) and on subsequent analysis of these via Campbell's Theorem. Specifically, the traditional integer-indexed sums in (20) and (21) are replaced by equivalent expressions indexed by points from a particular spatial point process. Several novel investigations are carried out in the paper. A comprehensive analytical characterization of the temporal birth-death mechanism is given. Additionally, we derive the general structure of the time-frequency correlation function for this type of time-variant channel models. A key aspect of our approach is a gradual identification of conditions under which the resulting channel models belong to the popular WSSUS class.

Several overall conclusions emerge in Paper A. The proposed point process perspective is analytically beneficial due to its inherent flexibilities with respect to dimensionality swapping and due to its ability to circumvent enumeration issues of traditional modeling approaches. The point process perspective is also highly attractive for simulation purposes. Channel models of type (20) can indeed be designed such that they belong to the WSSUS class. The general structure of the time-frequency correlation function reveals a product form consisting of a large-scale and a small-scale term. Finally, the paper strongly suggests (without definitive proof, however) that models of type (21) *cannot* be designed such that they belong to the WSSUS class.

Paper B – The topic of this paper is centered around the popular time-invariant channel model by Saleh and Valenzuela (the S-V model), which is of type (18). The paper presents a thorough and readily accessible point process analysis of the S-V model and its underlying two-layered structure. The motivation for revisiting the classical S-V model comes from the fact that it is being widely used in simulation studies, performance comparisons and evaluations[15]. However, due to its rather ad-hoc construction, the analytical properties of the original S-V channel model are not well-understood or not known, e.g. the shape of the power-delay profile.

The approach in the paper relies on an analytically tractable reformulation of the classical S-V model. Specifically, the collection of propagation delays emerging in two layers is formulated as a new point process. This new formulation facilitates analytical characterization via Campbell's Theorem. Hence, the main idea is to naturally exploit the fact that the original model construction relies on point processes. From this perspective the main investigations are driven by a question rooted in curiosity. What basic analytical properties can be readily established for the popular S-V model and its original two-layered construction?

---

[15]More precisely, a number of refined/extended S-V models are frequently employed, e.g. within the ultra-wideband activities based on the IEEE 802.15.3a and IEEE 802.15.4a standardizations.

The first main conclusion of Paper B is that the S-V model is comprised by the union of two dependent point processes, namely a homogeneous Poisson point process and an inhomogeneous Cox point process. Secondly, the intensity of path components rises linearly with propagation delay. Finally, the power-delay profile of the S-V model is not exponentially decaying, it consists of a sum of two exponentially decaying terms. Overall, the paper re-derives the intensity of path components and the channel's power-delay profile in a simpler and more insightful way compared to previous [19] and alternative [53] derivations. In essence, the above conclusions arise now as a direct result of the wide applicability and straightforward use of Campbell's Theorem.

Paper C – The topic of this paper is channel estimation in orthogonal frequency-division multiplexing (OFDM) systems. The work is motivated from the fact that the state-of-the-art channel estimation algorithm[16] for OFDM signalling suffers from an irreducible performance degradation due to its robust design. However, a notable advantage of this estimation algorithm is that it operates without knowledge on instantaneous radio channel parameters such as propagation delays and the number of path components. Previous studies have suggested that the robustly designed estimator can be outperformed by linear minimum mean squared error estimators exploiting/presupposing such *instantaneous information* about the radio channel.

The approach in the paper is based on two different time-variant radio channel models, one of type (19) and one of type (21). For both of these scenarios, the same three-step channel estimator is employed. Specifically, $H(t, f)$ is sampled at $M = 200$ evenly spaced pilot-subcarrier frequencies and from these samples the channel parameters (all path components) are estimated via the following steps:

1) $M_1 \times M_1$ covariance matrix estimation (Toeplitz structure) where $M_1 \leq M$,

2) Propagation delay estimation using the Unitary ESPRIT algorithm [54],

3) Linear minimum mean squared error estimation of path gains.

Two separate endpoint investigations are considered. The first investigation is on the bit-error-rate performance versus improved covariance matrix estimation in 1) via so-called spatial smoothing (which is possible due to the Toeplitz structure). The second investigation is on bit-error-rate performance versus increased temporal dynamic behavior of the channel, i.e. when changing the channel model from type (19) to (21).

The overall conclusions of Paper C are that appropriate channel model selection is crucial for performance assessment of receiver algorithms and that the robustly designed state-of-the-art channel estimator can be outperformed at the expense of higher computational complexity and provided that the number of path components in the radio channel is known.

---

[16] A robustly designed linear estimator derived from a minimum mean squared error criterion [45].

Paper D – The topic of this paper is geometric-stochastic channel modeling of scattering contributions induced from roadside vegetation in land-mobile-satellite applications. The motivation for this work is that scattering, shadowing, and obstruction caused by vegetation (e.g. trees) in the surrounding of mobile receivers of satellite navigation systems impair the overall system performance. Specifically, the delay dispersion caused by the physical size of trees can easily be of the same order of magnitude as the inverse signal bandwidth used in modern positioning systems.

The paper presents a channel modeling approach taking into account the geometry of the considered scenario, namely the position of a transmitter (a satellite), the trajectory of a mobile receiver (a car) as well as the location and the size of a scattering volume (a tree). The scattering mechanism in the tree is modeled as resulting from single-bounce point-source scatterers located randomly inside the tree canopy. We model the set of such scatterers as a marked spatial point process. Essentially, the considered channel model is of type (21) but restricted such that the number of path components $L(t) = L$ does not change within the same realization of the channel, it changes only from realization to realization. An integral-form expression of the channel's time-frequency correlation function is derived by invoking Campbell's Theorem. Yet, a closed-form approximation of the time-frequency correlation function is given for time lags corresponding to displacements along the receiver trajectory for which the plane wave assumption holds. The proposed channel model is verified and validated experimentally with wideband measurements and by means of Monte Carlo simulations.

One of the key conclusions of Paper D is that the channel transfer function $H(t, f)$ is non-stationary and that the (mobility induced) steady change of the propagation constellation is the main cause for the non-stationarity. Three distinct phases are identified within the temporal evolution of the time-variant channel transfer function. All three phases comply well with intuition regarding the expected behavior of $H(t, f)$ depending on whether the mobile receiver is approaching, passing straight by, or departing a single isolated roadside tree. In fact, for each fixed time instance, the channel transfer function $H(t, f)$ is found to be wide-sense stationary in frequency. The proposed model includes conveniently and adequately the delay and Doppler dispersion induced by the physical extent of the tree and the receiver's movement.

12   Conclusions and Outlook

Based on the four main contributions of this thesis and their individual findings (as reported above), we draw the following two overall conclusions:

- The theory of spatial point processes is highly facilitating for the stochastic modeling of various radio channels. This is true for purely stochastic time-invariant and time-variant channels models as well as for geometric-stochastic channel models.

- The theory of spatial point processes and its powerful tools, like Campbell's Theorem, are equally facilitating for the purpose of extracting analytical properties of the proposed channel models.

The concept of marked (spatial) point processes comprises a flexible and easily applicable tool for the "engineering treatment" of numerous radio channels. Knowledge on abstract measure theory is not needed in order to *apply* the theory of spatial point processes, at least not in the practical context of radio channel modeling and characterization. Beside these overall statements, a number of more concrete implications can be highlighted as well.

The point process perspective offers build-in flexibilities with respect to dimensionality swapping as well as a natural ability to circumvent inconvenient enumeration issues of traditional channel modeling approaches. Model extensions such as incorporation of additional dispersion effects (e.g. direction and polarization) can be straightforwardly accounted for by attaching new marks to existing point processes. A convenient aspect is that the overall notation and the indexing procedures stay virtually the same. Calculations involving Campbell's Theorem amounts to the same mechanical steps, the main difference being that the vector dimensionality of the marks/points has increased.

The point process perspective offers as well guidelines in the direction of alternative/improved/easier computer simulation of channel model realizations. The analytical insight gained in Paper A allows for the considered temporal birth-death channel to be initialized in equilibrium. Approximate simulation is avoided and less running time is required since no forerun is needed for the channel process to "*settle in*". Essentially, a flexible alternative to traditional block-fading simulations is also provided by the temporal birth-death channel model in Paper A. The channel can be simulated as a single long realization and it automatically reconfigures its path components and the number of these along the way. The analytical insight gained in Paper B suggests an alternative procedure for generating channel realizations from the classical model by Saleh & Valenzuela. Specifically, one can generate the homogeneous Poisson point process at first and then, conditioned on its realization, generate the Cox point process according to an inhomogeneous Poisson point process having a staircase-shaped intensity function.

New parameter estimation aspects naturally emerge due to the analytical benefits of the point process perspective, in particular due the wide applicability of Campbell's Theorem. The practical importance of the direct ability to analytically assess

time-frequency correlation functions and power-delay profiles is clearly evident. Key parameters of the proposed channel models now reveal themselves explicit in practically measurable quantities. This aspect opens up new and alternative possibilities for how to estimate these key parameters. Essentially, the proposed channel models can be rigorously calibrated and used as well for measurement prediction purposes. Such capabilities stand in notable contrast to the limitations of "*pure*" simulation models. For such models it is usually unknown whether potential interactions occur between the different model parameters. Furthermore, questions regarding stationarity properties often remain inconclusive for pure simulation models, simply because of their analytically intractable setup.

Novel capacity assessments and bounding techniques could potentially enter as a future byproduct of the perspectives offered by the facilitating theoretical framework for spatial point processes. Research along these lines have already been considered in [19] for ultra-wideband Saleh & Valenzuela type channel model extensions.

References

[1] T. Pedersen, "Contributions in radio channel sounding, modeling, and estimation," PhD thesis, Aalborg University, Denmark, 2009.

[2] R. S. Kennedy, *Fading Dispersive Communication Channels.* John Wiley & Sons, 1969.

[3] K. Gröchenig, *Foundations of Time-Frequency Analysis.* Birkhäuser, 2001.

[4] R. A. Kennedy, *Hilbert Space Methods in Signal Processing.* Cambridge University Press, 2013.

[5] O. Christensen, *An Introduction to Frames and Riesz Bases.* Birkhäuser, 2003.

[6] D. Slepian, "On bandwidth," *Proceedings of the IEEE*, vol. 64, no. 3, pp. 292–300, 1976.

[7] J. I. Richards and H. K. Youn, *Theory of Distributions: a non-technical introduction*, re-issued paperback ed. Cambridge University Press, 2007.

[8] P. A. Bello, "Characterization of randomly time-variant linear channels," *IEEE Transactions on Communication Systems*, pp. 360–393, 1963.

[9] P. Olofsson, *Probability, Statistics, and Stochastic Processes.* John Wiley & Sons, Inc., 2005.

[10] A. Papoulis, *Probability, Random Variables, and Stochastic Processes*, 3rd ed. McGraw-Hill, Inc., 1991.

[11] G. D. Durgin, *Space-Time Wireless Channels.* Pearson Education, Inc., 2003.

[12] P. Almers, E. Bonek, A. Burr, N. Czink, M. Debbah, V. Degli-Esposti, H. Hofstetter, P. Kyösti, D. Laurenson, G. Matz, A. F. Molisch, C. Oestges, and H. Özcelik, "Survey of channel and radio propagation models for wireless MIMO systems," *EURASIP Journal on Wireless Communications and Networking*, 2007.

[13] M. Franceschetti, "Stochastic rays pulse propagation," *IEEE Transactions on Antennas and Propagation*, vol. 52, no. 10, pp. 2742–2752, 2004.

[14] G. Matz and F. Hlawatsch, "Time-varying communication channels: Fundamentals, recent developments, and open problems," *Proc. EUSIPCO*, 2006.

[15] B. H. Fleury and P. E. Leuthold, "Radiowave propagation in mobile communications: An overview of european research," *IEEE Communications Magazine*, pp. 70–81, 1996.

[16] R. Vaughan and J. B. Andersen, *Channels, Propagation and Antennas for Mobile Communications.* The Institution of Electrical Engineers (IEE), 2003.

[17] A. Ridolfi, "Power spectra of random spikes and related complex signals," PhD thesis, École Polytechnique Fédérale de Lausanne (EPFL), Switzerland, 2004.

[18] R. F. Brøndum and E. Rubak, "Stochastic channel modelling - a bayesian approach using reversible jump markov chain monte carlo methods," Master's thesis, Aalborg University, Denmark, 2006.

[19] K. Hao, "Modeling and statistical analysis of ultra-wideband (UWB) channels and systems: A point-process approach," PhD thesis, University of Wisconsin-Madison, USA, 2006.

[20] M. Haenggi, J. G. Andrews, F. Baccelli, O. Dousse and M. Franceschetti, "Stochastic geometry and random graphs for the analysis and design of wireless networks," *IEEE Journal on Selected Areas in Communications*, vol. 27, no. 7, pp. 1029–1046, 2009.

[21] S. O. Rice, "Mathematical analysis of random noise," *Bell System Technical Journal*, vol. 23, pp. 282–332, 1944.

[22] ——, "Mathematical analysis of random noise (continued)," *Bell System Technical Journal*, vol. 24, pp. 46–156, 1945.

[23] L. Zadeh, "The determination of the impulsive response of variable networks," *Journal of Applied Physics*, vol. 21, pp. 642–645, 1950.

[24] ——, "Frequency analysis of variable networks," *Proceedings of IRE*, vol. 38, pp. 291–299, 1950.

[25] R. H. Clarke, "A statistical theory of mobile-radio reception," *Bell System Technical Journal*, pp. 957–1000, 1968.

[26] G. Matz, "Characterization of non-WSSUS fading dispersive channels," *IEEE International Conference on Communications*, pp. 2480–2484, 2003.

[27] ——, "On non-WSSUS wireless fading channels," *IEEE Transactions on Wireless Communications*, vol. 4, no. 5, pp. 2465–2478, 2005.

[28] J. D. Parsons, *The Mobile Radio Propagation Channel*, 2nd ed. John Wiley & Sons, Ltd., 2000.

[29] M. Pätzold, *Mobile Fading Channels.* John Wiley & Sons, Ltd., 2002.

[30] A. Goldsmith, *Wireless Communications.* Cambridge University Press, 2005.

[31] W. C. Jakes, *Microwave Mobile Communications.* John Wiley & Sons, Inc., 1974.

[32] T. Aulin, "A modified model for the fading signal at a mobile radio channel," *IEEE Transactions on Vehicular Technology*, vol. 28, no. 3, pp. 182–203, 1979.

[33] H. Hashemi, "Impulse response modeling of indoor radio propagation channels," *IEEE Journal on Selected Areas in Communications*, vol. 11, no. 7, pp. 967–978, 1993.

[34] ——, "The indoor radio propagation channel," *Proceedings of the IEEE*, vol. 81, no. 7, pp. 943–968, 1993.

[35] G. L. Turin, F. D. Clapp, T. L. Johnston, S. B. Fine, and D. Lavry, "A statistical model of urban multipath propagation," *IEEE Transactions on Vehicular Technologies*, vol. 21, no. 1, pp. 1–9, 1972.

[36] D. R. Cox and V. Isham, *Point Processes.* Chapman & Hall, 1980.

[37] J. F. C. Kingman, *Poisson Processes.* Oxford University Press, 1993.

[38] H. Suzuki, "A statistical model for urban radio propagation," *IEEE Transactions on Communications*, vol. 25, no. 7, pp. 673–680, 1977.

[39] D. L. Snyder and M. I. Miller, *Random Point Processes in Time and Space.* Springer, 1991.

[40] H. Suzuki, "A statistical model for urban radio propagation," PhD thesis, University of California, Berkeley, 1975.

[41] A. A. M. Saleh and R. A. Valenzuela, "A statistical model for indoor multipath propagation," *IEEE Journal on Selected Areas in Communications*, vol. 5, no. 2, pp. 128–137, 1987.

[42] B. H. Fleury, "An uncertainty relation for WSS processes and its application to WSSUS systems," *IEEE Transactions on Communications*, vol. 44, no. 12, pp. 1632–1634, 1996.

[43] J. Møller and R. P. Waagepetersen, *Statistical Inference and Simulation for Spatial Point Processes.* Chapman & Hall/CRC, 2004.

[44] A. J. Baddeley, *Spatial Point Processes and their Applications.* (in "Stochastic Geometry - Lecture Notes in Mathematics"), Springer, 2007.

[45] Y. (G.) Li, L. J. Cimini, Jr. and N. R. Sollenberger, "Robust channel estimation for OFDM systems with rapid dispersive fading channels," *IEEE Transactions on Communications*, vol. 46, no. 7, pp. 902–915, 1998.

[46] E. Biglieri, J. Proakis and S. Shamai (Shitz), "Fading channels: Information-theoretic and communications aspects," *IEEE Transactions on Information Theory*, vol. 44, no. 6, pp. 2619–2692, 1998.

[47] A. F. Molisch, *Wireless Communications*. John Wiley & Sons, Ltd., 2005.

[48] J. Karedal, F. Tufvesson, N. Czink, A. Paier, C. Dumard, T. Zemen, C. F. Mecklenbräuker and A. F. Molisch, "A geometry-based stochastic mimo model for vehicle-to-vehicle communications," *IEEE Transactions on Wireless Communications*, vol. 8, no. 7, pp. 3646–3657, 2009.

[49] H. Iwai and Y. Karasawa, "Wideband propagation model for the analysis of the effect of the multipath fading on the near-far problem in CDMA mobile radio systems," *IEICE Transactions on Communications*, vol. E76-B, no. 2, pp. 103–112, 1993.

[50] B. H. Fleury, U. P. Bernhard and R. Heddergott, "Advanced radio channel model for magic WAND," *ACTS Mobile Telecommunications Summit*, pp. 600–607, 1996.

[51] T. Zwick, C. Fischer and W. Wiesbeck, "A stochastic multipath channel model including path directions for indoor environments," *IEEE Journal on Selected Areas in Communications*, vol. 20, no. 6, pp. 1178–1192, 2002.

[52] S. J. Papantoniou, "Modelling the mobile radio channel," PhD thesis, Eidgeössische Technische Hochschule Zürich (ETHZ), Switzerland, 1990.

[53] J. A. Gubner, B. N. Bhaskar and K. Hao, "Multipath-cluster channel models," *IEEE International Conference on UWB*, pp. 292–296, 2012.

[54] M. Haardt and J. A. Nossek, "Unitary esprit: How to obtain increased estimation accuracy with a reduced computational burden," *IEEE Transactions on Signal Processing*, vol. 43, no. 5, pp. 1232–1242, 1995.

Part II

Appendices

Appendix/Paper A

Analysis of Stochastic Radio Channels with Temporal
Birth-Death Dynamics: A Marked Spatial Point Process
Perspective

Morten Lomholt Jakobsen, Troels Pedersen and Bernard Henri Fleury

Abstract

We employ the theory of spatial point processes to revisit and reinterpret a well-known class of time-variant stochastic radio channel models. Common for all models in this class is that individual multipath components are emerging and vanishing in a temporal birth-death alike manner, with the stochastic birth-death mechanism governed by two facilitating assumptions. Well-known analytical properties of this class of channel models are reestablished by simple arguments and several new results are derived. The primary tool used to obtain these results is Campbell's Theorem which for example enables novel assessment of the autocorrelation functions of random processes used in the general channel model description. Under facilitating assumptions the channel transfer function is shown to be wide-sense stationary in both time and frequency (despite the birth-death behavior of the individual multipath components). This identification is a direct result of the point process perspective and its inherent ability to circumvent cumbersome enumeration issues in traditional channel modeling approaches. Furthermore, the practical importance of being able to analytically characterize the temporal birth-death channel models is clearly evidenced since key parameters enter explicitly in measurable quantities such as the power-delay profile.

1   Introduction

In the historical development of *time-invariant* stochastic radio channel models still being favored nowadays, the first use of *point processes* can be traced back to the seminal work by Turin [1, 2]. Specifically, Turin suggested to model the occurrences of multipath delay components via a one-dimensional (possibly *inhomogeneous*) Poisson point process. One-dimensional point processes were similarly involved in the later developments by Suzuki [3] and Hashemi [4], namely as a convenient tool for modeling and simulation. Despite a pronounced use for the *modeling* of stochastic radio channels, neither point processes nor their underlying theoretical framework have been favored as tools for *analysis*. This trend clearly maintains in the popular contribution by Saleh and Valenzuela [5] as well as in the more recent extension by Spencer et al. [6]. Essentially, point processes are employed only in the channel model specifications whereas tools from the underlying theory have not been used for analytical characterizations. In fact, this trend is present also for certain *time-variant* channel models, see [7–10]. Part of the reason for this surprising trend is most likely attributed to scientific tradition and to the scarce proportion of readily accessible, engineering targeted literature on point processes around the time of Turin's initial work. The textbook by Snyder [11] is one of the earliest of its kind, targeted towards engineers, and covering numerous examples and application areas. However, the engineering targeted exposition in [11] (or its successor [12]) does not appear to have fully convinced the channel modeling

community to also start analyzing their models using the variety of well-established tools from the theory of point processes.

Recently, the theoretical framework of *spatial*[1] *point processes* has revealed itself an adequate tool for the analytical characterization of various stochastic radio channel models, see e.g. [13–17]. In [13], a point process approach has been employed to derive and analyze a non-stationary *geometric-stochastic* propagation model applicable within satellite-to-vehicle communications. The well-known impulse response model by Saleh and Valenzuela [5] and more recent variations of it [6] have been analyzed in [14–16] with new and detailed insight gained in direct consequence of the point process perspective. *Campbell's Theorem*, a standard tool from the theory of spatial point processes, has proven itself instrumental for achieving both well-known and new results via concise and rigorous arguments, e.g. as in [13] and [15].

Time- and space-varying multipath propagation phenomenons, such as path components which emerge and vanish again, occur due to movements of the communicating entities and the surrounding scatterers [18, 19]. To imitate such a phenomenon, the following two tractable assumptions have been invoked several times in the channel modeling literature:

- i) **Stationary emergences:** The collection of time instances where new path components emerge forms a stationary point process on the real line.

    [†] (Facilitating special-case: Poisson point process).

- ii) **i.i.d. lifetimes:** The lifetimes of individual path components are drawn independently and identically distributed.

    [†] (Facilitating special-case: Exponential distribution).

The earliest appearance of i)[†] and ii)[†] is in [7] but these two special-case assumptions have re-entered in several later contributions, e.g. [8–10]. Under the assumptions i)[†] and ii)[†], the instantaneous number of path components in the channel is a Poisson distributed random variable (with known mean parameter). This property is justified in [7] by reference to standard results from *queuing theory*. Basically, the random process governing the time-varying number of path components in the channel can be identified as an $M/M/\infty$ queue [20, Sec. 16-2]. This observation also appears elsewhere in literature, see e.g. [10, Sec. III-C], where the construct via i)[†] and ii)[†] is identified as a *birth-death process* or, in different terminology, as a *marked Poisson process*. Analytical benefits and additional insight can often be gained from such structural identifications, e.g. as in [15] and [16] via the point process perspectives. Surprisingly, the promising potential of the available theory of marked spatial point processes does not seem to

---

[1]When prepending the term "spatial" we refer to point processes in two dimensions or more. The essential distinction compared to one-dimensional point processes is the inherent absence of a natural ordering of the points.

have been exploited so far in literature on time-variant radio channel models. Yet, we emphasize that spatial point processes have already been successfully utilized in highly related areas of research, namely, for the design and analysis of *wireless networks*, see [21] and the extensive list of references therein.

In the present contribution we analyze the class of time-variant stochastic radio channel models which is based on the more general assumptions *i*) and *ii*) in contrast to the facilitating special-cases *i*)† and *ii*)†. Random processes essential for radio channel characterization are constructed from underlying spatial point processes and straightforward use of Campbell's Theorem facilitates novel analytical assessment of the associated autocorrelation functions. A key feature of the point process perspective is its natural ability to circumvent enumeration issues arising in traditional modeling approaches. Our first main contribution is an extensive analysis of the temporal birth-death mechanism induced from the assumptions *i*) and *ii*). We relate our analysis to the results already obtained in the literature regarding the special-cases *i*)† and *ii*)†. Secondly, we derive a novel and general expression for the *time-frequency correlation function* associated with the class of temporal birth-death channel models. From example cases we illustrate how a particular channel model can be readily extended by including additional marks in the point process construction. We show as well how the point process perspective offers crucial insight for the task of simulating channel realizations with temporal birth-death dynamics. Overall, our contributions are together comprised by the point process formulations and the analytical characterizations induced thereof. Our approach relies in a consistent way on simple arguments and standard results from the theory of spatial point processes. In particular, Campbell's Theorem repeatedly reveals itself a highly useful and easily applicable tool.

The paper is organized as follows. Sec. 2 provides the necessary background information on the class of temporal birth-death channel models with an overview of previous approaches and contributions. We then present a concise but self-contained introduction to the basics of spatial point processes in Sec. 3. Subsequently, we initiate our investigations of the class of time-variant channel models by analyzing and characterizing the temporal birth-death process in Sec. 4. We continue in Sec. 5 with an exhaustive analysis of the channel's time-frequency correlation function. Sec. 6 provides a selection of illustrative examples on how the channel model can be modified and extended together with details on its simulation aspects. Finally, we draw our conclusions in Sec. 6.

2   Radio Channel Models with Temporal Birth-Death Dynamics

The class of stochastic radio channel models under consideration is governed by the assumptions *i*) and *ii*) in Sec. 1. Common to the approaches [7–10] is that they essentially all propose to incorporate a time-varying multipath *channel impulse response* of

the form[2]

$$h(t,\tau) = \sum_{\ell=1}^{L(t)} \alpha_\ell(t) \delta\big(\tau - \tau_\ell(t)\big), \tag{A.1}$$

where $L(t)$ is the number of path components at time t, $\alpha_\ell(t)$ is the complex-valued gain of the ℓ'th path component, $\tau_\ell(t)$ is the associated propagation delay, and $\delta(\cdot)$ is the Dirac delta. The time-varying *channel transfer function* corresponding to (A.1) reads

$$H(t,f) = \sum_{\ell=1}^{L(t)} \alpha_\ell(t) \exp\big(-j2\pi f \tau_\ell(t)\big). \tag{A.2}$$

The above two expressions or slight variations thereof are standard in the channel modeling literature [18, 19]. The special-case which has attracted most attention is when $L(t) = L$ is constant (deterministic or random) within each realization of the channel. That is, numerous traditional channel modeling approaches are disregarding the case when the number of path components is allowed to vary *within* each channel realization. However, the channel models considered in [7–10] all incorporate a temporal birth-death feature via the integer-valued random process[3] $L(\cdot)$. Specifically, the transition times of $L(\cdot)$ are to be generated according to $i)$ and $ii)$ in Sec. 1, but common to the contributions [7–10] is that they all specialize exclusively to the cases $i)^\dagger$ and $ii)^\dagger$.

In [7] each amplitude $|\alpha_\ell|$ is constant with time and the amplitudes of emerging components are drawn i.i.d. according to a log-normal distribution. Hence, the conditional second moment of $|\alpha_\ell|$ does *not* depend on the associated propagation delay τ_ℓ. From narrowband considerations the propagation delays are also modeled to be constant with time and they are drawn i.i.d. from a uniform distribution.

The modeling in [9] is inspired by [7]. However, the amplitudes $|\alpha_\ell(t)|$ are now varying with time and to ensure smooth transitions when birth-death events occur, a sequence of root-raised cosine functions are incorporated in a multiplicative manner. Each propagation delay $\tau_\ell(t)$ is varying with time as a function of the receiver's position in space and as a function of a random *initial delay* (the propagation delay when a path emerges). The *power-delay profile* is targeted to exhibit an overall exponential decay. See [22] for further details.

In [8] each time-varying amplitude $|\alpha_\ell(t)|$ is smoothened using the non-negative part of an ordinary sine function. The sine is stretched in time to match the individual lifetimes and $|\alpha_\ell(t)|$ is scaled such that its conditional second moment depends on $\tau_\ell(t)$ in

---

[2]In fact [7–10] rely on a *space-varying* approach which subsequently can be converted into a time-varying equivalent by appropriately assuming a receiver trajectory (most often a straight line in space). Furthermore, [7] and [10] are both modeling the *line-of-sight* component via a separate stochastic mechanism which alternates between being active and inactive.

[3]By $L(\cdot)$ we refer to the entire random process while with $L(t)$ we indicate that the time instance t is fixed. Hence, $L(t)$ is a random variable.

an exponentially decaying manner. Each propagation delay $\tau_\ell(t)$ is varying as a function of the receiver's position together with an initial delay drawn from an exponential distribution. From this construction the power-delay profile appears to exhibit an overall exponential decay, but the sine smoothing and the average number of path components are both disregarded in the calculations.

The modeling in [10] is inspired by [8] and each path component is characterized by a transfer matrix (polarization, antenna characteristics, etc.) together with a propagation delay and directions of departure and arrival. Hence, the channel model in [10] accounts for small-scale fading, large-scale fading and polarization aspects. A key aspect is the modeling of path directions which are found to be Laplacian distributed for smaller propagation delays followed by migration into a uniform distribution for larger delays. For the purpose of computer simulation, a number of guidelines are proposed for controlling, initializing and time-discretizing the temporal birth-death mechanism.

2.1 Consequences of Temporal Birth-Death Dynamics

As just indicated, the individual contributions [7–10] rely on different assumptions on the path gains, propagation delays, incidence directions, and so on. The approaches, methodologies and techniques in use are rather distinct in general. But common to all approaches seems to be the fact that thorough analytical characterization and assessment of the resulting channel properties have been very difficult to carry out. Computer simulation does not adequately provide the desired insight and is often not tractable either – especially not when the number of overall model parameters grows as large as in [10].

The essential part of the analytical challenge lies in the birth-death behavior of the random process $L(\cdot)$ controlling the time-varying number of path components. Conceptually, the random process $L(\cdot)$ may appear straightforward to handle and despite the simplicity of the assumptions $i)$ and $ii)$, difficulties quickly arise in the attempt to compute correlation quantities such as $\mathbb{E}[L(t)L(t')]$ or $\mathbb{E}[H^*(t,f)H(t',f')]$, where $\mathbb{E}[\cdot]$ denotes expectation and $(\cdot)^*$ denotes complex conjugation. The difficulties emerge since for distinct time instances t and t', the integers $L(t)$ and $L(t')$ are not necessarily referring to the same path components anymore (glimpse at Fig. A.4 on page 62). Such enumeration issues occur in (A.1) and (A.2) whenever the random process $L(\cdot)$ experiences a transition. The immediate consequence is that re-enumeration via the integer index ℓ or other means of cumbersome bookkeeping is needed over and over again. Overall, the different issues emerging as a consequence of the temporal birth-death behavior of $L(\cdot)$ are reported in various degrees of detail in [7–10].

Fortunately, as we shall see in Sec. 4, Sec. 5 and Sec. 6, the numerous analytical and technical difficulties encountered in [7–10] are swiftly circumvented by use of marked spatial point processes. Specifically, we demonstrate in a unifying manner how thorough analytical insight can be obtained by virtue of this well-established mathematical frame-

work. The approach is fully general in the sense that our results apply to any temporal birth-death channel model from the class governed by *i*) and *ii*), in particular to the models in [7–10] which all rely on *i*)† and *ii*)†. However, as knowledge on the basics of spatial point processes will be essential for transparency in the later derivations, we provide in the following a concise, self-contained and engineering targeted introduction to this mathematical framework.

3   Spatial Point Processes

A *spatial point process* [12, 23–26] is a random *countable* collection Y of points sitting in d-dimensional Euclidian space S (either $\mathbb{R}^d$ or a subset of it). The term "spatial" is used here to stress the fact that d is larger than one, but the term is often skipped again for the sake of brevity. Since the peculiar ordering property of the real line obscures the overall theory, the reader is encouraged [24] to always think of the two-dimensional ($d = 2$) case, see Fig. A.1.

For reasons of practical applicability and simplicity it is convenient to restrict attention to the class of *locally finite* and *simple* point processes. Here, locally finite means that only a *finite* number of points are falling in every *bounded* region $B \subset \mathbb{R}^d$. Furthermore, the term "simple" indicates that no two points of the process coincide. Both conditions are to be satisfied with probability one. As no two points from Y coincide, each individual realization of Y can be identified as a countable set of points $\{\boldsymbol{y}_1, \boldsymbol{y}_2, \boldsymbol{y}_3, \ldots\}$, $\boldsymbol{y}_i \in S$. The counting index i on $\boldsymbol{y}_i$ is used here only to distinguish individual points and to indicate countability. This index does not imply any ordering of the points (recall Fig. A.1) and for this reason we deliberately skip it again.

3.1   Region Counts and the Intensity Function

A natural way of exploring the properties of a point process is to count the number of points falling in different regions [26]. Accordingly, for any set $B \subseteq S$ consider the *region count*

$$N_{_Y}(B) := |Y \cap B| = \sum_{\boldsymbol{y} \in Y} \mathbb{1}[\boldsymbol{y} \in B], \tag{A.3}$$

where $|\cdot|$ denotes set cardinality and $\mathbb{1}[\cdot]$ is a generic *indicator function* taking the value one if the logical statement in brackets is fulfilled and zero otherwise. As suggested by its name, the region count $N_{_Y}(B)$ in (A.3) gives the random number of points from Y falling within the region B. For *fixed* and *bounded* B, the region count $N_{_Y}(B)$ is an ordinary random variable with range $\mathbb{N}_0 := \{0\} \cup \mathbb{N}$. An example illustration was already provided in Fig. A.1. For a general point process Y, the probability distribution of $N_{_Y}(B)$ depends on the region B via its d-dimensional *Lebesgue measure*, shape, location, orientation, and

$N_Y(B) = 3$

$N_Y(B) = 4$
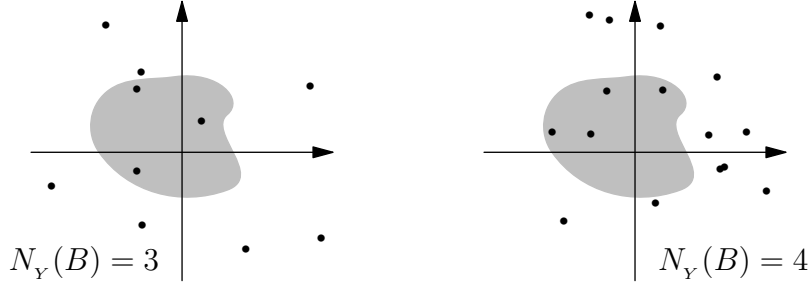
Fig. A.1: A pair of realizations of a two-dimensional point process Y. Notice that the points are not enumerated/ordered and observe that each realization has a different number of points $N_Y(B)$ falling in the gray-shaded region B.

so on. The region B can be very complicated but certain properties of the region counts are easily established. In particular we have $N_Y(\emptyset) = 0$ and also for disjoint regions $A, B \subset S$ it follows that $N_Y(A \cup B) = N_Y(A) + N_Y(B)$. Indeed, various complicated regions can be build up from simpler ones by use of set operations for which the behavior of $N_Y(\cdot)$ is obvious.

By forming the expected value of the region count $\mu_Y(B) := \mathbb{E}[N_Y(B)]$ we induce a *measure* on S, the so-called *intensity measure* of Y. If the intensity measure can be expressed as an integral

$$\mu_Y(B) = \int_B \varrho_Y(\boldsymbol{y})\mathrm{d}\boldsymbol{y}, \tag{A.4}$$

for some *locally integrable* function $\varrho_Y : S \to [0, \infty)$, then $\varrho_Y(\cdot)$ is called the *intensity function* of Y. For virtually all applications of practical relevance the intensity function does exist. If $\varrho_Y(\cdot)$ is constant on S then Y is called a *homogeneous* point process and otherwise Y is said to be *inhomogeneous*. In general, the shape of $\varrho_Y(\cdot)$ indicates where points are more likely to occur. Besides this intuitive feature the intensity function plays an important role for the use of *Campbell's Theorem* [24, Chap. 3], [26, Thm. 2.2]. This powerful and widely applicable theorem states that the identity

$$\mathbb{E}\Big[\sum_{\boldsymbol{y} \in Y} g(\boldsymbol{y})\Big] = \int_S g(\boldsymbol{y})\varrho_Y(\boldsymbol{y})\mathrm{d}\boldsymbol{y} \tag{A.5}$$

holds whenever the integral on the right is well-defined, where $g(\cdot)$ is any real- or complex-valued function defined on S. Campbell's Theorem is particularly useful as it enables straightforward calculation of expected values of scalar random variables of the form

$$\sum_{\boldsymbol{y} \in Y} g(\boldsymbol{y}). \tag{A.6}$$

When dealing with point processes one frequently encounters random variables of the type in (A.6). One example already appeared in (A.3) where $g(\cdot)$ is the indicator function for a region B. As we shall see in Sec. 4 and Sec. 5, the expression in (A.2) can as well be reformulated into a sum indexed by a certain point process like the generic expression in (A.6). This convenient form facilitates analysis via Campbell's Theorem.

3.2 Marked Point Processes

Let Y be a point process on $S \subseteq \mathbb{R}^d$ and consider the procedure of attaching a random label or a *mark* $\boldsymbol{m_y}$ to each point $\boldsymbol{y} \in Y$. These marks can be of very general type but they must all belong to the same space M. By attaching random marks to the points of a point process, several underlying characteristics can be studied in a natural and concise manner [23]. This will be evident in Sec. 4 and Sec. 5.

Definition 1. Let Y be a simple and locally finite point process on $S \subseteq \mathbb{R}^d$ and let M be some space. If a random mark $\boldsymbol{m_y} \in M$ is attached to each point $\boldsymbol{y} \in Y$, then

$$X := \{(\boldsymbol{y}, \boldsymbol{m_y}) : \boldsymbol{y} \in Y\} \tag{A.7}$$

is called a *marked spatial point process* with points in S and marks in M.

By construction, X is a simple and locally finite random subset of $S \times M$. Accordingly, a marked point process X with points in S and marks in M can always be viewed as an *unmarked* point process on $S \times M$. However, the converse is not true since an arbitrary point process cannot always be projected onto a lower dimensional space and viewed as a marked point process. Such a collection of projected points is not necessarily simple nor locally finite.

3.3 Poisson Point Processes

The most fundamental type of spatial point processes is the *Poisson*[4] class:

Definition 2. [25, Def. 3.2] A point process Y on $S \subseteq \mathbb{R}^d$ is called a *Poisson point process* with intensity function $\varrho_Y(\cdot)$ if:

1) For any region $B \subseteq S$ with $\mu_Y(B) = \int_B \varrho_Y(\boldsymbol{s})\mathrm{d}\boldsymbol{s} < \infty$ the region count $N_Y(B)$ is Poisson distributed with mean $\mu_Y(B)$.

---

[4]A highly accessible introduction to Poisson point processes can be found in the book [24] by Kingman. Although not crucial, his approach and choice of presentation is better perceived with some minor knowledge on abstract *measure theory*. In contrast, several other books on spatial point processes require a solid background in measure theory just to get started.

2) Conditioned on the event $N_Y(B) = n \in \mathbb{N}$ such that $0 < \mu_Y(B) < \infty$, the joint distribution of $Y \cap B$ is the same as that of n points drawn i.i.d. according to the probability density function $f_B(\cdot)$, where

$$f_B(\boldsymbol{s}) := \frac{\varrho_Y(\boldsymbol{s})}{\mu_Y(B)} \mathbb{1}[\boldsymbol{s} \in B], \quad \boldsymbol{s} \in S.$$

We write $Y \sim \mathtt{PoissonPP}(S, \varrho_Y)$.

For a Poisson point process the individual region counts are Poisson distributed random variables. Hence the name of the process. Poisson point processes are flexible and mathematically tractable in the sense of their stability with respect to several manipulations [25, Chap. 3], e.g. independent *superposition*, independent *thinning* and independent *displacement*.

A particularly useful property of Poisson point processes arise via the *Marking Theorem* [24, Sec. 5.2], [25, Prop. 3.9]. This theorem states that if mutually independent marks are attached to a Poisson point process, then the distended collection (of points and marks) is again a Poisson point process (in a higher dimensional space) and the associated intensity function is known. Loosely speaking, the Poisson property of the region counts are sustained when blowing up the dimensionality. Notice that mutual independence is the key requirement of the Marking Theorem, i.e. the marks need not be identically distributed, for instance. Notice also that the Marking Theorem does not apply to point processes in general, only to Poisson point processes. This partly explains the facilitating aspect of the assumption $i)^\dagger$ in Sec. 1.

4   Characterization of the Temporal Birth-Death Process $L(t)$

In this section we assess the fundamental properties of the temporal birth-death mechanism associated with the class of time-variant stochastic radio channel models invoking the assumptions $i)$ and $ii)$ from Sec. 1. Our approach is to reformulate and incorporate $i)$ and $ii)$ using a marked point process. This perspective facilitates a convenient definition of the random process $L(\cdot)$ which we briefly introduced in Sec. 2. We show that $L(\cdot)$ is strict-sense stationary and we calculate its mean by use of Campbell's Theorem. Subsequently we extract a partial but crucial share of the second-order properties of $L(\cdot)$, again by application of Campbell's Theorem. Furthermore, we illustrate for the facilitating special-case $i)^\dagger$ how additional insight can be gained from changing perspective. Specifically, via the Marking Theorem for Poisson point processes we swap to a higher dimensional representation and from this new perspective we readily identify that $L(t)$ is Poisson distributed for any fixed $t \in \mathbb{R}$. Finally, we indicate that $i)$ and $ii)$ are essential for preserving analytical tractability of $L(\cdot)$ as even minor relaxation attempts turn $L(\cdot)$ into a non-stationary random process.

4.1   Definition of $L(\cdot)$ Using a Marked Point Process

We begin by setting up a useful notation to incorporate assumption i) from Sec. 1. We introduce Y to represent the one-dimensional *stationary*[5] point process describing the time instances where new path components emerge. For instance, Y could be a Poisson point process, a *renewal* point process [12, Chap. 6], a *Cox* point process [25, Chap. 5], and so on. A stationary point process is necessarily homogeneous [26, Cor. 1], and so we introduce the intensity function $\varrho_Y(\cdot)$ of Y such that $\varrho_Y(y) = \lambda_e$ is constant for all $y \in \mathbb{R}$. The subscript on the positive constant λ_e is used to abbreviate the term "emerge".

Secondly, we need to incorporate assumption ii) from Sec. 1. To allocate the *period* (or lifetime) of each path component, a random non-negative mark p_y is attached to each element $y \in Y$ (lifetimes are necessarily non-negative). The letter p is used to emphasize the interpretation of each mark as a "period" while the subscript y on p_y serves as a *unique* identifier for its underlying point (with probability one). Hence, instead of a traditional integer-index looping across $\mathbb{N}$, the countable collection of periods $\{p_y : y \in Y\}$ is now *indexed using the points from* Y. The periods are drawn i.i.d. according to some probability density function $f_{\text{period}}(\cdot)$ with non-negative support and finite first-order moment

$$\mathbb{E}[p_y] = \mathbb{E}[p_\star] = \int_0^\infty p f_{\text{period}}(p)\mathrm{d}p. \tag{A.8}$$

In (A.8) we use the wildcard notation $\mathbb{E}[p_\star]$ to denote the mean of a "typical/arbitrary" mark $p_\star$ (as they are all drawn i.i.d.). By construction, the random collection

$$X := \{(y, p_y) : y \in Y\} \tag{A.9}$$

is a marked point process on $\mathbb{R} \times \mathbb{R}_+$ with points in $\mathbb{R}$ and marks in $\mathbb{R}_+$. This marked point process is analytically convenient as it allows directly for random variables of type (A.6) to be established. Furthermore, we shall often find it convenient to also change our view upon X. Sometimes we view it as a marked point process and sometimes as an unmarked point process in two-dimensional space (which being more attractive depends on context).

By use of the random collection X in (A.9), the number of "active" path components at time t can now be formulated as

$$L(t) := \sum_{y \in Y} \mathbb{1}[y < t]\,\mathbb{1}[y + p_y > t], \quad t \in \mathbb{R}. \tag{A.10}$$

An arbitrary component (y, p_y) from (A.9) contributes to the value of the sum in (A.10) only if it *emerges before* and *vanishes after* time t (incorporated by the product of the

---

[5]In the sense of spatial point processes which similarly to ordinary random processes means that all distributional properties are preserved under arbitrary fixed translations [26, Def. 1.7].

two indicator functions). Obviously, $L(\cdot)$ as defined by (A.10) is a continuous-time random process with range $\mathbb{N}_0$ (once more glimpse at Fig. A.4 on page 62).

As an immediate consequence of i) and ii), we show in Appendix 7 that the random process $L(\cdot)$ is *strict-sense stationary*. Intuitively, this is also to be expected since the underlying point process Y is stationary and since the marks/periods attached to it are mutually independent and identically distributed. By strict-sense stationarity, $L(\cdot)$ is also *wide-sense stationary* which means that $\mathbb{E}[L(t)]$ does not depend on t and $\mathbb{E}[L(t)L(t')]$ depends on $t' - t$ only.

4.2 First- And Second-Order Properties of $L(\cdot)$

Using Campbell's Theorem we can readily compute the mean of $L(\cdot)$ as follows:

$$
\begin{aligned}
\mathbb{E}[L(t)] &= \mathbb{E}\big[\mathbb{E}[L(t)\,|\,Y]\big] \\
&= \mathbb{E}\Big[\sum_{y \in Y} \mathbb{1}[y < t]\,\mathbb{E}\big[\mathbb{1}[y + p_y > t]|Y\big]\Big] \\
&= \mathbb{E}\Big[\sum_{y \in Y} \underbrace{\mathbb{1}[y < t]\mathrm{Pr}(p_y > t - y\,|\,y)}_{g(y;t)}\Big]. \\
&= \int_{\mathbb{R}} g(y;t)\varrho_Y(y)\mathrm{d}y \qquad \text{(Campbell's Theorem)} \\
&= \int_{-\infty}^{t} \mathrm{Pr}(p_y > t - y)\lambda_{\mathrm{e}}\mathrm{d}y.
\end{aligned}
\tag{A.11}
$$

Performing the variable substitution $\xi := t - y$ yields

$$
\mathbb{E}[L(t)] = \lambda_{\mathrm{e}} \int_0^{\infty} \mathrm{Pr}(p_{t-\xi} > \xi)\mathrm{d}\xi = \lambda_{\mathrm{e}}\mathbb{E}[p_\star],
\tag{A.12}
$$

i.e. the mean $\mathbb{E}[L(t)]$ does not depend on t, in accordance with $L(\cdot)$ being strict-sense stationary. Readers familiar with queueing theory will recognize the final expression in (A.12) to be consistent with well-known results for the $M/G/\infty$ queue [20, Sec. 16-2], [23, Sec. 5.6 (iii)], i.e. when specializing i) to the case i)†.

The interpretation of (A.12) is in fact rather intuitive: The average number of path components in the channel is governed by the *rate* (λ_{e}) at which new components emerge, together with the *inverse rate* ($\mathbb{E}[p_\star]$) at which they vanish again. The mean $\mathbb{E}[L(t)]$ is *not* affected by the exact shape of the probability density function $f_{\mathrm{period}}(\cdot)$ shared by all the marks. Only the first-order moment $\mathbb{E}[p_\star]$ matters.

By strict-sense stationarity we know that the autocorrelation function $\mathbb{E}[L(t)L(t')]$ will depend only on the time difference $t' - t$. To obtain further insight we introduce and split the autocorrelation function as

$$
R_L(t, t') := \mathbb{E}[L(t)L(t')] = \mathbb{E}[(\diamond_1)] + \mathbb{E}[(\diamond_2)],
\tag{A.13}
$$

with the definitions

$$(\diamond_1) := \sum_{y \in Y} \mathbb{1}[y < \min\{t, t'\}, \ y + p_y > \max\{t, t'\}] \tag{A.14}$$

$$(\diamond_2) := \sum_{y, \widetilde{y} \in Y}^{\neq} \mathbb{1}[y < t, \ y + p_y > t]\mathbb{1}[\widetilde{y} < t', \ \widetilde{y} + p_{\widetilde{y}} > t'].$$

The splitting in (A.13) reflects a deliberate choice as the first quantity $(\diamond_1)$ gives the random number of terms (y, p_y) from (A.9) contributing *jointly* to both $L(t)$ and $L(t')$. The mean of $(\diamond_1)$ is readily assessed by the same manipulations as those leading to (A.11), in particular Campbell's Theorem, such that

$$\mathbb{E}[(\diamond_1)] = \mathbb{E}\big[\mathbb{E}[(\diamond_1)|Y]\big] = \lambda_{\mathrm{e}} \int_{|t'-t|}^{\infty} \Pr(p_\star > \xi)\mathrm{d}\xi \tag{A.15}$$

with $|t' - t| = \max\{t, t'\} - \min\{t, t'\}$.

The second quantity $(\diamond_2)$ is not as easily handled as $(\diamond_1)$ and its interpretation is also not as straightforward (the symbol $\neq$ above the summation in $(\diamond_2)$ is used to indicate that the sum is taken over pairwise distinct points y and $\tilde{y}$). Calculating the mean of $(\diamond_2)$ is indeed possible but at the same time also more involved as it requires to know the statistical properties on joint occurrences of points from Y. In general, such knowledge is not available through the intensity function of Y. On the other hand, this information is contained in a function sometimes called the *second-order product density* [25, Def. 4.3] or the *second moment density* [26, Def. 2.5]. In the sequel we calculate for illustration purposes the mean of $(\diamond_2)$ for the tractable special-case $i)^\dagger$.

As expected, the quantity in (A.15) depends only on the time difference $\Delta t := t' - t$, and not on the specific time instances t and t' (by strict-sense stationarity). In general, without having calculated $\mathbb{E}[(\diamond_2)]$, we know that this quantity can also at most be a function of Δt. Opposite to the mean $\mathbb{E}[L(t)]$ in (A.12) which is affected only by the first-order moment of $f_{\mathrm{period}}(\cdot)$, the exact shape of this probability density function affects directly the autocorrelation function $\mathbb{E}[L(t)L(t')]$ in (A.13). As will be shown in Sec. 5, the quantity in (A.15) plays a crucial role as it influences the *time-frequency correlation function* of the channel. To the contrary, the quantity $\mathbb{E}[(\diamond_2)]$ does not and so indicates the main reason why we do not insist on calculating this particular term.

To the best of our knowledge, equally concise and rigorous derivations of the results (A.12) and (A.15) have not appeared elsewhere in literature. The novelty here is that our conclusions are valid for the general assumptions $i)$ and $ii)$ and that our observations emerge as a concise and direct result of the point process perspective, in particular, as a result of using Campbell's Theorem.

4.3   The Poisson Special-Case $i)^{\dagger}$

In the following we specialize $i)$ to the facilitating case $i)^{\dagger}$ and view the marked point process in (A.9) from a new perspective. Specifically, since we now have (see Sec. 3.3)

$$Y \sim \texttt{PoissonPP}(\mathbb{R}, \varrho_{Y}), \qquad \varrho_{Y}(y) = \lambda_{\mathrm{e}}, \ y \in \mathbb{R},$$

we can directly employ the Marking Theorem and swap to a higher dimensional point process representation. Due to $ii)$, the marks $\{p_y : y \in Y\}$ are mutually independent and each individual period p_y does not depend on $Y \backslash \{y\}$. Then, by the Marking Theorem [25, Prop. 3.9], it follows that the marked collection X in (A.9) is itself a Poisson point process, namely

$$X \sim \texttt{PoissonPP}(\mathbb{R} \times \mathbb{R}_{+}, \varrho_{X}).$$

The associated intensity function $\varrho_{X}(\cdot)$ reads [25, Prop. 3.9]

$$\varrho_{X}(\boldsymbol{x}) = \varrho_{Y}(y) f_{\mathrm{period}}(p), \qquad \boldsymbol{x} = (y, p). \tag{A.16}$$

To ease the notation it is often convenient to drop the index y on p_y as we just did. We simply think of each $\boldsymbol{x} \in X$ as a two-dimensional point (y, p) and not as a one-dimensional point with a mark attached. Notice that neither $\varrho_{Y}(\cdot)$ nor $f_{\mathrm{period}}(\cdot)$ depends on y. Hence, the intensity function $\varrho_{X}(\cdot)$ varies only with its second argument p via the shape of $f_{\mathrm{period}}(\cdot)$.

In view of this new, two-dimensional perspective it is a straightforward exercise to see that $L(t)$ is Poisson distributed for any fixed $t \in \mathbb{R}$. In fact, $L(t)$ as defined in (A.10) can now beneficially be recognized as a region count associated with the point process X. The exact region in question must necessarily be indexed by time t and from inspection of the two indicator functions in (A.10) we "mechanically" define

$$B_t := \{(y, p) : y < t, \ y + p > t\} \subset \mathbb{R} \times \mathbb{R}_{+}. \tag{A.17}$$

With this definition of the region B_t it follows that $L(t)$ as defined in (A.10) coincides directly with the number of points from X falling within B_t, i.e. (see also Fig. A.2)

$$L(t) = N_{X}(B_t), \quad t \in \mathbb{R}. \tag{A.18}$$

Since X is a Poisson point process the region count $N_{X}(B_t)$ is a Poisson distributed random variable. By the equality in (A.18) it follows immediately that $L(t)$ is Poisson distributed. Notice the simplicity of this crucial argument and notice how it relates naturally to the point process framework. In particular, no results from queuing theory were needed as compared to the approach in [7].

Under the facilitating assumption $i)^{\dagger}$, we have now shown that the strict-sense stationary random process $L(\cdot)$ has Poisson distributed marginals, i.e. the random variable
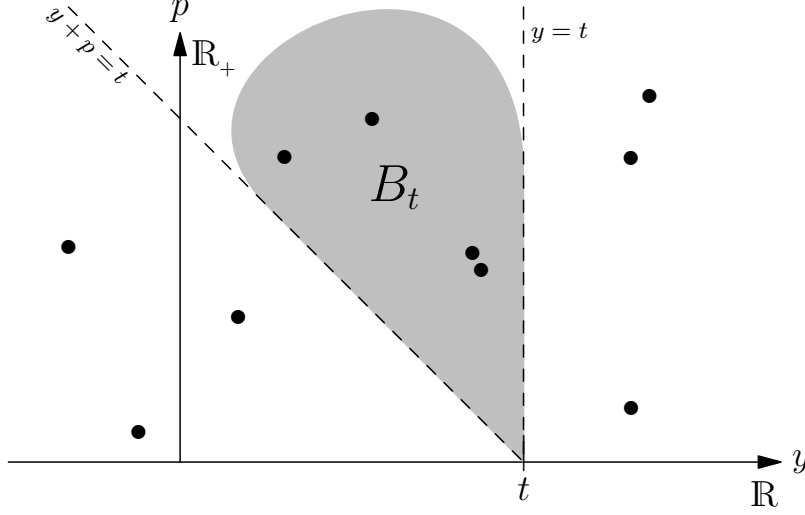
Fig. A.2: The region $B_t \subset \mathbb{R} \times \mathbb{R}_+$ for arbitrary $t \in \mathbb{R}$ with black bullets representing points from X. Points falling within B_t indicate path components which are *active* in the radio channel at time t, i.e. $L(t) = N_X(B_t)$. Notice that the collection of points from X contributing jointly to both $L(t)$ and $L(t')$ are exactly those falling in the region $B_t \cap B_{t'}$.

$L(t)$ is *Poisson distributed* for any fixed t. For the general case i), the marginal distribution of $L(t)$ depends crucially on the exact type of point process we assume for Y. In particular, the distribution of $L(t) = N_X(B_t)$ depends on the properties inherited by the marked collection X when viewed as a two-dimensional point process. In the facilitating special-case i)† both Y and X are Poisson point processes, but in the general case no such exceptional circumstances enter. The equality in (A.18) is of course valid in the general case but without knowledge on the distribution of the region counts for X, this two-dimensional perspective does (in principle) not lead to any further insight. Yet, in the general case we have calculated in (A.12) the mean $\mathbb{E}[L(t)]$ by use of Campbell's Theorem. It is nonetheless surprisingly informative to reconsider the steps leading to (A.12) in the light of our two-dimensional perspective when X is of Poisson type. Specifically, the mean of the region count $N_X(B_t)$, and hence the mean of $L(t)$, is given by the value of the associated intensity measure at B_t, namely as (recall the general relationship in (A.4))

$$\mu_X(B_t) = \int_{B_t} \varrho_X(\boldsymbol{x})\mathrm{d}\boldsymbol{x} = \lambda_e \int_0^\infty p f_{\text{period}}(p)\mathrm{d}p = \lambda_e \mathbb{E}[p_\star].$$

The above step is natural in the sense that is it "dictated" by the point process framework (to get the intensity measure just integrate the intensity function). In particular,

we did not even make use of Campbell's Theorem as opposed to the more involved steps leading to $(A.12)^6$.

Another immediate analytical benefit of Y and X being Poisson point processes is that we can readily calculate the cumbersome autocorrelation term $\mathbb{E}[(\diamond_2)]$ from $(A.13)$. Specifically, since Y is a Poisson point process, special-case use of Campbell's Theorem yields [25, Prop. 4.1]

$$\mathbb{E}[(\diamond_2)] = \mathbb{E}[L(t)]\mathbb{E}[L(t')] = (\lambda_\mathrm{e}\mathbb{E}[p_\star])^2.$$

Hence, under the facilitating assumption $i)^\dagger$ we find the autocorrelation function of $L(\cdot)$ to be

$$R_L(t,t') = \mathbb{E}[(\diamond_1)] + \mathbb{E}[(\diamond_2)]$$
$$= \lambda_\mathrm{e} \int_{|\Delta t|}^{\infty} \Pr(p_\star > \xi)\mathrm{d}\xi + (\lambda_\mathrm{e}\mathbb{E}[p_\star])^2. \qquad (A.19)$$

Notice by evaluating $(A.19)$ at $\Delta t = 0$, one immediately identifies the well-known property that for a Poisson distributed random variable, the mean and the variance coincide.

Example 1. Assume as in [7–10] that the i.i.d. collection of periods $\{p_y : y \in Y\}$ is generated according to an exponential distribution with mean $\mathbb{E}[p_\star] = 1/\lambda_\mathrm{v}$ (subscript used to abbreviate the term "vanish"). Carrying out the integral in $(A.15)$ then leads to the following special-case form of the autocorrelation function in $(A.19)$:

$$R_L(t,t') = \frac{\lambda_\mathrm{e}}{\lambda_\mathrm{v}} \exp\big(-\lambda_\mathrm{v}|\Delta t|\big) + \Big(\frac{\lambda_\mathrm{e}}{\lambda_\mathrm{v}}\Big)^2.$$

Example 2. For comparison, assume instead a uniform distribution for the periods with the same mean parameter $1/\lambda_\mathrm{v}$. We select the uniform distribution on the interval $[0, \frac{2}{\lambda_\mathrm{v}}]$. In this case the autocorrelation function in $(A.19)$ reads

$$R_L(t,t') = \lambda_\mathrm{e}\Big(\frac{\lambda_\mathrm{v}}{4}|\Delta t|^2 - |\Delta t| + \frac{1}{\lambda_\mathrm{v}}\Big)\mathbb{1}\Big[|\Delta t| \le \frac{2}{\lambda_\mathrm{v}}\Big] + \Big(\frac{\lambda_\mathrm{e}}{\lambda_\mathrm{v}}\Big)^2.$$

As intuitively expected, when the periods are uniformly distributed on the interval $[0, \frac{2}{\lambda_\mathrm{v}}]$, we find that the Poisson distributed random variables $L(t)$ and $L(t')$ are uncorrelated whenever t and t' are displaced further than the overall extent of the interval. □

The result in $(A.19)$ was derived in [23, Sec. 5.6 (iii)] under the facilitating special-case assumption $i)^\dagger$. However, the derivations are more notably involved as [23, Sec. 5.6 (iii)] does not rely on the easy applicability of Campbell's Theorem.

---

[6]This interesting observation is well-aligned with the claim by Kingman in the preface of his book [24], namely that the theory of (Poisson) point processes is more natural and powerful in higher dimensions.

4.4   Relaxing The General Assumptions $i)$ and $ii)$

A compelling motivation for employing the special-case assumptions $i)^\dagger$ and $ii)^\dagger$ is that these together lead to (quoting [7]) *simple mathematics.* As illustrated in the previous subsection, the Poisson assumption $i)^\dagger$ is indeed facilitating for analytical investigations. In Sec. 6.3 we illustrate how $i)^\dagger$ and $ii)^\dagger$ are also particularly convenient from the point of view of computer simulation. The core of the current contribution, however, relies on the more general assumptions $i)$ and $ii)$. An interesting and practically relevant question is whether these general assumptions can be relaxed while preserving the ability to assess and comprehend the analytical properties inherited by $L(\cdot)$. The answer is that relaxations are not to be entirely ruled out, but the resulting constructions tend to grow overly cumbersome.

From the general result in (A.12), one may tend to think that the equation $\mathbb{E}[L(t)] = \lambda_\mathrm{e}\mathbb{E}[p_\star]$ would stay unaffected if we relaxed $i)$ and $ii)$ such that Y would just be homogenous (not stationary) and such that the marks would hold the same mean $\mathbb{E}[p_\star]$ (but not necessarily be identically distributed). Obviously, $L(\cdot)$ would then no longer be strict-sense stationary as all arguments from Appendix 7 would break down. However, $L(\cdot)$ could potentially remain wide-sense stationary. A simple construction inspired from Examples 1 and 2 in the previous subsection suggests that this is not the case.

Example 3. Consider drawing the periods using a threshold procedure at the origin such that

$$p_y \sim f_\mathrm{period}(p) = \begin{cases} \lambda_\mathrm{v}\mathrm{e}^{-\lambda_\mathrm{v}p} & \text{if } y \geq 0, \\ \frac{\lambda_\mathrm{v}}{2}\mathbb{1}[0 \leq p \leq \frac{2}{\lambda_\mathrm{v}}] & \text{if } y < 0. \end{cases} \qquad (A.20)$$

One can then readily check via (A.12) that the particular construction in (A.20) gives rise to a mean function depending on time in such a way that $\mathbb{E}[L(t)] = \frac{\lambda_\mathrm{e}}{\lambda_\mathrm{v}}$ for $t < 0$ and

$$\mathbb{E}[L(t)] = \frac{\lambda_\mathrm{e}}{\lambda_\mathrm{v}}\big(1 - \mathrm{e}^{-\lambda_\mathrm{v}t}\big) + \lambda_\mathrm{e}\Big(\frac{\lambda_\mathrm{v}}{4}t^2 - t + \frac{1}{\lambda_\mathrm{v}}\Big)\mathbb{1}\Big[0 \leq t \leq \frac{2}{\lambda_\mathrm{v}}\Big]$$

for $t \geq 0$ (see Fig. A.3). Hence, the mean $\mathbb{E}[L(t)]$ is clearly affected by the sudden change of the mark distribution as given in (A.20). However, as time progresses the aftereffect of this change in $f_\mathrm{period}(\cdot)$ becomes less and less noticeable (the birth-death mechanism stabilizes again). $\qquad\square$

The example-construction in (A.20) shows that it greatly affects the properties of the temporal birth-death process $L(\cdot)$ when the periods are not identically distributed. The influence of (A.20) on the autocorrelation function $\mathbb{E}[L(t)L(t')]$ is even more complicated than for the mean $\mathbb{E}[L(t)]$. In conclusion, to preserve analytical tractability of the birth-death process $L(\cdot)$, the assumption $ii)$ cannot be relaxed. Assumption $i)$ can be relaxed in the sense of replacing the term "stationary" with "homogeneous", and the resulting birth-death process $L(\cdot)$ will *sometimes* remain wide-sense stationary but examples can readily be constructed where this is not the case.
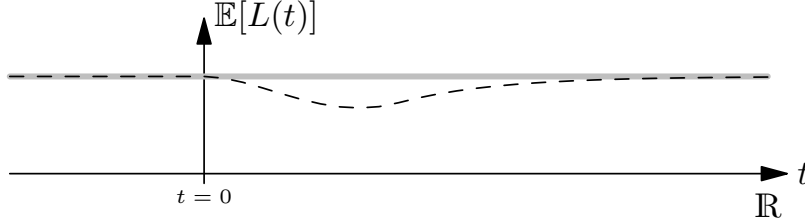
Fig. A.3: The effect of (A.20) upon the mean $\mathbb{E}[L(t)]$ from (A.12) as a result of an attempt to relax the assumptions $i)$ and $ii)$.

5   The Time-Frequency Correlation Function

In this section our goal is to calculate the *time-frequency correlation function*

$$R_H(t, t', f, f') := \mathbb{E}[H^*(t, f)H(t', f')]. \tag{A.21}$$

This function is often considered for radio channel characterization as the information it carries is useful for several reasons [27]. Among others, the time-frequency correlation function reveals if the time-variant channel transfer function $H(\cdot, \cdot)$ in (A.2) is wide-sense stationary (in time, in frequency or in both domains simultaneously). This knowledge is crucial since in practice we typically ask for stochastic models which indeed are wide-sense stationary, mainly to facilitate analytical insight and to simplify our system designs. A frequently recurring example application of the time-frequency correlation function emerges in *linear minimum mean-squared error* channel estimation (see e.g. [28] for an OFDM use case). Wide-sense stationarity of $H(\cdot, \cdot)$ in both time and frequency notably simplifies the design and implementation of such channel estimators. Furthermore, wide-sense stationarity of $H(\cdot, \cdot)$ in frequency allows for inferring on the rate of decay of received power versus propagation delay, namely, to infer on the channel's power-delay profile. Power-delay profiles are crucial to the design of modern positioning and communication systems and such profiles are often estimated in practice using channel sounding measurements.

Calculating the correlation function in (A.21) is conceptually straightforward when the number of path components (deterministic or random) remains fixed within each realization of the channel in (A.2). The traditional procedure is to introduce two separate integer-indices ℓ and k, one for each term in (A.21), and then to pair together those path components for which $\ell = k$. However, in the current time-variant setup we cannot compute (A.21) by traditional means since the temporal birth-death process $L(\cdot)$ is changing without explicit reference to the enumeration of the underlying random quantities (path gains, propagation delays, etc.) describing $H(\cdot, \cdot)$ in (A.2). The overall situation and the enumeration problem are together illustrated in Fig. A.4. Hence, with the considered class of temporal birth-death channel models, we necessarily need to ac-
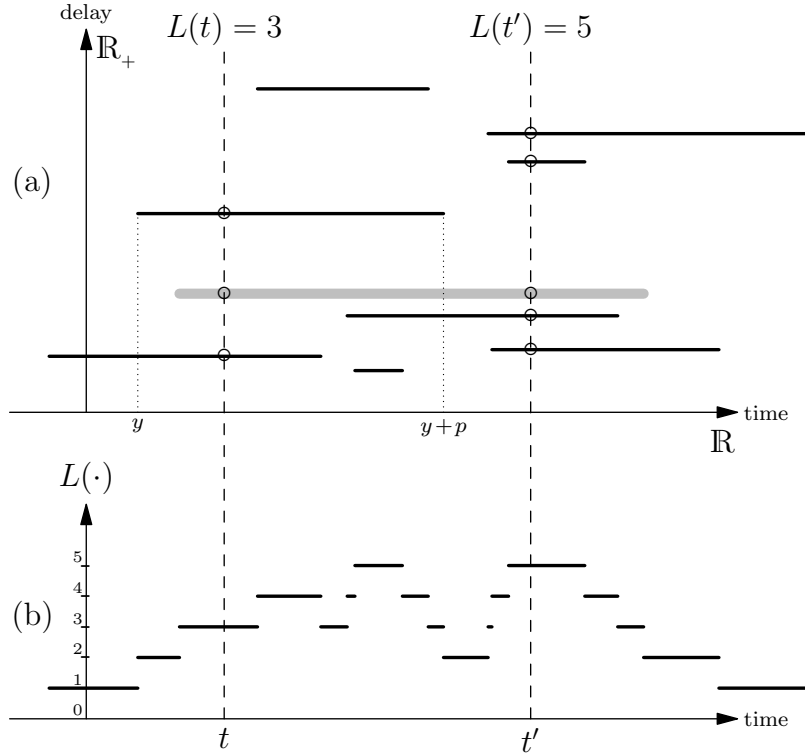
Fig. A.4: Line segments in (a) indicating the time instances of birth-death transition of the random process $L(\cdot)$ in (b). In this particular illustration, notice that only a single path component (thick gray line) contributes jointly to both $L(t)$ and $L(t')$.

count for the enumeration issues. As we shall see in the sequel, the use of marked spatial point processes paves the way and provides at the same time a number of substantial analytical advantages.

5.1 Using the Point Process X to Reformulate the Channel Transfer Function $H(\cdot, \cdot)$

To compute (A.21) we bypass the enumeration problem by adopting our previously introduced point process perspective. The basic idea is to replace the integer-indexed sum in the traditional expression (A.2) by a point process indexed sum similar to the one in (A.10). Initially, we start out with a *simplified setup* as it allows to apply once more the procedure of attaching marks to a point process (as done in Sec. 4). Specifically, we

now introduce the marked point process

$$\left\{ \left(\boldsymbol{x}, (\alpha_{\boldsymbol{x}}, \nu_{\boldsymbol{x}}, \tau_{\boldsymbol{x}}) \right) : \boldsymbol{x} \in X \right\}, \tag{A.22}$$

where the i.i.d. mark collection $\{(\alpha_{\boldsymbol{x}}, \nu_{\boldsymbol{x}}, \tau_{\boldsymbol{x}}) : \boldsymbol{x} \in X\}$ is indexed using the points from the two-dimensional point process X as defined in (A.9). Each three-dimensional mark $(\alpha_{\boldsymbol{x}}, \nu_{\boldsymbol{x}}, \tau_{\boldsymbol{x}}) \in \mathbb{C} \times \mathbb{R} \times \mathbb{R}_+$ is drawn from some joint probability distribution (shared by all marks as they are drawn i.i.d.). Each mark designates a triplet of a path gain, a Doppler shift, and a propagation delay, respectively. The point process construction in (A.22) is fundamentally similar to the one in (A.9), and we use (A.22) to restrict and reformulate the traditional expression (A.2) such that

$$H(t, f) = \sum_{\boldsymbol{x} \in X} \mathbb{1}[\boldsymbol{x} \in B_t] \alpha_{\boldsymbol{x}} \mathrm{e}^{j2\pi t \nu_{\boldsymbol{x}}} \mathrm{e}^{-j2\pi f \tau_{\boldsymbol{x}}}, \tag{A.23}$$

where B_t is the triangular shaped region defined in (A.17) and shown in Fig. A.2. By recalling (A.18), notice how the indicator function in (A.23) ensures to exactly pinpoint those $L(t)$ path components which should contribute to the time-variant channel transfer function at time t. By comparing (A.23) with the traditional expression (A.2) it is readily seen how we have simplified the model of the channel transfer function. Specifically, we have substituted the two original collections of random processes $\{\alpha_\ell(t)\}$ and $\{\tau_\ell(t)\}$ by simpler terms $\{(\alpha_{\boldsymbol{x}}, \nu_{\boldsymbol{x}}, \tau_{\boldsymbol{x}}) : \boldsymbol{x} \in X\}$ which do not depend on time t and so allows to be naturally incorporated as marks attached to X. This deliberate simplification ensures transparency in the forthcoming derivation. In Sec. 5.3 we relax this simplified assumption and discuss the general case as well.

In addition to the expression in (A.23), we employ the reasonable assumption that the marks are drawn such that

$$\mathbb{E}[\alpha_{\boldsymbol{x}} \,|\, \nu_{\boldsymbol{x}}, \tau_{\boldsymbol{x}}] = \mathbb{E}[\alpha_\star \,|\, \nu_\star, \tau_\star] = 0, \qquad \boldsymbol{x} \in X, \tag{A.24}$$

where we make use of a wildcard notation like in (A.8). The assumption in (A.24) is usually justified from a default argument of uniformly distributed *initial phases*. By (A.24), we can readily show that $\mathbb{E}[H(t, f)] = \mathbb{E}\big[\mathbb{E}[H(t, f) | X]\big] = 0$, i.e. the channel transfer function in (A.23) has zero mean.

5.2 Applying Campbell's Theorem to Calculate the Time-Frequency Correlation Function

To calculate the time-frequency correlation function we enter (A.23) in (A.21) and proceed at first via intermediate conditioning on X such that

$$R_H(t, t', f, f') = \mathbb{E}\big[\mathbb{E}[H^*(t, f) H(t', f') \,|\, X]\big] \tag{A.25}$$

$$= \mathbb{E}\Big[\sum_{\boldsymbol{x} \in X} \mathbb{1}[\boldsymbol{x} \in B_t \cap B_{t'}] \mathbb{E}\big[|\alpha_{\boldsymbol{x}}|^2 \mathrm{e}^{j2\pi(\Delta t \nu_{\boldsymbol{x}} - \Delta f \tau_{\boldsymbol{x}})}\big] \Big] \tag{A.26}$$

where in (A.26) we have introduced the notation $\Delta f := f' - f$. The innermost expectation in (A.26) is with respect to the joint distribution of the mark $(\alpha_{\boldsymbol{x}}, \nu_{\boldsymbol{x}}, \tau_{\boldsymbol{x}})$. The equality between (A.25) and (A.26) is established by use of (A.24) together with the fact that the three-dimensional marks are mutually independent. Hence, all cross terms vanish in the innermost expectation in (A.25). The outermost expectation in (A.26) can be computed using Campbell's Theorem. This operation is straightforward since the indicator function of the region $B_t \cap B_{t'}$ is the only term left depending on the underlying points from X (not its marks). Accordingly, we have that

$$\mathbb{E}\Big[\sum_{\boldsymbol{x} \in X} \mathbb{1}[\boldsymbol{x} \in B_t \cap B_{t'}]\Big] = \mathbb{E}[N_X(B_t \cap B_{t'})] = \mu_X(B_t \cap B_{t'}).$$

Finally, the time-frequency correlation function reads

$$R_H(t, t', f, f') = \mu_X(B_t \cap B_{t'}) \mathbb{E}\big[|\alpha_\star|^2 e^{j2\pi(\Delta t \nu_\star - \Delta f \tau_\star)}\big] \tag{A.27}$$

with the first term $\mu_X(B_t \cap B_{t'})$ providing the expected number of points from X contributing *jointly* to both $H(t, \cdot)$ and $H(t', \cdot)$, recall Fig. A.2. Notice that the region count $N_X(B_t \cap B_{t'})$ is exactly the random quantity $(\diamond_1)$ defined in (A.14) in Sec. 4.2 and its expectation has already been calculated in (A.15). Since the general expression in (A.15) is a function of Δt only, the time-frequency correlation function in (A.27) is of the form

$$R_H(t, t', f, f') = \underbrace{R_1(\Delta t)}_{\mu_X(\cdot)} \underbrace{R_2(\Delta t, \Delta f)}_{\mathbb{E}[\cdot]} \tag{A.28}$$

which depends on time and frequency differences only. Hence, *the time-variant channel transfer function $H(\cdot, \cdot)$ in (A.23) is wide-sense stationary in both time and frequency.*

The general expression in (A.27) is one of our main results. The product form of (A.27) stated explicitly in (A.28) holds an attractive and intuitive interpretation. The first term $R_1(\Delta t)$ gives the temporal (large-scale) correlation properties of the birth-death process $L(\cdot)$. The second term $R_2(\Delta t, \Delta f)$ reports the "traditional" time-frequency correlation properties of each individual path component (small-scale). If we specialize to the traditional modeling approach where $L(t) = L$ is constant within individual channel realizations (deterministic or random), then all we have to modify is the term $R_1(\Delta t)$. If L is a fixed constant then $R_1(\Delta t)$ is to be replaced by L itself, whereas if L is a random variable, then $R_1(\Delta t)$ is to be replaced by $\mathbb{E}[L]$. Hence, for the temporal birth-death case it seems reasonable that $R_1(\Delta t)$ should be given by $\mathbb{E}[N_X(B_t \cap B_{t'})]$, i.e. the expected number of path components contributing jointly to both $H(t, \cdot)$ and $H(t', \cdot)$.

5.3 Towards a More General Model for the Channel Transfer Function $H(\cdot, \cdot)$

With the simplified model (A.23) and the result (A.27) in mind, we may naturally seek a more general expression for $H(\cdot, \cdot)$ with the path gains and the propagation delays being described according to random processes as also suggested by the original model in (A.2). To obtain such we depart from (A.23) and via term-by-term substitution we introduce instead

$$H(t, f) = \sum_{\boldsymbol{x} \in X} \mathbb{1}[\boldsymbol{x} \in B_t] \alpha_{\boldsymbol{x}}(t) \mathrm{e}^{-j 2 \pi f \tau_{\boldsymbol{x}}(t)}. \tag{A.29}$$

The only difference now between (A.29) and the traditional expression in (A.2) is that the new collection $\{\alpha_{\boldsymbol{x}}(t) : \boldsymbol{x} \in X\}$ is used in substitute for $\{\alpha_\ell(t)\}$, and similarly, the new collection $\{\tau_{\boldsymbol{x}}(t) : \boldsymbol{x} \in X\}$ is used in substitute for $\{\tau_\ell(t)\}$. That is, *we use the points from X to index two individual sequences of random processes while simultaneously generating the birth-death process $L(\cdot)$ using the very same points from X*. Notice carefully that (A.2) and (A.29) portray the very same random quantity, just represented in two different ways.

With the general expression (A.29) in place, a relevant task is now to identify what properties the two newly indexed sequences of random processes must possess in order for $H(\cdot, \cdot)$ to be wide-sense stationary in both time and frequency. Hence, the fundamental question we ask is the following: When will

$$R_H(t, t', f, f') = \mathbb{E}[H^*(t, f) H(t', f')] \stackrel{?}{=} \widetilde{R}_H(\Delta t, \Delta f)$$

be a function of Δt and Δf only? The relevance of this question needs hardly no motivation as the class of doubly wide-sense stationary stochastic channel models has been favored both in literature and practice ever since Bello introduced his seminal *WSSUS characterization* [27]. Bello did not assume a specific form of the time-variant channel transfer function as we do here. Instead he treated $H(\cdot, \cdot)$ as a generic stochastic process and we extend our analysis in a similar fashion in Sec. 5.5, but for now we restrict to the repeatedly favored multipath model in (A.29).

At a first glance it may seem a rather innocent question when asking for how and when (A.29) will be doubly wide-sense stationary. *Surprisingly, it seems that the question is not so innocent after all.* In the spirit of Bello's WSSUS framework we invoke the popular assumption that the random processes $\{\alpha_{\boldsymbol{x}}(t) : \boldsymbol{x} \in X\}$ are mutually uncorrelated and that they all hold zero mean (compare with (A.24) of the simplified setup). Then, our analysis narrows down to deal with a random process including only a single path component, namely $\widetilde{H}(t, f) = \alpha(t) \mathrm{e}^{-j 2 \pi f \tau(t)}$. If we then further make the simplistic assumption of $\alpha(\cdot)$ and $\tau(\cdot)$ being independent random processes it means that we need to draw our conclusions based on

$$R_{\widetilde{H}}(t, t', f, f') = \mathbb{E}[\alpha^*(t) \alpha(t')] \mathbb{E}\left[\mathrm{e}^{-j 2 \pi (f' \tau(t') - f \tau(t))}\right].$$

Obviously, the random process $\alpha(\cdot)$ must be wide-sense stationary in order to make the first expectation a function of Δt only. Surprisingly, the only way for the second expectation to be a function of Δf is when the random process $\tau(\cdot)$ has constant realizations (and hence it does not at all depend on t and t'). A detailed but simple argument for this claim can be found in Appendix 7.

5.4 Principal Representation of $H(\cdot, \cdot)$ and Its Associated Time-Frequency Correlation Function

The insight gained by now motivates the assumption of random but constant propagation delays as well as wide-sense stationary path gain processes. Accordingly, we thus introduce an expression of the channel transfer function such that

$$H(t, f) = \sum_{\boldsymbol{x} \in X} \mathbb{1}[\boldsymbol{x} \in B_t] \alpha_{\boldsymbol{x}}(t) \mathrm{e}^{-j2\pi f \tau_{\boldsymbol{x}}}. \tag{A.30}$$

This expression can be seen as a natural intermediate between (A.23) and (A.29) with the ability to result in being doubly wide-sense stationary. We make use of a collection of random *processes* (path gains) together with a collection of random *marks* (propagation delays) with both collections being indexed via the points from X. We assume that the marks $\{\tau_{\boldsymbol{x}} : \boldsymbol{x} \in X\}$ comprise an i.i.d. collection drawn from a probability density function $f_{\mathrm{delay}}(\cdot)$. Conditioned on the marks, we further assume that the random processes $\{\alpha_{\boldsymbol{x}}(t) : \boldsymbol{x} \in X\}$ all hold zero mean, are mutually uncorrelated, and individually exhibits an autocorrelation function parameterized via the corresponding mark. Specifically, for all $t, t' \in \mathbb{R}$ we assume that

$$\mathbb{E}[\alpha_{\boldsymbol{x}}^*(t) \alpha_{\widetilde{\boldsymbol{x}}}(t') \,|\, \tau_{\boldsymbol{x}}, \tau_{\widetilde{\boldsymbol{x}}}] = 0, \qquad \boldsymbol{x} \neq \widetilde{\boldsymbol{x}}, \tag{A.31}$$

$$\mathbb{E}[\alpha_{\boldsymbol{x}}^*(t) \alpha_{\boldsymbol{x}}(t') \,|\, \tau_{\boldsymbol{x}}] = R_\alpha(\Delta t; \tau_{\boldsymbol{x}}), \tag{A.32}$$

allowing (for instance) to conveniently assign conditional average power to each random process $\alpha_{\boldsymbol{x}}(\cdot)$ as a function of its corresponding propagation delay $\tau_{\boldsymbol{x}}$.

By repeating the procedures and calculations from Sec. 5.2 we now obtain a time-frequency correlation function for the model in (A.30) reading

$$R_H(t, t', f, f') = R_1(\Delta t) \mathbb{E}\big[R_\alpha(\Delta t; \tau_\star) \mathrm{e}^{-j2\pi \Delta f \tau_\star}\big], \tag{A.33}$$

with $R_1(\Delta t) = \mu_X(B_t \cap B_{t'})$ and where the expectation is with respect to $f_{\mathrm{delay}}(\cdot)$, i.e. we utilize again a wildcard notation $\tau_\star$ to represent a typical mark. By (A.33), the time-variant channel transfer function $H(\cdot, \cdot)$ in (A.30) is also wide-sense stationary in both time and frequency.

5.5 The Channel Transfer Function $H(\cdot, \cdot)$ as a Sum of Generic WSSUS Components

To complete the current investigations we extend our previous model of $H(\cdot, \cdot)$ such that its individual time-frequency contributions are no longer of any particular form. Specifically, we let

$$H(t, f) = \sum_{\boldsymbol{x} \in X} \mathbb{1}[\boldsymbol{x} \in B_t] H_{\boldsymbol{x}}(t, f), \qquad (A.34)$$

and we augment the model in (A.34) with the tractable assumptions that the individual component processes fulfill:

$$\mathbb{E}[H_{\boldsymbol{x}}(t, f) | \boldsymbol{x}] = 0, \qquad \boldsymbol{x} \in X, \qquad (A.35)$$
$$\mathbb{E}[H_{\boldsymbol{x}}^*(t, f) H_{\widetilde{\boldsymbol{x}}}(t', f') | \boldsymbol{x}, \widetilde{\boldsymbol{x}}] = R_2(\Delta t, \Delta f) \mathbb{1}[\boldsymbol{x} = \widetilde{\boldsymbol{x}}]. \qquad (A.36)$$

For the model in (A.34) we obtain, analogously to previous expressions, a time-frequency correlation function reading

$$R_H(t, t', f, f') = R_1(\Delta t) R_2(\Delta t, \Delta f). \qquad (A.37)$$

To summarize this section we emphasize the sole tool which enabled our novel assessment of the time-frequency correlation function with the general product form as given in (A.27), (A.28), (A.33) and (A.37). In a nutshell, our key step was to reformulate the traditional expression (A.2) to circumvent the enumeration problem induced by the traditional integer-indexing of path components. Specifically, we reformulated (A.2) using the point process X defined in (A.9) which is the very same random collection we also used for generating the temporal birth-death process $L(\cdot)$ in Sec. 4. Through X, we then introduced several candidate representations in direct substitute of the traditional and widely used model (A.2) of the channel transfer function. All substitute representations were essentially of type (A.6) and hence appropriate for analysis using Campbell's Theorem.

6 Selected Examples and Simulation Aspects

This section provides a selection of examples intended to concretize the general results obtained in Sec. 4 and Sec. 5. In particular, the goal is to highlight the practical implications of our novel findings as well as to illustrate the benefits of the spatial point process perspective in terms of modeling flexibility and computer simulation. Specifically, we show via concrete examples how the key parameters of the temporal birth-death channel model enter explicitly in quantities which can be measured in practice, e.g. the power-delay profile. Furthermore, depending on its purpose, we show how the channel

model can be readily modified to incorporate fewer or more stochastic features. Finally, we illustrate from a simulation technical point of view the facilitating and convenient aspects of the assumptions $i)^{\dagger}$ and $ii)^{\dagger}$.

6.1   Power-Delay Profile Induced From A Separation Property

In Sec. 5.4 we did not introduce a specific choice for the autocorrelation function $R_{\alpha}(\cdot;\cdot)$ in (A.32). By making such a choice and by making also explicit choices about the probability density functions $f_{\text{period}}(\cdot)$ and $f_{\text{delay}}(\cdot)$, we readily end up with a final and concrete expression for the time-frequency correlation function in (A.33).

Example 4. A simple choice for the autocorrelation function $R_{\alpha}(\cdot;\cdot)$ in (A.32) is to assume that

$$\mathbb{E}[\alpha_{\boldsymbol{x}}^{*}(t)\alpha_{\boldsymbol{x}}(t')\,|\,\tau_{\boldsymbol{x}}] = R_{\alpha}(\Delta t;\tau_{\boldsymbol{x}}) = \sigma_{\alpha}^{2}(\tau_{\boldsymbol{x}})J_{0}(2\pi\eta\Delta t),$$

where $J_{0}(\cdot)$ is the zeroth-order Bessel function of the first kind, η is a positive parameter to be specified, and $\sigma_{\alpha}^{2}(\cdot)$ is assigning conditional average power to each random process $\alpha_{\boldsymbol{x}}(\cdot)$ as a function of its corresponding propagation delay $\tau_{\boldsymbol{x}}$. Similar assumptions (or choices) are often found in literature [8, 28] and the use of the Bessel function $J_{0}(\cdot)$ originates from Clarke's seminal work [29]. Notice that we in fact assume the correlation function to be the same for all individual path gain processes $\{\alpha_{\boldsymbol{x}}(t) : \boldsymbol{x} \in X\}$, except for an individual scaling by $\sigma_{\alpha}^{2}(\tau_{\boldsymbol{x}})$. With these choices the time-frequency correlation function in (A.33) is readily seen to factorize in a product of time-frequency separated terms, namely as

$$R_{H}(t,t',f,f') \ = R_{\text{time}}(\Delta t)R_{\text{freq}}(\Delta f), \tag{A.38}$$

$$R_{\text{time}}(\Delta t) := R_{1}(\Delta t)J_{0}(2\pi\eta\Delta t), \tag{A.39}$$

$$R_{\text{freq}}(\Delta f) := \mathbb{E}\big[\sigma_{\alpha}^{2}(\tau_{\star})\mathrm{e}^{-j2\pi\Delta f\tau_{\star}}\big]. \tag{A.40}$$

The product form in the right-hand side of (A.38) reflects the separation property mentioned briefly in [28]. An immediate and practically convenient consequence of the separation property in (A.38) is that it notably simplifies the design of linear minimum mean-squared error estimators of the channel transfer function $H(\cdot,\cdot)$, e.g. for OFDM applications [28].

Notice how even (A.39) factorizes, namely as a product of *large-scale* and *small-scale* fading induced correlation properties (recall also the discussion below (A.28) in Sec. 5.2). To further concretize (A.39) we could invoke assumption $ii)^{\dagger}$ as [7–10] and like we also did in Example 1 in Sec. 4.2. The large-scale correlation term $R_{1}(\Delta t)$ would then exhibit an exponential decay and specifically we would have

$$R_{\text{time}}(\Delta t) = \frac{\lambda_{\text{e}}}{\lambda_{\text{v}}} \exp(-\lambda_{\text{v}}|\Delta t|)J_{0}(2\pi\eta\Delta t).$$

Exponentially decaying correlation functions for large-scale fading processes (*shadowing*) have been suggested in literature several times, see e.g. [30] for one of the earliest occurrences. We selected here the Bessel function $J_0(\cdot)$ as the small-scale correlation structure only to provide a concrete and popular example. Obviously, we could have made any other selection for the normalized correlation function and substituted it directly into (A.39) instead of $J_0(\cdot)$.

The expression in (A.40) holds important information as well. Specifically, as we can readily identify (A.40) as the Fourier transform

$$R_{\text{freq}}(\Delta f) = \mathcal{F}\{\sigma_\alpha^2(\cdot)f_{\text{delay}}(\cdot)\}(\Delta f)$$

we find that the *power-delay profile* of the channel is

$$P_{\text{delay}}(\tau) := R_{\text{time}}(0)\mathcal{F}\{R_{\text{freq}}(\cdot)\}(\tau) = \frac{\lambda_{\text{e}}}{\lambda_{\text{v}}}\sigma_\alpha^2(\tau)f_{\text{delay}}(\tau).$$

This function characterizes the rate of decay of received power versus propagation delay. Knowledge of the power-delay profile (sometimes also called the *delay-power spectrum*) is crucial for localization aspects and wireless communications in general. Motivated by empirical observations, a standard assumption is that $P_{\text{delay}}(\cdot)$ exhibits an overall exponential decay. In [8, 9] such an exponential decay is maintained by appropriate selections of the conditional power assigning function $\sigma_\alpha^2(\cdot)$ and the probability density function $f_{\text{delay}}(\cdot)$.

To conclude this example we stress the importance of being able to calculate and analytically assess the functions $R_{\text{time}}(\cdot)$, $R_{\text{freq}}(\cdot)$, $P_{\text{delay}}(\cdot)$ and so on. The importance consists in that key parameters of the channel model such as λ_{e} and λ_{v} enter explicit in these practically measurable quantities. In turn, this allows for rigorous parameter estimation and it enables also the temporal birth-death channel model to be utilized as a tool for measurement prediction. Such capabilities stand in notable contrast to the limitations of "pure" simulation models, where we usually do not know if potential interactions occur between model parameters and where questions regarding stationarity properties most often remain inconclusive.   □

At a first glance it may seem quite restrictive that we in the above example assumed a shared normalized correlation function for all individual path gains $\{\alpha_{\boldsymbol{x}}(t) : \boldsymbol{x} \in X\}$. A straightforward way to generalize this is to introduce a second collection of i.i.d. marks. We illustrate this idea in the sequel.

6.2   Modeling Flexibility

The forthcoming example illustrates an important attribute of the point process perspective: Once the underlying point process X from (A.9) is in place, we can in a natural and straightforward manner change the modeling details of the channel transfer

function. Specifically, we can swap in dimensionality by attaching fewer or more marks to each $\boldsymbol{x} \in X$ depending on the degree of features we wish the random process $H(\cdot, \cdot)$ to exhibit. Yet, the notation is nearly not affected by such changes and the crucial details in the derivation of the resulting time-frequency correlation function (Sec. 5.2) stay virtually unaffected. This attractive fact stand in notable contrast to a variety of model extensions proposed in literature. Certain well-known model extensions appear essentially to lack structure or to suffer from the absence of a profound theoretical modeling framework. Examples include Spencer's extension [6] of Saleh and Valenzuela's model [5] together with the ultra-wideband model [31] which is fundamentally based on [5] as well.

To extend the temporal birth-death channel model in (A.30) we can for example make use of the marked point process

$$\big\{\big(\boldsymbol{x}, (\tau_{\boldsymbol{x}}, \theta_{\boldsymbol{x}})\big) : \boldsymbol{x} \in X\big\}. \tag{A.41}$$

Conceptually we are attaching two-dimensional marks $(\tau_{\boldsymbol{x}}, \theta_{\boldsymbol{x}})$ and the collection in (A.41) can of course be seen as a point process in a four-dimensional space (which may sometimes be useful, but not always). The new collection $\{\theta_{\boldsymbol{x}} : \boldsymbol{x} \in X\}$ is modeling azimuth (incidence) directions for the individual path components as also focused on in e.g. [6] and [10]. Each $\theta_{\boldsymbol{x}}$ is drawn independently from a probability density function $f_{\text{azimuth}}(\cdot)$ with support set $[-\pi, \pi]$ and the assumption in (A.32) is then replaced (with minor notational abuse) according to

$$\mathbb{E}[\alpha_{\boldsymbol{x}}^*(t)\alpha_{\boldsymbol{x}}(t') \,|\, \tau_{\boldsymbol{x}}, \theta_{\boldsymbol{x}}] = \sigma_\alpha^2(\tau_{\boldsymbol{x}})R_\alpha(\Delta t; \theta_{\boldsymbol{x}}) \tag{A.42}$$

such that each path gain $\alpha_{\boldsymbol{x}}(\cdot)$ holds an individual *normalized* autocorrelation function $R_\alpha(\cdot; \theta_{\boldsymbol{x}})$ parameterized by $\theta_{\boldsymbol{x}}$. When repeating the derivation in Sec. 5.2 based on (A.42) we find that the resulting time-frequency correlation function now takes the form

$$R_H(t, t', f, f') = R_1(\Delta t)\mathbb{E}[R_\alpha(\Delta t; \theta_\star)]\mathbb{E}\big[\sigma_\alpha^2(\tau_\star)\mathrm{e}^{-j2\pi\Delta f \tau_\star}\big], \tag{A.43}$$

where the first expectation is with respect to $f_{\text{azimuth}}(\cdot)$ and the second with respect to $f_{\text{delay}}(\cdot)$. The above modification appears intuitively reasonable when comparing (A.43) with the previous expressions (A.33) and (A.38) for the time-frequency correlation function.

Example 5. Conditioned on the two marks $(\tau_{\boldsymbol{x}}, \theta_{\boldsymbol{x}})$, we could for instance generate each path gain process $\alpha_{\boldsymbol{x}}(\cdot)$ in terms of azimuth-dispersed sub-components such that

$$\alpha_{\boldsymbol{x}}(t) := \sqrt{\frac{\sigma_\alpha^2(\tau_{\boldsymbol{x}})}{M}} \sum_{m=1}^{M} A_m \exp\big(j2\pi\eta\cos(\varphi_m)t\big), \quad t \in \mathbb{R},$$

where $\{A_m\} \overset{\text{i.i.d.}}{\sim} \mathcal{CN}(0,1)$ and $\{\varphi_m\} \overset{\text{i.i.d.}}{\sim} \mathcal{VM}(\theta_{\boldsymbol{x}}, \kappa)$. Here we use $\mathcal{CN}$ and $\mathcal{VM}$ to denote the *complex normal* distribution and the *von Mises* distribution, respectively. Furthermore, (M, η, κ) are fixed parameters to be set according to the particular context (environment, physical speeds, carrier wavelength, etc.) but they are not of main concern at present.

It follows readily that $\alpha_{\boldsymbol{x}}(t)|(\tau_{\boldsymbol{x}}, \theta_{\boldsymbol{x}}) \sim \mathcal{CN}(0, \sigma_\alpha^2(\tau_{\boldsymbol{x}}))$, and with some minor calculations we get (recall (A.42))

$$R_\alpha(\Delta t; \theta_{\boldsymbol{x}}) = \mathbb{E}[\exp(j2\pi\eta\cos(\varphi_\star)\Delta t)\,|\,\theta_{\boldsymbol{x}}] \tag{A.44}$$

$$= \frac{I_0\big(\sqrt{\kappa^2 - (2\pi\eta\Delta t)^2 + j4\pi\kappa\eta\Delta t\cos(\theta_{\boldsymbol{x}})}\,\big)}{I_0(\kappa)},$$

where in (A.44) the expectation is with respect to an arbitrary $\varphi_\star$ drawn from the von Mises density

$$f_{\mathcal{VM}}(\varphi; \theta_{\boldsymbol{x}}, \kappa) = \frac{\exp(\kappa\cos(\varphi - \theta_{\boldsymbol{x}}))}{2\pi I_0(\kappa)}, \quad \varphi \in [-\pi, \pi),$$

and where $I_0(\cdot)$ denotes the zeroth-order *modified* Bessel function of the first kind. We refer to [32] for more details on the von Mises distribution and the properties of the resulting correlation function. The current goal is to realize how our modeling choices affect the time-frequency correlation function in (A.43). Specifically, we then need to average (A.44) with respect to the density $f_{\text{azimuth}}(\cdot)$, i.e.

$$\mathbb{E}[R_\alpha(\Delta t; \theta_{\boldsymbol{x}})] = \mathbb{E}\big[\mathbb{E}[\exp(j2\pi\eta\cos(\varphi_\star)\Delta t)\,|\,\theta_{\boldsymbol{x}}]\big]$$

$$= \iint f_{\text{azimuth}}(\theta) f_{\mathcal{VM}}(\varphi; \theta, \kappa) \mathrm{e}^{j2\pi\eta\cos(\varphi)\Delta t} \mathrm{d}\varphi\mathrm{d}\theta, \tag{A.45}$$

where the region of integration is $[-\pi, \pi) \times [-\pi, \pi)$. The expression in (A.45) is difficult to assess except for certain special cases of the density $f_{\text{azimuth}}(\cdot)$. However, if we employ the assumption that $f_{\text{azimuth}}(\cdot)$ is the uniform density on $[-\pi, \pi)$, then (A.45) simplifies to the standard expression $J_0(2\pi\eta\Delta t)$ from Example 4. To see this, simply swap the order of integration in (A.45) and notice that $\int f_{\mathcal{VM}}(\varphi; \theta, \kappa)\mathrm{d}\theta = 1$ since the individual roles of the "variables" φ and θ are interchangeable in the von Mises density. Hence, from the very beginning we could have made the default selection of the Bessel function $J_0(2\pi\eta\Delta t)$ for the shared correlation function in (A.32). However, we could also have employed individual correlation functions as just shown. Yet, with the particular choices made, in fact, the time-frequency correlation function in (A.43) would coincide with the one from Example 4. □

The above example illustrated a particular choice and recipe for how each path gain process $\alpha_{\boldsymbol{x}}(\cdot)$ could be parameterized and generated in a computer simulation. In the following we highlight a few selected details on tractable simulation procedures for the underlying birth-death process $L(\cdot)$. In addition to its analytical advantages, the point process perspective proves itself also particularly valuable for simulation purposes.

6.3 Simulation Aspects Regarding the Point Process X and the Temporal Birth-Death Process

The approaches in [7–10] rely exclusively on the assumptions $i)^\dagger$ and $ii)^\dagger$. This can be motivated by the fact that these two assumptions together endow the resulting channel model with *simple mathematics* [7]. In fact, $i)^\dagger$ and $ii)^\dagger$ are also particularly convenient in terms of computer simulation, especially due to our theoretical knowledge from Sec. 4 regarding the point process X.

The contribution in [7] focuses on modeling and experimental investigations and does not cover aspects related to computer simulation. Both [8] and [9] mention a few simulation aspects with example visualizations of generated channel impulse responses. However, exact details or guidelines are not provided, in particular, the enumeration issues related to the birth-death transitions of $L(\cdot)$ are not mentioned. In contrast, [10] proposes a number of heuristic guidelines for controlling, initializing and time-discretizing the temporal birth-death mechanism. For instance, the random process $L(\cdot)$ is always initialized such that no path components are present. Hence, if the *origin* is selected to be the arbitrary starting time, then [10] systematically assigns $L(0) = 0$. The motivation for this is (quoting [10, Sec. III-C]): *To avoid the problem of defining a specific starting state.* It is then suggested to initially let the process run long enough to yield the "correct" value for $\mathbb{E}[L(t)]$. Based on $ii)^\dagger$, a value is then given for the minimum forerun needed to yield an error of at most 1% (in a certain sense). The actual simulation should subsequently take place after this forerun[7].

With our theoretical knowledge from Sec. 4, approximate simulation guidelines like the one mentioned above can be entirely circumvented. In particular, rather than *defining* a starting state, $L(0)$ should be drawn from a Poisson distribution instead of being systematically assigned to zero. Conditioned on $L(0)$, the task is then to calculate the conditional joint distribution of *emergence times* and *lifetimes* of those $L(0)$ path components which necessarily are present in the channel at initialization time $t = 0$. Obviously, all $L(0)$ path components must have emerged before time $t = 0$.

Example 6. Our goal in this example is to show the facilitating aspects of $i)^\dagger$ by itself. Accordingly, we combine $i)^\dagger$ with $ii)$. In the following we show how to initialize the birth-death process $L(\cdot)$ using emergence times and lifetimes drawn from the equilibrium distribution.

Initially, recall Fig. A.2 and shift the region B_t to the origin. Since X as defined in (A.9) is a Poisson point process we have that $L(0) = N_X(B_0)$ is a Poisson distributed random variable with mean $\mu_X(B_0) = \lambda_e \mathbb{E}[p_\star]$. Hence, we start by drawing the non-negative integer $L(0)$. By the second item of Definition 2 in Sec. 3, we should then draw

---

[7]This procedure resembles the well-known *burn-in* periods often used in *Markov Chain Monte Carlo* (MCMC) simulations [25, Sec. 8.1.2]. Such a burn-in is employed to ensure that the marginal distribution of the Markov chain's current state is sufficiently close to its (unknown) *equilibrium distribution* for all practical purposes.

the $L(0)$ points $X \cap B_0$ mutually independent and identically distributed according to

$$f_{B_0}(\boldsymbol{x}) = \frac{\varrho_X(\boldsymbol{x})}{\mu_X(B_0)} \mathbb{1}[\boldsymbol{x} \in B_0] = \frac{f_{\text{period}}(p)}{\mathbb{E}[p_\star]} \mathbb{1}[(y, p) \in B_0],$$

where the intensity function $\varrho_X(\cdot)$ is taken from (A.16). Due to the shape of the un-bounded triangular region B_0, it is most convenient to draw each two-dimensional point $\boldsymbol{x} = (y, p)$ by a two-step procedure. Marginalizing $f_{B_0}(\cdot)$ with respect to each of y and p yields respectively

$$f_y(y) := \int f_{B_0}(y, p) \mathrm{d}p = \frac{\mathbb{1}[y < 0]}{\mathbb{E}[p_\star]} \int_{-y}^{\infty} f_{\text{period}}(p) \mathrm{d}p = \frac{\Pr(p_\star > -y)}{\mathbb{E}[p_\star]} \mathbb{1}[y < 0], \quad (A.46)$$

and

$$f_p(p) := \int f_{B_0}(y, p) \mathrm{d}y = \frac{f_{\text{period}}(p)}{\mathbb{E}[p_\star]} \int_{-p}^{0} 1 \mathrm{d}y = \frac{p f_{\text{period}}(p)}{\mathbb{E}[p_\star]}. \quad (A.47)$$

(Notice that both $f_y(\cdot)$ and $f_p(\cdot)$ integrate to unity). The corresponding conditional distributions read

$$f_{y|p}(y|p) = \frac{f_{B_0}(y, p)}{f_p(p)} = \frac{1}{p} \mathbb{1}[y \in (-p, 0)] \quad (A.48)$$

and

$$f_{p|y}(p|y) = \frac{f_{B_0}(y, p)}{f_y(y)} = \frac{f_{\text{period}}(p)}{\Pr(p_\star > -y)} \mathbb{1}[p > -y], \quad (A.49)$$

(which also both integrate to unity as can be readily verified). Now, to generate a point $\boldsymbol{x} = (y, p)$, we can first generate the emergence time y according to $f_y(\cdot)$ in (A.46) and then generate the corresponding[8] period p according to $f_{p|y}(\cdot|y)$ in (A.49). Alternatively, we can first generate the period via (A.47) and then generate the corresponding emergence time via (A.48). The approach most preferable for implementation depends on our choice of the density $f_{\text{period}}(\cdot)$. In essence, to initialize the temporal birth-death process $L(\cdot)$ in equilibrium at time $t = 0$ we do as follows:

1. Draw $L(0) = N_X(B_0)$ from a Poisson distribution with mean $\lambda_e \mathbb{E}[p_\star]$.

2. Draw the points $X \cap B_0$ i.i.d. according to (A.46) and (A.49) (alternatively, use (A.47) and (A.48)).

---

[8] In this construction y and p are obviously dependent since we have conditioned on the fact that exactly $L(0)$ path components are present at time $t = 0$. To the contrary, the periods of those path components to emerge in the future are to be drawn independently of their times of emergence.

Accordingly, the temporal birth-death process $L(\cdot)$ exhibits its exact theoretical properties at initialization time $t = 0$ without imitating a forerun from the infinite past.

$\qquad\qquad\qquad\qquad\qquad\qquad\qquad\qquad\qquad\qquad\qquad\qquad\qquad\qquad$ $\square$

The example above illustrates in a convincing manner the benefits and the potential of the point process perspective. In contrast to the approximate and heuristic initialization guideline in [10], the channel can now be initialized exact (in equilibrium) from a "mechanic procedure" dictated by the properties of the Poisson point process X (Definition 2 in Sec. 3).

7   Conclusion

The theoretical framework of spatial point processes and its powerful tools, like Campbell's Theorem, comprise a natural environment for the engineering treatment of various stochastic radio channel models. Our analysis of the class of temporal birth-death channel models, governed by the assumptions $i)$ and $ii)$ in Sec. 1, supports this conclusion and the usefulness of Campbell's Theorem has been demonstrated repeatedly. Overall, the proposed point process perspective is analytically beneficial due to its inherent flexibilities with respect to dimensionality swapping and its ability to circumvent inconvenient enumeration issues of traditional modeling approaches. Specifically, the key technique we employed was to replace traditional integer-indexed sums by equivalent expressions indexed by points from spatial point processes. In essence, this allows for keeping track of individual path components by use of the same stochastic mechanism which is also generating the temporal birth-death behavior of the channel. In addition to its analytical advantages, the point process perspective has proven itself particularly valuable for simulation purposes as well. A complete and categorized overview of our findings is given in Fig. A.5.

In Sec. 4 we have shown that the temporal birth-death process $L(\cdot)$ is strict-sense stationary. The mean of $L(\cdot)$ does not depend on the exact shape of the probability density function induced via $ii)$, only the its first-order moment matters. However, the autocorrelation function of $L(\cdot)$ is directly affected via its shape. Finally, we indicated in Sec. 4 the crucial roles of $i)$ and $ii)$ in the sense that relaxation attempts in general turn $L(\cdot)$ into a non-stationary random process.

We derived in Sec. 5 a general expression of the channel's time-frequency correlation function. To the best of our knowledge this expression has not appeared elsewhere in the channel modeling literature. The time-frequency correlation function is comprised by the product of a large-scale and a small-scale term. Under facilitating assumptions we have shown that the channel transfer function becomes wide-sense stationary in both time and frequency despite the birth-death behavior of the channels individual path components.
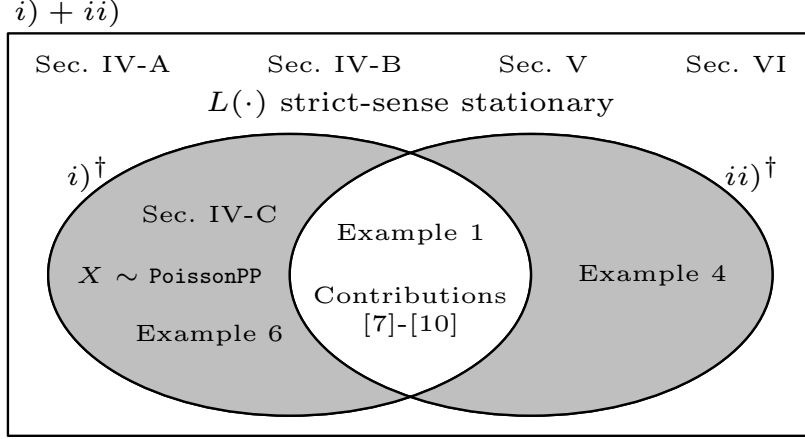
$i) + ii)$

Sec. IV-A   Sec. IV-B   Sec. V   Sec. VI

$L(\cdot)$ strict-sense stationary

$i)^{\dagger}$

Sec. IV-C

$X \sim$ PoissonPP

Example 6

Example 1

Contributions
[7]-[10]

$ii)^{\dagger}$

Example 4

Fig. A.5: Overview of the present contribution in the form of a Venn-diagram. Notice that we have not indicated Sec. 4.4 anywhere in the figure as this paragraph attempts to relax the assumptions $i)$ and $ii)$ displayed in terms of the rectangular box.

We have shown and demonstrated via concrete examples in Sec. 6 the paramount ability to calculate and assess the time-frequency correlation function by analytical means. The key parameters of the birth-death channel model enter explicitly in practically measurable quantities such as temporal correlation functions and the power-delay profile. Immediate practical implications are that new parameter estimation procedures can be rigorously suggested and that the class of temporal birth-death channel models can as well be used as a tool for measurement prediction (as compared to a model class useful merely for simulation purposes).

Appendix A: Strict-Sense Stationarity of the Temporal Birth-Death Process $L(t)$

Proposition. As a consequence of $i)$ and $ii)$, the random process $L(\cdot)$ defined in (A.10) is strict-sense stationary.

Proof. To see that $L(\cdot)$ is strict-sense stationary we have to show (for any fixed time shift $s \in \mathbb{R}$ and for any $k \in \mathbb{N}$) that

$$\Pr\big(L(t_1 + s) \leq n_1, \ldots, L(t_k + s) \leq n_k\big) \tag{A.50}$$

does not depend on our choice of s. However, the common time shift in (A.50) corresponds in fact to nothing but a translation of the point process Y since by the definition

of $L(t)$ in (A.10) we have

$$L(t_i + s) = \sum_{y \in Y} \mathbb{1}[y < t_i + s, \ y + p_y > t_i + s]$$

$$= \sum_{\widetilde{y} \in \widetilde{Y}} \mathbb{1}[\widetilde{y} < t_i, \ \widetilde{y} + p_{\widetilde{y+s}} > t_i], \quad i = 1, \ldots, k,$$

where $\widetilde{Y} := Y - s$ is the random collection $\{y - s : y \in Y\}$ of shifted points. Indeed, for any fixed $s \in \mathbb{R}$, the shifted collection $\widetilde{Y}$ is a stationary point process on the entire real line with the same distributional properties as Y. Additionally, the marks/periods are drawn i.i.d. irrespectively of the underlying point pattern and from this we now conclude that

$$\big(L(t_1 + s), \ldots, L(t_k + s)\big) \sim \big(L(t_1), \ldots, L(t_k)\big).$$

That is, (A.50) does not depend on s and so the random process $L(\cdot)$ defined in (A.10) is strict-sense stationary. $\qquad\square$

Appendix B: On Conditions for Wide-Sense Stationarity

Proposition. Let $\tau(\cdot)$ be real-valued random process for which the product-moment $\mathbb{E}[\tau(t)\tau(t')]$ exists for all $t, t' \in \mathbb{R}$. Then the function

$$g(t, t', f, f') := \mathbb{E}\big[e^{-j2\pi(f'\tau(t') - f\tau(t))}\big] \tag{A.51}$$

depends at most on $\Delta f = f' - f$ only if $\tau(\cdot)$ is a random process with constant realizations.

Proof. Observe that the expectation in (A.51) relates directly to the *characteristic function* (or the *moment generating function*) of the bivariate random variable $(X, Y) = \big(\tau(t), \tau(t')\big)$. Consider for simplicity the moment generating function

$$\mathcal{M}_{XY}(f_1, f_2) := \mathbb{E}\big[e^{f_1 X + f_2 Y}\big], \tag{A.52}$$

which relates to the characteristic function $\mathcal{C}_{XY}(\cdot, \cdot)$ by evaluating (A.52) at (jf_1, jf_2). Moreover, it is readily seen that we directly obtain (A.51) by evaluating (A.52) at $(j2\pi f, -j2\pi f')$. Requiring (A.51) to be a function of Δf essentially means that we require $\mathcal{M}_{XY}(f_1, f_2) = M(f_1 + f_2)$, for some function $M(\cdot)$. Then by using the fact that (A.52) is a moment generating function it follows for all $n, m \in \mathbb{N}_0$ that

$$\frac{\partial^n}{\partial f_1^n} \frac{\partial^m}{\partial f_2^m} \mathcal{M}_{XY}(f_1, f_2)\Big|_{(0,0)} = \mathbb{E}[X^n Y^m] = M^{(n+m)}(0),$$

where $M^{(k)}(\cdot)$ denotes the k'th order derivative of $M(\cdot)$. Hence, for first- and second-order properties of X and Y we find that $\mathbb{E}[X] = \mathbb{E}[Y]$ and $\mathbb{E}[X^2] = \mathbb{E}[XY] = \mathbb{E}[Y^2]$, which means that the *correlation coefficient* ρ_{XY} between X and Y is such that $|\rho_{XY}| = 1$. Accordingly, X and Y are related via some affine transform $Y = aX + b$ but only $a = 1$ and $b = 0$ together fulfills the first- and second-order requirements for X and Y, and these two random variables were arbitrary samples from the random process $\tau(\cdot)$.$\square$

References

[1] G. L. Turin, "Communication Through Noisy, Random-Multipath Channels", Doctoral thesis, Massachusetts Institute of Technology, 1956.

[2] G. L. Turin, F. D. Clapp, T. L. Johnston, S. B. Fine, and D. Lavry, "A statistical model of urban multipath propagation", IEEE Trans. Vehic. Techn., Vol. 21, No. 1, pp. 1-9, 1972.

[3] H. Suzuki, "A statistical model for urban radio propagation", Doctoral thesis, University of California, Berkeley, 1975. See also IEEE Trans. Commun., Vol. 25, No. 7, pp. 673-680, 1977.

[4] H. Hashemi, "Simulation of the urban radio propagation channel", Doctoral thesis, University of California, Berkeley, 1977. See also IEEE Trans. Vehic. Techn., Vol. 28, No. 3, pp. 213-225, 1979.

[5] A. A. M. Saleh and R. A. Valenzuela, "A statistical model for indoor multipath propagation", IEEE J. Selec. Areas in Commun., Vol. 5, No. 2, pp. 128-137, 1987.

[6] Q. H. Spencer, B. D. Jeffs, M. A. Jensen, and A. L. Swindlehurst, "Modeling the statistical time and angle of arrival characteristics of an indoor multipath channel", IEEE J. Selec. Areas in Commun., Vol. 18, No. 3, pp. 347-360, 2000.

[7] S. J. Papantoniou, "Modelling the Mobile Radio Channel", PhD thesis, ETHZ, Switzerland, 1990.

[8] H. Iwai and Y. Karasawa, "Wideband Propagation Model for the Analysis of the Effect of the Multipath Fading on the Near-Far Problem in CDMA Mobile Radio Systems", IEICE Trans. Commun., Vol. E76-B, No. 2, pp. 103-112, 1993.

[9] B. H. Fleury, U. P. Bernhard and R. Heddergott, "Advanced Radio Channel Model for Magic WAND", ACTS Mobile Telecommun. Summit, pp. 600-607, 1996.

[10] T. Zwick, C. Fischer and W. Wiesbeck, "A Stochastic Multipath Channel Model Including Path Directions for Indoor Environments", IEEE J. Selec. Areas in Commun., Vol. 20, No. 6, pp. 1178-1192, 2002.

[11] D. L. Snyder, "Random Point Processes", John Wiley & Sons, 1975.

[12] D. L. Snyder and M. I. Miller, "Random Point Processes in Time and Space", Springer, 1991.

[13] F. M. Schubert, M. L. Jakobsen, and B. H. Fleury, "Non-Stationary Propagation Model for Scattering Volumes with an Application to the Rural LMS Channel", IEEE Trans. on Anten. and Prop., Vol. 61, No. 5, pp. 2817-2828, 2013.

[14] J. A. Gubner, B. N. Bhaskar and K. Hao, "Multipath-Cluster Channel Models", IEEE Int. Conf. on UWB, pp. 292-296, 2012.

[15] M. L. Jakobsen, T. Pedersen and B. H. Fleury, "Analysis of the Stochastic Channel Model by Saleh & Valenzuela via the Theory of Point Processes", Proc. Int. Zurich Seminar on Commun., Switzerland, pp. 115-118, 2012.

[16] K. Hao, "Modeling and Statistical Analysis of Ultra-Wideband (UWB) Channels and Systems: A Point-Process Approach", PhD thesis, University of Wisconsin-Madison, USA, 2006.

[17] A. Ridolfi, "Power Spectra of Random Spikes and Related Complex Signals", PhD thesis, EPFL, Switzerland, 2004.

[18] H. Hashemi, "The Indoor Radio Propagation Channel", Proc. IEEE, Vol. 81, No. 7, pp. 943-968, 1993.

[19] H. Hashemi, "Impulse Response Modeling of Indoor Radio Propagation Channels", IEEE J. Selec. Areas in Commun., Vol. 11, No. 7, pp. 967-978, 1993.

[20] A. Papoulis, "Probability, Random Variables and Stochastic Processes", McGraw-Hill, 3rd ed., 1991.

[21] M. Haenggi, J. G. Andrews, F. Baccelli, O. Dousse and M. Franceschetti, "Stochastic Geometry and Random Graphs for the Analysis and Design of Wireless Networks", IEEE J. Selec. Areas in Commun., Vol. 27, No. 7, pp. 1029-1046, 2009.

[22] R. Heddergott, U. P. Bernhard and B. H. Fleury, "Stochastic Radio Channel Model for Advanced Indoor Mobile Communication Systems", IEEE PIMRC, pp. 140-144, 1997.

[23] D. R. Cox and V. Isham, "Point Processes", Chapman & Hall, 1980.

[24] J. F. C. Kingman, "Poisson Processes", Oxford University Press, 1993.

[25] J. Møller and R. P. Waagepetersen, "Statistical Inference and Simulation for Spatial Point Processes", Chapman & Hall/CRC, 2004.

[26] A. J. Baddeley, "Spatial Point Processes and their Applications" (in "Stochastic Geometry - Lecture Notes in Mathematics"), Springer, 2007.

[27] P. A. Bello, "Characterization of Randomly Time-Variant Linear Channels", IEEE Trans. on Commun. Systems, pp. 360-393, 1963.

[28] Y. (G.) Li, L. J. Cimini, Jr. and N. R. Sollenberger, "Robust Channel Estimation for OFDM Systems with Rapid Dispersive Fading Channels", IEEE Trans. on Commun., Vol 46., No. 7, pp. 902-915, 1998.

[29] R. H. Clarke, "A Statistical Theory of Mobile-Radio Reception", Bell Syst. Tech. J., pp. 957-1000, 1968.

[30] M. Gudmundson, "Correlation model for shadow fading in mobile radio systems", IEE Elect. Lett., Vol. 27, No. 23, pp. 2145-2146, 1991.

[31] A. F. Molisch, D. Cassioli, C.-C. Chong, S. Emami, A. Fort, B. Kannan, J. Karedal, J. Kunisch, H. G. Schantz, K. Siwiak and M. Z. Win, "A Comprehensive Standardized Model for Ultrawideband Propagation Channels", IEEE Trans. on Anten. and Prop., Vol. 54, No. 11, pp. 3151-3166, 2006.

[32] A. Abdi, J. A. Barger and M. Kaveh, "A Parametric Model for the Distribution of the Angle of Arrival and the Associated Correlation Function and Power Spectrum at the Mobile Station", IEEE Trans. on Vehic. Techn., Vol. 51, No. 3, pp. 425-434, 2002.

Appendix/Paper B

Analysis of the Stochastic Channel Model by Saleh &
Valenzuela via the Theory of Point Processes

Morten Lomholt Jakobsen, Troels Pedersen and Bernard Henri Fleury

Abstract

In this paper we revisit the classical channel model by Saleh & Valenzuela via the theory of spatial point processes. By reformulating this model as a particular point process and by repeated application of Campbell's Theorem we provide concise and elegant access to its overall structure and underlying features, like the intensity function of the component delays and the delay-power intensity. The flexibility and clarity of the mathematical instruments utilized to obtain these results lead us to conjecture that the theory of spatial point processes provides a unifying mathematical framework to define, analyze, and compare most channel models already suggested in literature and that the powerful tools of this framework have not been fully exploited in this context yet.

1 Introduction

Literature regarding channel models for (indoor) radio propagation dates back earlier than 1960, and most commonly the wireless multipath channel is characterized via its (time and space varying) impulse response [1]. Two classic and seminal contributions within channel modeling are those by Turin et al. [2] and Saleh & Valenzuela [3]. To some extent the (indoor) model by Saleh & Valenzuela can be seen as a generalization of the (urban) model by Turin. Specifically, the generalization aimed at mimicking cluster alike behavior since this effect was reported to have been observed experimentally.

Ever since the model by Saleh & Valenzuela (for short the S-V model) was proposed in 1987, many refined or marginally extended variants have appeared, see e.g. [4] and [5]. Unfortunately, these channel models have not been developed within any unifying mathematical framework. Instead their treatment is of rather ad-hoc nature and, as a result, their inherent features remain essentially veiled and any two different models are not easily comparable.

Recently the authors of [6] and [7] reformulated and outlined the S-V model in terms of marked point processes. The S-V model has also been revisited in [8] by use of shot-noise tools and point process theory. Among other things the analysis in [7] and [8] show that the overall intensity of the relative delays of multipath components grows linearly with the propagation delay. Unfortunately, the mathematical tools used in [7] to extract the features of the model are not directly associated with the general theory of point processes. On the other hand, the tools used in [8] are rather advanced and the derivations less transparent. Accordingly, the potential theoretical benefits arising through these point process reformulations are not immediately evident.

In this paper we showcase how the general theory of spatial point processes provides an insightful view upon the inherent structure and features of the classical S-V model. Like [7] and [8] we revisit the model and reformulate it as a particular point process. Aligned with [7] we show that the component delays consist of the union of a Poisson

point process and a Cox point process and we derive the associated intensity function as an immediate consequence of Campbell's Theorem. The derivation in [7] is similar but with no reference to Campbell's Theorem. Furthermore, and in contrast to the involved proofs relying on shot-noise tools in [8], we obtain the delay-power intensity in a simple and direct way by invoking once more Campbell's Theorem. These results demonstrate the potential of this well-known theorem from the theory of spatial point processes in the context of stochastic channel modeling. In view of this, our conclusion is that the theory of spatial point processes and its powerful tools have not been fully exploited yet to analyze the properties of most proposed stochastic channel models. This theory appears to provide the necessary unifying framework for which these models can be contrasted within.

2 Point Process Framework

We assume familiarity with the basics of the theory of spatial point processes (see [9, Sec. 1.3, Chap. 2] and [10, Sec. 1.5, 6.2] for highly recommendable introductions). Concepts from abstract measure theory will be kept at a minimum.

2.1 Locally finiteness and simplicity

Denote by Y a *locally finite* and *simple* point process defined on a d-dimensional space $S \subseteq \mathbb{R}^d$. For intuitive, practical and mathematical reasons, these two properties are convenient to impose since several technical aspects can then be disregarded. A point process is locally finite if the number of points falling in every *bounded Borel set $B \subseteq S$* is *almost surely* finite. A point process is simple if, almost surely, no two points of the process coincide. Accordingly, any realization of the point process Y can be identified as a countable set of points $\{\boldsymbol{y}_1, \boldsymbol{y}_2, \boldsymbol{y}_3, \dots\}$, $\boldsymbol{y}_i \in S$, where the index i of $\boldsymbol{y}_i$ serves solely as a dummy label. Thus, the index is used only to distinguish points and to indicate countability. It does not indicate any ordering of the points.

2.2 The intensity function and Campbell's Theorem

Consider the *counting function* defined, using a generic indicator function $\mathbb{1}[\cdot] \in \{0, 1\}$, as

$$N_Y(B) := \sum_{\boldsymbol{y} \in Y} \mathbb{1}[\boldsymbol{y} \in B],$$

which equals the random number of points from Y falling in the set B. For any fixed and *bounded B*, the count $N_Y(B)$ is a non-negative integer-valued random variable. The expected value of the counting function $\mu_Y(B) := \mathbb{E}[N_Y(B)]$ defines a *measure* on S,

the so-called *intensity measure* of Y. If the intensity measure can be expressed as

$$\mu_Y(B) = \int_B \varrho_Y(\boldsymbol{y})\mathrm{d}\boldsymbol{y}, \quad B \subseteq S,$$

for a *locally integrable* function $\varrho_Y : S \to [0, \infty)$, then ϱ_Y is called the *intensity function* of Y. The case when the intensity function exists is by far the most important for applications [11]. The importance of the intensity function is evident from the following result, often referred to as *Campbell's Theorem*.

Campbell's Theorem. Let Y be a point process on $S \subseteq \mathbb{R}^d$ with intensity function ϱ_Y. Then for a real or complex-valued *measurable* function $h : S \to \mathbb{R}$ (or $\mathbb{C}$), the random variable $\sum\limits_{\boldsymbol{y} \in Y} h(\boldsymbol{y})$ has expected valued

$$\mathbb{E}\left[\sum_{\boldsymbol{y} \in Y} h(\boldsymbol{y})\right] = \int_S h(\boldsymbol{y})\varrho_Y(\boldsymbol{y})\,d\boldsymbol{y}, \tag{B.1}$$

provided that the integral on the right exists.

Proofs with varying degrees of detail can be found in [9, Sec. 3.2], [11, Prop. 4.1] and [12, Thm. 2.2]. Often, the theorem is stated only for non-negative functions h, since the equality in (B.1) is then unconditionally true, i.e. the integral is always well-defined but possibly divergent. When h is real-valued some care must be taken since the integral at the right hand side of (B.1) has no meaning if the positive and the negative part of h are not integrable. Similar care must be taken for complex h.

2.3   Poisson and Cox point processes

We now define two classes of point processes which are particularly important for our treatment in the forthcoming section, namely Poisson point processes and Cox point processes. These definitions can be found in many text books covering the theory of spatial point processes. Our treatment is directly inspired by [11] and the interested reader may consult [10–12] for further details.

Definition. A point process Y on $S \subseteq \mathbb{R}^d$ is called a *Poisson point process* with intensity function ϱ_Y if:

(i) For any $B \subseteq S$ with $\mu_Y(B) = \int_B \varrho_Y(\boldsymbol{s})\mathrm{d}\boldsymbol{s} < \infty$ the count $N_Y(B)$ is Poisson distributed with mean $\mu_Y(B)$.

(ii) Given that $N_Y(B) = n \in \mathbb{N}$ where $0 < \mu_Y(B) < \infty$, the distribution of $Y \cap B$ is the same as that of n points drawn i.i.d. according to f_B, where

$$f_B(\boldsymbol{s}) := \frac{\varrho_Y(\boldsymbol{s})\mathbb{1}[\boldsymbol{s} \in B]}{\mu_Y(B)}.$$

We write $Y \sim \texttt{PoissonPP}\big(S, \, \varrho_{Y}\big)$.

Definition. Let $Z(\boldsymbol{s})$, $\boldsymbol{s} \in S$, be a non-negative random field such that, almost surely, every realization of Z is a locally integrable function on S. If a point process Y, conditioned on Z, is a Poisson point process with intensity function Z, then Y is called a *Cox point process driven by Z*.

Cox point processes (also often referred to as *doubly stochastic Poisson point processes* [10]) are flexible models for clustered point patterns. Specifically, the two-level construction most commonly entails the Cox class to exhibit so-called *over-dispersion* compared to the Poisson class [11, Sec. 5.2].

3   The Model by Saleh & Valenzuela

In this section we analyze the impulse response of the classical S-V model within the framework of spatial point processes. The main purpose of this effort is to straightforwardly derive the features of this model through a flexible and powerful theory. Several relevant aspects of the model are revealed through this reformulation, e.g. its overall delay intensity, a concise and clear derivation of the average power gain and, a simple derivation of the delay-power intensity as well.

3.1   Classical formulation

Saleh & Valenzuela define the channel impulse response with *cluster* and *within-cluster* delays as [3, Eq. (25)]

$$h(t) = \sum_{\ell=0}^{\infty} \sum_{k=0}^{\infty} \beta_{k,\ell} \exp(j\theta_{k,\ell}) \delta\big(t - (T_\ell + \tau_{k,\ell})\big), \tag{B.2}$$

where δ is the Dirac delta and j is the imaginary unit. The index ℓ indicates a certain cluster and k is the within-cluster index. By definition in [3], $T_0 = 0$ and $\tau_{0,\ell} = 0$ for each $\ell \in \mathbb{N}_0 := \{0\} \cup \mathbb{N}$. Beside these fixed delay components, a sequence of Poisson point processes are suggested such that

- $\big\{T_\ell\big\}_{\ell \in \mathbb{N}} \sim \texttt{PoissonPP}\big(\mathbb{R}_+, \, \Lambda\big)$

- $\big\{\tau_{k,\ell}\big\}_{k \in \mathbb{N}} \sim \texttt{PoissonPP}\big(\mathbb{R}_+, \, \lambda\big)$ for each $\ell \in \mathbb{N}_0$,

with $\Lambda, \lambda > 0$ being two parameters. Moreover, conditional second-order moments are modeled such that [3, Eq. (26)]

$$\mathbb{E}\big[\beta_{k,\ell}^2 \,\big|\, T_\ell, \tau_{k,\ell}\big] = Q \exp\big(-T_\ell/\Gamma\big) \exp\big(-\tau_{k,\ell}/\gamma\big), \tag{B.3}$$

with $\Gamma, \gamma > 0$ and Q being the average power gain of the first component within the first cluster (i.e. corresponding to the fixed delay T_0). Conditioned on all T_ℓ's and all $\tau_{k,\ell}$'s, the $\beta_{k,\ell}$'s are assumed to be mutually independent random variables. Specifically, each power gain $\beta_{k,\ell}^2$, conditioned on T_ℓ and $\tau_{k,\ell}$, should follow an exponential distribution with mean parameter decaying as described by (B.3). Fig. B.1 illustrates the Poisson point processes involved in the S-V model.

Finally, it was mentioned in [3] that practically the doubly-infinite sum in (B.2) should "stop" whenever each of the exponentially decaying terms in (B.3) had become small enough. Through the insight gained via the forthcoming reformulation of this classical channel model we are able to motivate a less heuristic "stopping criterion".

3.2 Point process formulation

Naturally, we select the space $S = \mathbb{R}_+$ and let $T_0 = 0$ as above. In addition, we introduce the point processes:

$$C := \big\{T_\ell\big\}_{\ell \in \mathbb{N}} \qquad\qquad \big(\text{all } \textit{cluster} \text{ delays except } T_0\big)$$

$$W_\ell := \big\{T_\ell + \tau_{k,\ell}\big\}_{k \in \mathbb{N}} \qquad\qquad \big(\text{delays } \textit{within} \text{ the } \ell\text{'th cluster}\big)$$

$$W := \bigcup_{\ell=0}^{\infty} W_\ell \qquad\qquad \big(\text{all } \textit{within-cluster} \text{ delays}\big)$$

$$Y := C \cup W \qquad\qquad \big(\text{all propagation delays except } T_0\big).$$

Notice that C is the Poisson point process specified at first in the previous paragraph. Its intensity function has a simple form, namely $\varrho_C(t) = \Lambda$ for all $t \in S$. By conditioning, we immediately identify a sequence of Poisson point processes

$$W_\ell \big| T_\ell \sim \texttt{PoissonPP}\Big(\mathbb{R}_+,\ \lambda \mathbb{1}\big[t > T_\ell\big]\Big), \quad \ell \in \mathbb{N}_0,$$

and since the Poisson class is stable with respect to countable superpositions [11, Prop. 3.6], we see that

$$W \big| C \sim \texttt{PoissonPP}\Big(\mathbb{R}_+,\ \widetilde{\varrho}_W\Big),$$

with the staircase-alike intensity function

$$\widetilde{\varrho}_W(t) = \lambda + \lambda \sum_{c \in C} \mathbb{1}\big[t > c\big], \quad t \in S. \tag{B.4}$$

Accordingly, we identify that the point process W, without conditioning on C, is a Cox point process driven by a stochastic process Z having the same functional form as $\widetilde{\varrho}_W$ in (B.4) but with C being random. The intensity function of the Cox point process W
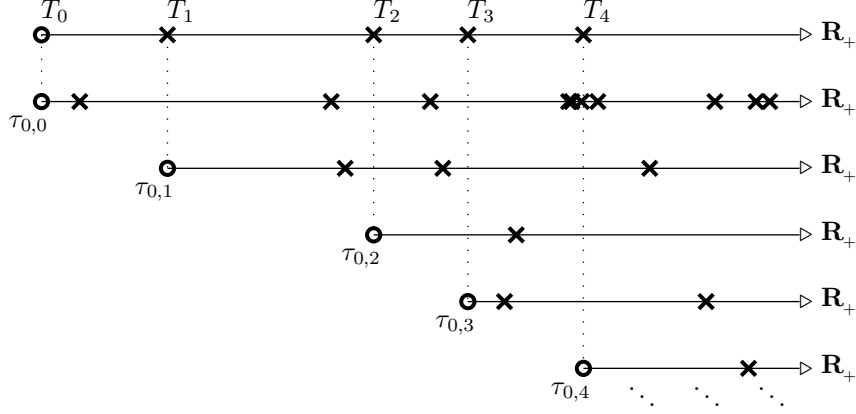
Fig. B.1: Realization of Poisson point processes corresponding to the S-V model. Circle points indicate fixed delay components. The top process occurs with rate Λ while each of the lower processes occurs with rate λ. A new point process is initialized whenever a new point emerges from the top process.

is $\varrho_W(t) = \mathbb{E}\big[Z(t)\big]$ [11, Sec. 5.2], and by direct application of Campbell's Theorem we get

$$\varrho_W(t) = \lambda + \lambda\mathbb{E}\left[\sum_{c\in C}\mathbb{1}\big[t > c\big]\right] = \lambda + \lambda\Lambda t, \quad t \in S.$$

Since $Y = C \cup W$ is a union of almost surely disjoint point processes, its associated intensity function reads [10, Sec. 6.2.3]

$$\varrho_Y(t) = \varrho_C(t) + \varrho_W(t) = \Lambda + \lambda + \lambda\Lambda t, \quad t \in S.$$

It is interesting to notice that the entire set of propagation delays (excluding the first component T_0) is the *union of a Poisson point process and a Cox point process*. Of course, the realization of W depends upon the realization of C, i.e. these two point processes are not independent. In [7] this interpretation was inherently adopted, without being explicitly mentioned. Another interesting yet expected observation is that the intensity function ϱ_Y rises linearly with propagation delay, see Fig. B.2. The jump of height $\Lambda + \lambda$ at $T_0 = 0$ in the graph of ϱ_Y appears due to the cluster delays and the delays within the very first cluster. The term $\lambda\Lambda t$ result from the fact that, on average, a total of Λt additional clusters emerge during the interval $[0, t]$, with each and every one of them spawning further delay components at rate λ.
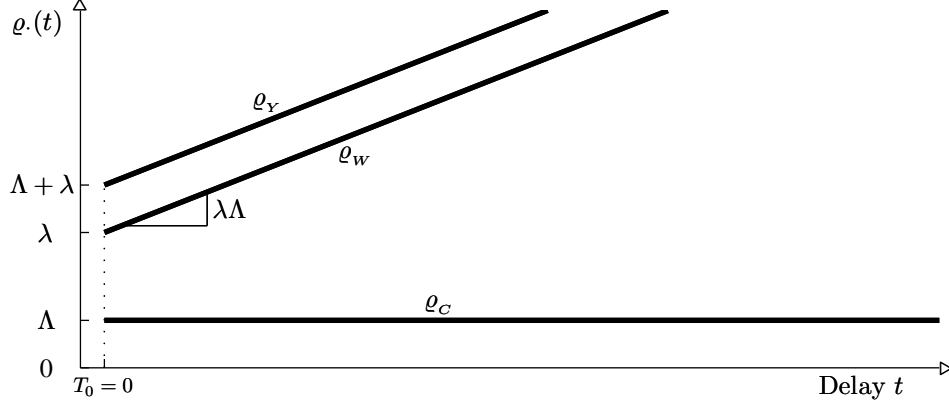
Fig. B.2: Intensity functions associated with the S-V model.

3.3   Multipath power gain

Analogous to the approach in [3], we consider the following non-negative random variable

$$G := \sum_{\ell=0}^{\infty} \sum_{k=0}^{\infty} \beta_{k,\ell}^2, \tag{B.5}$$

referred to as the total *multipath power gain* [3]. By splitting G into three terms corresponding to T_0 and arrivals in C and W, its expectation can be calculated as

$$\mathbb{E}\big[G\big] = \mathbb{E}\big[\beta_{0,0}^2\big] + \mathbb{E}\bigg[\underbrace{\sum_{\ell=1}^{\infty} \beta_{0,\ell}^2}_{(\star)}\bigg] + \mathbb{E}\bigg[\underbrace{\sum_{\ell=0}^{\infty} \sum_{k=1}^{\infty} \beta_{k,\ell}^2}_{(\diamond)}\bigg].$$

As in [3] we write $\beta\big(T_\ell, \tau_{k,\ell}\big)$ in substitute for $\beta_{k,\ell}$ to facilitate a comprehensible notation in the following. For additional clarity we introduce the function

$$f\big(t, \tilde{t}\big) := Q \exp\big(-t/\Gamma - \tilde{t}/\gamma\big), \quad t, \tilde{t} \in S.$$

Notice that $f\big(T_\ell, \tau_{k,\ell}\big) = f\big(T_\ell, (T_\ell + \tau_{k,\ell}) - T_\ell\big)$ coincides with the expression in (B.3). Then, by intermediate conditioning on C, we calculate the expectation of the term $(\star)$ as

$$\mathbb{E}\big[(\star)\big] = \mathbb{E}\bigg[\sum_{c \in C} \beta^2(c,0)\bigg] = \mathbb{E}\bigg[\sum_{c \in C} \mathbb{E}\underbrace{\big[\beta^2(c,0)\,\big|\,C\big]}_{f(c,0)}\bigg] = Q\Lambda\Gamma,$$

where the final step follows by application of Campbell's Theorem. Next, by defining $C_0 := \{T_0\} \cup C$ and with a similar sequence of manipulations involving intermediate conditioning and Campbell's Theorem, we find the expected value of $(\diamond)$ to be[1]

$$\mathbb{E}\big[(\diamond)\big] = \mathbb{E}\bigg[\sum_{c \in C_0} \sum_{w \in W_c} \beta^2(c, w - c)\bigg] \tag{B.6}$$

$$= \mathbb{E}\bigg[\sum_{c \in C_0} \mathbb{E}\bigg[\sum_{w \in W_c} \mathbb{E}\big[\underbrace{\beta^2(c, w - c)|c, w}_{f(c, w-c)}\big]\bigg]\bigg] = Q\big(1 + \Lambda\Gamma\big)\lambda\gamma.$$

Accordingly, the average total power gain is given by

$$\mathbb{E}\big[G\big] = \mathbb{E}\big[\beta_{0,0}^2\big] + \mathbb{E}\big[(\star)\big] + \mathbb{E}\big[(\diamond)\big]$$
$$= \quad Q \quad + \quad Q\Lambda\Gamma \quad + \quad Q\big(1 + \Lambda\Gamma\big)\lambda\gamma$$
$$= Q\big(1 + \lambda\gamma\big)\big(1 + \Lambda\Gamma\big), \tag{B.7}$$

as was also reported in a footnote in [3]. Yet, the original sequence of arguments used to obtain this result may appear less instructive, see [3, Eq. (27), (31)] for comparison. Notice that, depending on how we choose to write out the product in (B.7), we end up with different interpretations of individual average power contributions.

3.4   Delay-power intensity

Motivated by the definition of G in (B.5) together with the relationship in (B.7), we consider

$$p(t) := \sum_{\ell=0}^{\infty} \sum_{k=0}^{\infty} \beta_{k,\ell}^2 \delta\big(t - (T_\ell + \tau_{k,\ell})\big).$$

We wish to calculate how the average power gains are distributed across delay. From (B.7) we already know the mean total power gain, yet we seek to obtain further insight. The above definition of $p(t)$ is motivated by the fact that $\int_0^{\infty} p(t)\mathrm{d}t = G$, and since $\mathbb{E}[G]$ is finite, the non-negative random variable G is itself finite almost surely. Accordingly, we define

$$P(t) := \mathbb{E}\big[p(t)\big], \quad t \in S,$$

and we refer to this function as the *delay-power intensity*. By similar manipulations as in the previous paragraph (conditioning, Campbell's Theorem, etc.) we find

$$\frac{P(t)}{Q} = \delta(t) + \begin{cases} k_1 \exp\big(-\frac{1}{\Gamma}t\big) + k_2 \exp\big(-\frac{1}{\gamma}t\big), & \Gamma \neq \gamma \\ \varrho_{\scriptscriptstyle Y}(t) \exp\big(-\frac{1}{\gamma}t\big) & , \;\; \Gamma = \gamma \end{cases}$$

---

[1] Note that in (B.6) we abuse notation since the collections W_c are not explicitly defined. We only defined these as W_ℓ via the counting index ℓ.
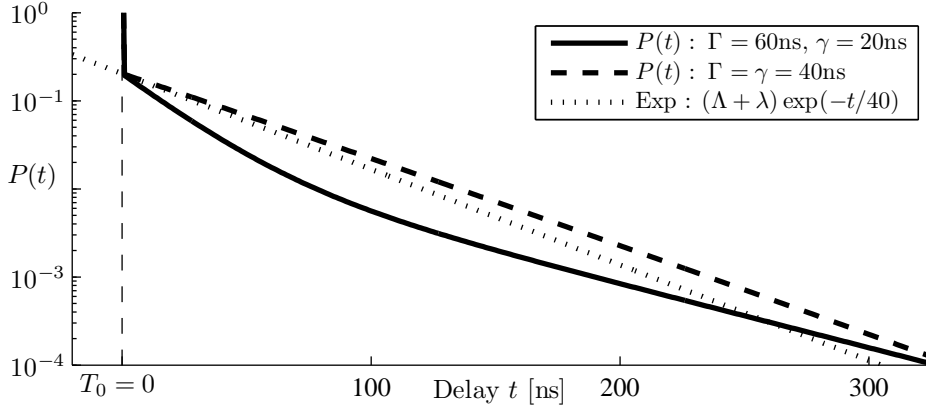
Fig. B.3: Delay-power intensity of the S-V model (solid line). The parameter values of $\Lambda, \lambda, \Gamma, \gamma$ correspond to the estimates reported in [3]. The dashed curve correspond to the selection $\Gamma = \gamma = 40\text{ns}$. For comparison, the dotted curve provides a purely exponential decay.

where we have conveniently introduced the two constants

$$k_1 := \Lambda\left(1 + \lambda\frac{\Gamma\gamma}{\Gamma-\gamma}\right) \quad \text{and} \quad k_2 := \lambda\left(1 - \Lambda\frac{\Gamma\gamma}{\Gamma-\gamma}\right).$$

The same expression for $P(t)$ is obtained in [8, Chap. 2,3] using rather involved shot-noise tools with weighty notational overhead. Notice the particular relationship

$$\mathbb{E}[G] = \mathbb{E}\left[\int_0^\infty p(t)\mathrm{d}t\right] = \int_0^\infty \mathbb{E}\big[p(t)\big]\mathrm{d}t = \int_0^\infty P(t)\mathrm{d}t.$$

The delay-power intensity of the S-V model is depicted in Fig. B.3. Notice that $P(t)$ is *not exponentially decaying*, not even when $\Gamma = \gamma$ since ϱ_Y rises linearly (compare with the dotted line in Fig. B.3).

Finally, as mentioned in the beginning of this section, we are now able to motivate a simple "stopping criterion" suitable, e.g. for simulation purposes. Specifically, select a delay threshold $t_{\max}(\alpha)$ such that

$$\int_0^{t_{\max}(\alpha)} P(t)\mathrm{d}t = \alpha\mathbb{E}[G],$$

for a relevant choice of $\alpha \in (0,1)$, e.g. $\alpha = 0.99$.

4   Conclusion

In this contribution we have revisited the radio channel model by Saleh & Valenzuela (the S-V model) within the framework of spatial point processes. We have shown that the component delays in the S-V model emerge from the union of a Poisson point process and a Cox point process. Furthermore, we have demonstrated that the intensity function of the component delays and the delay-power intensity can be derived in a straightforward and rigorous manner as an immediate consequence of Campbell's Theorem.

The above results indicate that the theory of spatial point processes yields a natural, unifying theoretical framework for dealing with stochastic channel models. This applies in particular to most channel models already suggested in literature, including the models by Turin et al. [2], Spencer et al. [4], and Chong et al. [5]. Our results also reveal that the powerful tools available in this framework, like Campbell's Theorem, have not been exploited to their full extent in this context yet. Overall the considered application to the S-V model and to some extent the work in [6–8] show that the resulting mathematical treatments inherit clarity and conciseness, in addition to rigorousness, in contrast to the traditionally used ad-hoc and heuristic arguments.

Acknowledgment

References

[1] H. Hashemi, "The Indoor Radio Propagation Channel", *Proc. IEEE*, '93.

[2] G. L. Turin et al, "A statistical model of urban multipath propagation", *IEEE Trans. Vehic. Techn.*, 1972.

[3] A. A. M. Saleh and R. A. Valenzuela, "A statistical model for indoor multipath propagation", *IEEE J. Selected Areas in Commun.*, 1987.

[4] Q. H. Spencer et al, "Modeling the statistical time and angle of arrival characteristics of an indoor multipath channel", *IEEE JSAC*, 2000.

[5] C.-C. Chong et al, "A modified S-V clustering channel model for the UWB indoor residential environment", *IEEE VTC*, 2005.

[6] A. Ridolfi, "Power Spectra of Random Spikes and Related Complex Signals", PhD thesis, EPFL, Lausanne, Switzerland, 2004.

[7] R. F. Brøndum and E. Rubak, "Stochastic Channel Modelling - A Bayesian approach using reversible jump Markov chain Monte Carlo methods", Master's thesis, Aalborg University, Denmark, 2006.

[8] K. Hao, "Modeling and Statistical Analysis of Ultra-Wideband (UWB) Channels and Systems: A Point-Process Approach", PhD thesis, University of Wisconsin-Madison, Wisconsin, USA, 2006.

[9] J. F. C. Kingman, "Poisson Processes", Oxford University Press, 1993.

[10] J. Illian et al, "Statistical Analysis and Modelling of Spatial Point Patterns", John Wiley & Sons, 2008.

[11] J. Møller and R. P. Waagepetersen, "Statistical Inference and Simulation for Spatial Point Processes", Chapman & Hall/CRC, 2004.

[12] A. J. Baddeley, "Spatial Point Processes and their Applications" (in "Stochastic Geometry - Lecture Notes in Mathematics"), Springer, 2007.

Appendix/Paper C

Parametric Modeling and Pilot-Aided Estimation of the Wireless Multipath Channel in OFDM Systems

Morten Lomholt Jakobsen, Kim Laugesen, Carles Navarro Manchón,
Gunvor E. Kirkelund, Christian Rom and Bernard Fleury

Abstract

In this paper we present a refined model of the wireless multipath channel along with a thorough analysis on the impact of spatial smoothing techniques when used for improved channel estimation. The state-of-the-art channel estimation algorithm for pilot-aided OFDM systems is robustly designed and operates without knowledge of the time-varying multipath propagation delays in the wireless channel. However, algorithms exploiting knowledge of these time-varying delay parameters can outperform the state-of-the-art solution. We demonstrate from simulations how the Unitary ESPRIT algorithm together with spatial smoothing techniques exhibit a promising potential for multipath propagation delay estimation. Furthermore, we show that the optimum smoothing parameters depend notably on the channel model assumed, specifically in terms of the dynamical behavior of the multipath delays.

1   Introduction

During the last decade, the technique of *orthogonal frequency-division multiplexing* (OFDM) has entered and settled within several wireless standards, e.g. European digital audio broadcasting, IEEE 802.11a wireless local area networking and 3GPP *long term evolution* (LTE). The reasons for OFDM being widely selected are manifold. A few motivations include the flexibility in spectrum occupancy, robustness against inter-symbol-interference and easy integration with multiple antenna techniques.

Today, even higher data rates are demanded - calling for larger digital constellation sizes and coherent detection. Channel estimation is therefore required and commonly achieved using pilot symbol transmissions. In principle, the channel estimation may be conducted in a completely non-parametric manner. However, this approach conflicts with the requirement of high data rates due to the dimensionality of the estimation problem and also due to the time-varying behavior of the wireless channel (expensive time-frequency overhead of pilot symbols). With the aim of lowering the dimension of the estimation task and the amount of pilot symbols needed, a parametric structure of the wireless multipath channel is typically imposed [1–4]. Yet, the parametric channel model assumed in scientific literature and wireless standards [5] does not adequately reflect dynamic environments, e.g. with a mobile receiver. For instance, the multipath propagation delays, the inter-delay gaps and the overall number of delays are often modeled as persistently fixed - even though the receiver is assumed to be moving. Furthermore, it is common to include modeling of the Doppler frequency shifts experienced by the receiver [2, 4] - despite the fact that Doppler shifts and delay fluctuations are indisputably related. Hence, the default and widely used modeling of the wireless channel is counterintuitive and inadequate.

When employing the state-of-the-art channel estimator [1] (robust design), the fluc-

tuating behavior of the multipath delays are of no importance since a continuum of equally powered channel components is assumed. However, this robust design yields an irreducible performance degradation which is avoidable if instead a channel estimator presupposing knowledge of the time-varying delays is used. Hence, if sufficiently accurate delay estimates can be obtained, the robust state-of-the-art channel estimator [1] can be outperformed. Yet, for this opposing solution to earn practical attention it requires a sufficiently accurate/realistic model of the wireless multipath channel.

In recent literature [2] the ESPRIT algorithm [6] has been proposed to serve as initial multipath delay acquisition tool for pilot-aided OFDM systems. The ESPRIT algorithm is an eigenvalue decomposition based method which exhibits satisfactory estimation performance when the multipath propagation delays in the channel model stay persistently fixed. However, in more realistic scenarios the propagation delays will fluctuate over time, the overall number of delays will change and also the inter-delay gaps will vary. Thus, depending on the individual realizations of the channel the delays will sometimes tend to cluster while other times tend to be more dispersed. Such effects are typically not captured by the channel models in use. Accordingly, promising simulation-based algorithm performance may implicitly give rise to erroneous comprehension - directly inherited from the inappropriate channel modeling.

In this paper we present an advanced multipath channel model which manages to mimic an increased amount of real-world channel effects. Compared to the default state-of-the-art channel model, this advanced model is of supplementary dynamic nature and therefore allows for interesting simulation-based comparisons. In terms of channel estimation performance we compare the state-of-the-art algorithm [1] with the *linear minimum mean squared error* (LMMSE) estimator [2] using Unitary ESPRIT [7] as multipath delay estimation tool. Additionally, a key contribution of this paper is a thorough analysis of the performance gain obtained when applying a spatial smoothing scheme for improved delay estimation accuracy. The smoothing scheme is also employed in [2], yet no analysis of its impact is provided and no justification for the smoothing parameters are given. We investigate how to optimize the smoothing parameters depending on the dynamical behavior of the wireless multipath channel model assumed.

The remaining parts of this paper are organized as follows. In Section 2 a scenario involving an OFDM system is described and the signal model is presented. The channel models considered are introduced and discussed in Section 3. In Section 4 we briefly describe the main principles of the ESPRIT algorithm. Performance evaluations are conducted and compared in terms of Monte-Carlo simulations in Section 5. Concluding remarks are provided in Section 6.

2 OFDM Signal Model

We consider a single-input single-output OFDM system designed with a total of N subcarriers. The effective spectrum occupied by the system is often adjusted by forcing

certain subcarriers inactive, for instance at each edge of the overall bandwidth. Accordingly, only $N_u \leq N$ subcarriers are used for actual transmissions.

The OFDM signal is generated as follows. Initially, a stream of raw information bits are modulated onto a set of PSK/QAM symbols which are then multiplexed with a sequence of M pilot symbols. After multiplexing the sequence consists of exactly N_u symbols $x_1, x_2, \ldots, x_{N_u}$, and these are intended for transmission. Finally, OFDM modulation by means of an IFFT is performed and a cyclic prefix is inserted.

The received signal is OFDM demodulated by discarding the samples corresponding to the cyclic prefix and the N time-domain samples left are exposed to a FFT. We assume that the channel remains static during transmission of each OFDM symbol and furthermore that the duration of the cyclic prefix exceeds the maximum excess delay of the channel. The OFDM demodulated signal at the receiver is then given as

$$\boldsymbol{r} = \left[r_1, r_2, \ldots, r_{N_u}\right]^\top = \mathbf{X}\boldsymbol{h} + \boldsymbol{w}, \tag{C.1}$$

where $\mathbf{X} = \operatorname{diag}\left\{x_1, x_2, \ldots, x_{N_u}\right\}$ is a diagonal matrix built from the transmitted symbols and $\boldsymbol{h} = [h_1, h_2, \ldots, h_{N_u}]^\top$ contains as components the channel frequency responses at the N_u active subcarriers. Circular symmetric additive white Gaussian noise contributions with variance σ^2 are contained in the vector $\boldsymbol{w} = [w_1, w_2, \ldots, w_{N_u}]^\top$.

2.1 Pilot Symbol Observations

The received pilot symbol observations are used to estimate the channel frequency response at all subchannels carrying non-redundant data symbols. Conveniently, we define the following subset of indices

$$\mathcal{P} := \left\{p(1), p(2), \ldots, p(M)\right\} \subset \left\{1, 2, \ldots, N_u\right\},$$

which identifies the M subcarriers used for pilot symbol transmissions. We extract the M equations from (C.1) corresponding to the indices contained in $\mathcal{P}$ and define

$$y_m := \frac{r_{p(m)}}{x_{p(m)}}, \qquad m = 1, 2, \ldots, M,$$

which we can appropriately and compactly formulate as

$$\boldsymbol{y} := \left(\mathbf{X}_{\mathcal{P}}\right)^{-1}\boldsymbol{r}_{\mathcal{P}} = \boldsymbol{h}_{\mathcal{P}} + \left(\mathbf{X}_{\mathcal{P}}\right)^{-1}\boldsymbol{w}_{\mathcal{P}}, \tag{C.2}$$

meanwhile the subscript notation should be obvious to interpret. We assume that all pilot symbols hold unit power, whereby the statistics of the noise term $\left(\mathbf{X}_{\mathcal{P}}\right)^{-1}\boldsymbol{w}_{\mathcal{P}}$ remains unchanged. Hence, the observations available in (C.2) are known to the receiver due to the pilot symbol data and $\boldsymbol{y}$ yields the true channel frequency responses (at the pilot subcarriers) embedded in zero-mean complex Gaussian noise. To properly estimate

the channel frequency responses at *all* active subcarriers, i.e. the vector $\boldsymbol{h}$ in (C.1), a parametric model of the wireless channel is invoked. In this way the dimension is notably reduced since the task is now altered to estimate only a relatively small number of channel model parameters.

3   Multipath Channel Models

Two different multipath channels are presented in this section. The overall model for these two channels is the same and the first configuration described is simpler but unrealistic with respect to certain physical interpretations. The second configuration described is more dynamic and sophisticated while easier to accept from a physical point of view. In the entire paper we assume a non-line-of-sight, far-field scenario where *only* the receiver is moving.

The model commonly used to describe a time-varying multipath channel impulse response is given by

$$g(t,\tau) = \sum_{\ell=1}^{L(t)} \alpha_\ell(t)\delta\big(\tau - \tau_\ell(t)\big), \tag{C.3}$$

where δ is the Dirac delta. Each complex-valued amplitude α_ℓ, $\ell = 1, 2, \ldots, L(t)$, is typically modeled as a wide-sense stationary, zero-mean complex Gaussian process [1–4]. The processes $\{\alpha_\ell\}$ are furthermore assumed to be mutually uncorrelated, i.e. the channel described by (C.3) is a so-called *wide-sense stationary* and *uncorrelated scattering* [8] (WSSUS) Rayleigh fading channel.

3.1   Static Reference Channel

The simpler and static channel model is described according to a relaxed version of (C.3) reading

$$g(t,\tau) = \sum_{\ell=1}^{L} \alpha_\ell(t)\delta(\tau - \tau_\ell). \tag{C.4}$$

The overall number L of echoes in the channel is fixed and also the delay parameters $\{\tau_\ell\}$ are persistently static. All amplitude processes $\{\alpha_\ell\}$ are assumed to share the same normalized autocorrelation function, given in terms of the zeroth-order Bessel function of the first kind. Accordingly, the normalized Doppler power spectrum associated with each echo is bathtub-shaped and usually referred to in terms of Clarke or Jakes, see [9, Sec. 3.2] and the references therein. Such modeling is based on the assumption of a *uniform scattering environment*, a scenario which is difficult to accept by physical means. Specifically, it is hard to imagine a propagation environment such that the transmitted signal is scattered into plenty reflections arriving uniformly from every direction, all equally delayed, and thereby combining into one of the L dominant echoes

in the channel. Nonetheless, such a channel model is usually assumed, e.g. by 3GPP in [5].

3.2 Dynamic Channel

A more realistic model would allow for the delay parameters to fluctuate over time as a result of receiver mobility. Also, the overall number of echoes in the channel may change from time to time due to blocking obstacles in the environment. Hence, a channel impulse response as described by (C.3) is appropriate and notably more realistic than the model in (C.4). Initially, for $\ell = 1, 2, \ldots, L(t)$, the channel echoes are modeled as

$$\alpha_\ell(t) = \sqrt{\frac{Q_\ell}{R}} \sum_{r=1}^{R} \exp\left(j2\pi f_D \cos(\theta_{\ell,r})t + j\varphi_{\ell,r}\right), \tag{C.5}$$

where Q_ℓ is the average power of the ℓ'th echo, f_D denotes the maximum Doppler frequency and $\{\varphi_{\ell,r}\}$ are i.i.d. uniform initial phases. In contrast to the uniform scattering environment, each channel echo α_ℓ in (C.5), is (heuristically) modeled from R azimuth excited subcomponents centered around a nominal angle of arrival $\bar{\theta}_\ell$. Specifically, the modeling reads

$$\bar{\theta}_\ell \overset{\text{i.i.d.}}{\sim} \mathcal{U}(-\pi, \pi) \qquad \text{and} \qquad \theta_{\ell,r} \big| \bar{\theta}_\ell \overset{\text{i.i.d.}}{\sim} \text{vM}(\bar{\theta}_\ell, \kappa),$$

where the notation $\text{vM}(\bar{\theta}_\ell, \kappa)$ refers to the *von Mises* distribution with location parameter $\bar{\theta}_\ell$ and concentration parameter $\kappa \geq 0$, see [10] for details. In this setup the channel echoes do *not* share the same normalized autocorrelation function and the Doppler power spectra are therefore individual too.

Following the modeling suggestion in [11], it is convenient to let transitions of arising channel echoes occur according to a homogeneous Poisson process with rate λ_A. Assigning i.i.d. exponential lifetimes with mean $1/\lambda_B$ to the echoes then results in $L(t)$ being a Poisson distributed random variable with $\mathbb{E}[L(t)] = \lambda_A/\lambda_B$. For simplicity and due to our receiver mobility assumption, it is furthermore convenient to model the delay fluctuations from straight line advancements, i.e.

$$\tau_\ell(t) = \tau_{\ell,0} + \frac{f_D \cos(\bar{\theta}_\ell)}{f_c}(t - t_{\ell,0}), \qquad t \geq t_{\ell,0},$$

where f_c denotes the carrier frequency of the communication system and $t_{\ell,0}$ is the birth time of the ℓ'th echo. The distribution of the initial delays $\{\tau_{\ell,0}\}$ can be specified as desired - a simple choice is to select the uniform distribution on an appropriate interval. The average power terms $\{Q_\ell\}$ may then be assigned according to an exponentially decaying function (i.e. the power delay profile is specified). The straight line advancements of the multipath delays are illustrated in Fig. C.1 which reports a ten seconds
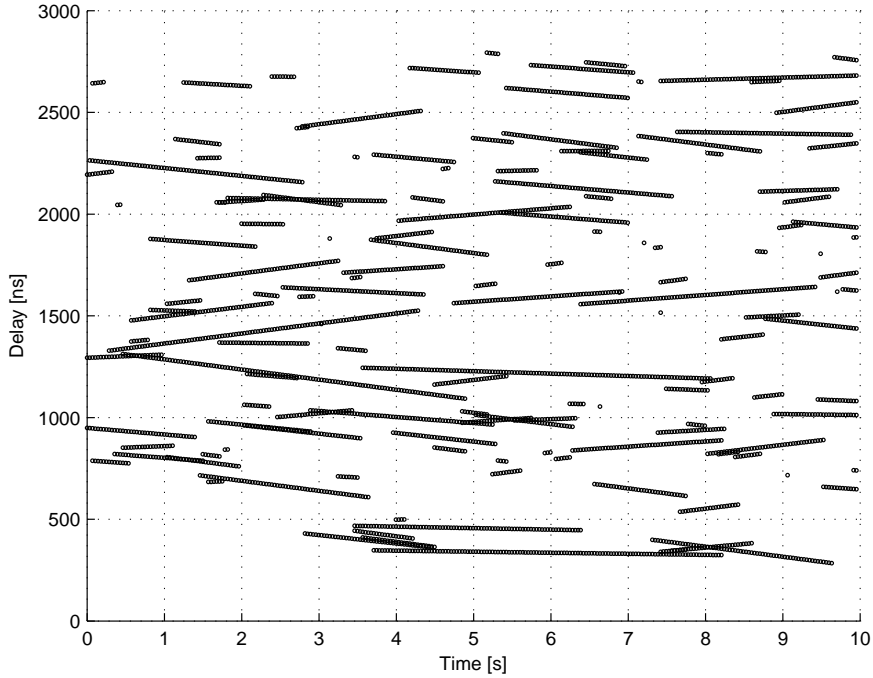
Fig. C.1: Contiguous realization of the dynamic channel with maximum Doppler frequency $f_D = 100$Hz and carrier frequency $f_c = 2$GHz.

realization of the dynamic channel with $\mathbb{E}\big[L(t)\big] = 15$ delays on average. As can be seen from the figure the channel exhibits a reasonable amount of dynamical behavior, e.g. the overall number of delays is changing over time and also the straight line patterns of the delays are quite apparent.

The simpler and more static channel model described comprises the state-of-the-art reference. The intention with the more realistic and dynamic channel model described is to mimic a time-varying and fluctuating behavior of $L(t)$, $\big\{\tau_\ell(t)\big\}$ and $\big\{|\tau_\ell(t) - \tau_k(t)|\big\}$. Our goal is to investigate how incorporation of such dynamics affects the pilot-aided channel estimation performance.

4 Propagation Delay Estimation

Assuming the reference channel model (C.4) as described in Section 3.1, we reformulate the observation model (C.2) as

$$\boldsymbol{y} = \mathbf{T}(\boldsymbol{\tau})\boldsymbol{\alpha} + \boldsymbol{n}, \tag{C.6}$$

where we have introduced a $M \times L$ matrix $\mathbf{T}(\boldsymbol{\tau})$, the vector $\boldsymbol{\alpha} = [\alpha_1, \alpha_2, \ldots, \alpha_L]^\top$ and the additive noise vector $\boldsymbol{n}$. The matrix $\mathbf{T}(\boldsymbol{\tau})$ depends on the delay parameters and the pilot symbol positions in such a way that its (m, ℓ)'th entry reads

$$\mathbf{T}_{m,\ell} = \exp\Big(-j2\pi \frac{p(m)}{N}\frac{\tau_\ell}{T_{\mathrm{s}}}\Big), \qquad \begin{matrix} m = 1, 2, \ldots, M, \\ \ell = 1, 2, \ldots, L, \end{matrix}$$

where T_{s} denotes the sampling time of the communication system. Notice that the L columns building up the matrix $\mathbf{T}(\boldsymbol{\tau})$ are of identical structure and by system design the parameters N, T_{s} and $\mathcal{P}$ are known - only the delays $\{\tau_\ell\}$ are unknown. The theoretical covariance matrix associated with $\boldsymbol{y}$ reads

$$\mathbf{R} := \mathbb{E}\Big[\boldsymbol{y}\boldsymbol{y}^H\Big] = \mathbf{T}(\boldsymbol{\tau})\mathbf{A}\mathbf{T}^H(\boldsymbol{\tau}) + \sigma^2\mathbf{I}_M, \tag{C.7}$$

where we have implicitly assumed that any component of $\boldsymbol{\alpha}$ is statistically independent of any component of $\boldsymbol{n}$. Furthermore, $\mathbf{A} := \mathbb{E}\big[\boldsymbol{\alpha}\boldsymbol{\alpha}^H\big]$ is a $L \times L$ diagonal matrix due to the uncorrelated scattering assumption. Notice in (C.7), that since the delay parameters are assumed static the covariance matrix $\mathbf{R}$ does not change over time.

Now, any vector in the null space of $\mathbf{T}^H(\boldsymbol{\tau})$ is an eigenvector of $\mathbf{R}$ with associated eigenvalue σ^2. Therefore, the particular eigenvectors of $\mathbf{R}$ not belonging to the null space of $\mathbf{T}^H(\boldsymbol{\tau})$ are all associated with eigenvalues strictly greater than σ^2. This key fact provides insight on how the signal subspace and the noise subspace can be separated according to the individual magnitudes of the eigenvalues. From a proper design of the set $\mathcal{P}$, the structure inherited by the matrix $\mathbf{T}(\boldsymbol{\tau})$ allows for two specific submatrices to be related by a simple rotational (i.e. unitary) transform. Estimation of this unitary transform is essentially how the ESPRIT algorithm is used to estimate the unknown delay parameters, see [2].

Obviously, the theoretical covariance matrix $\mathbf{R}$ is not available. Instead the ESPRIT algorithm is applied to some 'prudent' estimate of the matrix. Observations which we denote by $\big\{\boldsymbol{y}_k\big\}$ are collected temporally, and in a generic manner we arrange K of such vectors in the $M \times K$ matrix

$$\mathbf{Y} := \begin{bmatrix} | & | & & | \\ \boldsymbol{y}_1 & \boldsymbol{y}_2 & \cdots & \boldsymbol{y}_K \\ | & | & & | \end{bmatrix}. \tag{C.8}$$

The estimate used could then be the sample covariance matrix

$$\widehat{\mathbf{R}} := \frac{1}{K}\mathbf{Y}\mathbf{Y}^H \qquad \text{or} \qquad \widetilde{\mathbf{R}} := \frac{1}{2}\Big(\widehat{\mathbf{R}} + \mathbf{J}\widehat{\mathbf{R}}^\top \mathbf{J}\Big),$$

where $\widetilde{\mathbf{R}}$ is the centrosymmetric equivalent[1] of $\widehat{\mathbf{R}}$. Here $\mathbf{J}$ denotes the $M \times M$ reversal matrix with 1's in its entire anti-diagonal and 0's elsewhere, see [12, Sec. 4.8, 6.5.8].

If instead we assume the more realistic and dynamic channel model (C.3) as described in Section 3.2, the entire situation is crucially altered. In (C.6), the delay parameter $\boldsymbol{\tau} = \boldsymbol{\tau}(t)$ is now time-variant and the basis of the underlying signal subspace is therefore changing over time (potentially, the dimension changes too, e.g. while gathering data for the matrix $\mathbf{Y}$). Essentially, the rotational transform to be estimated is time-variant since the delay parameters no longer stay fixed and hence, the basic assumptions for ESPRIT are not satisfied. Yet, by considering only time frames of sufficiently short duration, the delay fluctuations can be considered negligible. Finally, to achieve improved estimation accuracy and reduced complexity we employ Unitary ESPRIT [7], not standard ESPRIT.

4.1 Spatial Smoothing

To decrease any disturbing impact from the time-varying delay parameters it seem obvious to use an observation matrix $\mathbf{Y}$ where K is as small as possible. With K small, only a few observations are collected in the time direction and this fact complies well with the rigorous latency requirements of today's communication systems. If the number of pilot symbols M is relatively large and if the set $\mathcal{P}$ is designed appropriately, we can apply a so-called spatial smoothing technique. By doing so we artificially build up more time-direction observations by suffering on overall dimension (aperture) in the frequency direction. By applying a vertical sliding window of size $M_1 \leq M$ to the $M \times K$ matrix in (C.8) we obtain a new observation array of size

$$M_1 \times K(M - M_1 + 1).$$

Notice how the attribute of wide-sense stationarity in the frequency domain (inherited from the uncorrelated scattering assumption in the delay domain) is paramount when applying the smoothing window. Obviously, the number M_1 should be chosen according to a trade-off between aperture and estimation accuracy. Choosing M_1 smaller generates more snapshots while is (simultaneously) penalized by poorer ability to resolve closely displaced delay parameters. Notice that with $K = 1$ the data matrix $\mathbf{Y}$ in (C.8) has unit rank and consequently $\widehat{\mathbf{R}}$ only holds a single nonzero eigenvalue. In this case we should indeed make sure that $M - M_1 + 1$ exceeds the total number of delays in the channel

---

[1] The theoretical covariance matrix in (C.7) is Toeplitz when the subcarrier spacings between adjacent pilots are all identical.

- otherwise there are not enough nonzero eigenvalues for ESPRIT to process. Spatial smoothing techniques are commonly employed to decorrelate coherent signal sources, see e.g. [13] and the references therein.

5 Performance Evaluation

In this section we evaluate the pilot-assisted channel estimation performance of the LMMSE estimator from [2] using Unitary ESPRIT as delay estimation tool. For all configurations considered we evaluate uncoded *bit-error-rate* (BER) performance of the OFDM system. We investigate the impact of spatial smoothing as a function of the window size M_1 and the two different channel models are treated separately. We consider a 3GPP LTE alike scenario with system parameters:

$$N = 2048, \ N_u = 1200, \ T_{\mathrm{s}} = 32.55\mathrm{ns}, \ M = 200.$$

The duration of the cyclic prefix is 4.69μs, corresponding to 144 T_{s}-samples. A total of 14 OFDM symbols are transmitted every millisecond and four of these carry $M = 200$ pilots each. We assume the pilot symbols to be evenly positioned along the $N_u = 1200$ active subchannels with a fixed spacing of six subcarriers, i.e.

$$\mathcal{P} = \big\{3, 9, 15, \dots, 597, 603, \dots, 1185, 1191, 1197\big\}. \tag{C.9}$$

The set of pilot symbol positions $\mathcal{P}$ in (C.9) represents a uniform linear array of sensors with maximum overlap. The carrier frequency of the system is assumed to be $f_c = 2$GHz and we consider a receiver traveling at walking speed, i.e. the maximum Doppler frequency is assumed to be $f_D = 10$Hz. The digital modulation scheme used is QPSK (gray coded), both for data symbols and pilot symbols.

5.1 Performance in Static Reference Channel

As the static reference channel we employ the 3GPP EVA-profile from [5, Annex B.2] which constantly holds $L = 9$ multipath echoes with fixed delays and its maximum excess delay is approximately half the duration of the cyclic prefix. To visualize how the window size M_1 impacts the overall system performance, we consider a span from $M_1 = 200$ towards $M_1 = 10$, corresponding to no smoothing and full-scale smoothing, respectively. Figure C.2 reports the uncoded BER-performance of the OFDM system as a function of the window size M_1. We always feed the true number of delays (i.e. $L = 9$) directly to Unitary ESPRIT, since estimation of the number of channel echoes is not an objective in this paper. In Fig. C.2, it is interesting to note that a rather wide range of window sizes are leading to the same degree of performance (near to that of using known channel coefficients). Even with $K = 1$ we realize that near-optimal performance is achievable. However, additional smoothing is required and the
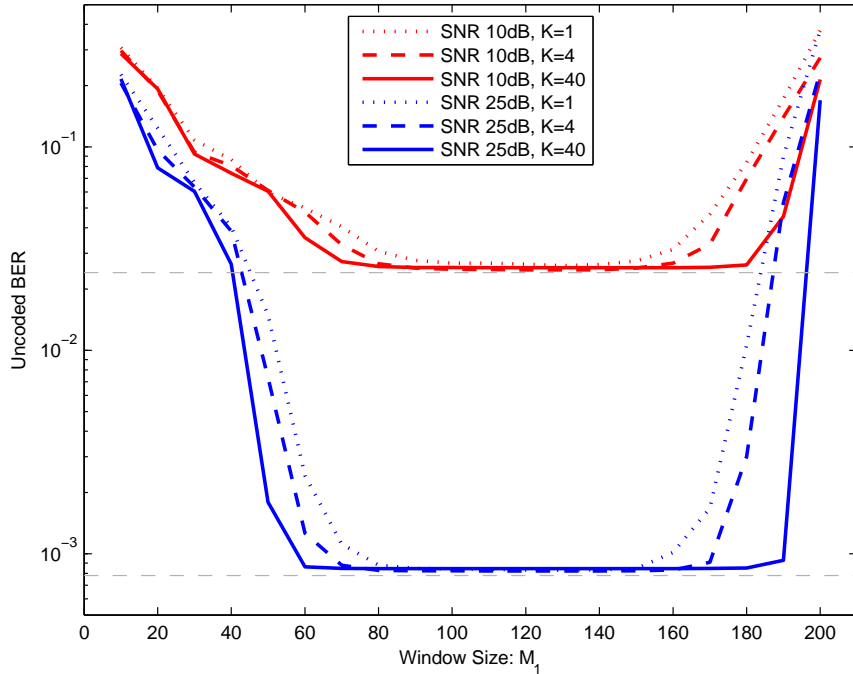
Fig. C.2: BER performance as a function of M_1. The two grey-dashed lines indicate the BER performance at 10dB and 25dB of *signal-to-noise ratio* (SNR) using true/known channel frequency responses.

range of window sizes inheriting splendid performance is more tight when K is smaller. Notice also the immediate and steep performance gains obtained when M_1 decreases from its maximum value $M = 200$. This behavior partly reflects the fact that rank is building up in the covariance matrix estimate, cf. the discussion at the end of Section 4. Finally, recall that the inter-delay gaps are persistently fixed in this scenario and hence, the resolvability issues for Unitary ESPRIT to deal with are identical/constant for *all* individual channel realizations.

5.2   Performance in Dynamic Multipath Channel

With a channel inheriting additional dynamical behavior we now repeat the same simulation study as just described in the previous section. Hence, we wish to visualize the impact of the window size M_1 in a scenario where the delay resolvability issue is non-constant across the individual realizations of the channel. For simulation technical
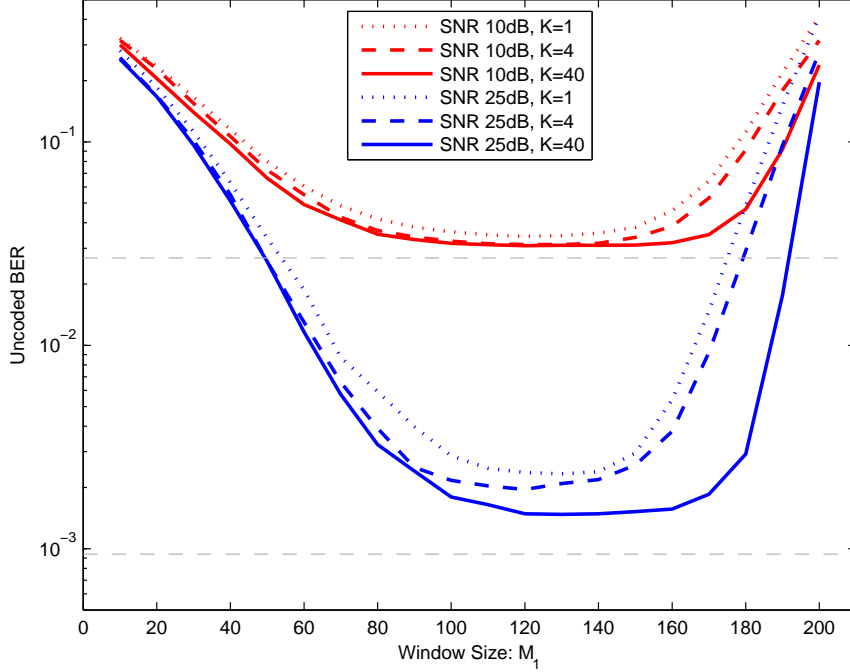
Fig. C.3: BER performance as a function of M_1. The two grey-dashed lines indicate the BER performance at 10dB and 25dB of SNR using true/known channel frequency responses.

reasons the dynamic channel holds fifteen echoes on average[2], i.e. $L(t)$ is Poisson distributed with mean parameter equal to 15. The maximum excess delay is the same as for the static reference channel and also the power delay profile is similar to that of the static reference channel. Since $\mathbb{E}\big[L(t)\big] = 15$, then roughly anything from five to twenty-five echoes can be observed in the instantaneous realizations of the channel. In some realizations the delays will tend to cluster while in others tend to be more dispersed. As before, we feed the true number of delays to Unitary ESPRIT such that it always seeks for the instantaneous amount of channel echoes. Figure C.3 illustrates how the window size M_1 affects the system performance in this case.

As can be readily seen from Fig. C.3, the wide range of window sizes leading to the same degree of performance is not present anymore. The curves are still bathtub shaped, however, notably less steep and edged compared to Fig. C.2. Also, none of the curves appear tight along the known channel bound as in the first case considered.

---

[2]Basically, we require $P\big(L(t) = 0\big)$ to be negligible.

This is jointly caused by the fact that more delays have to be estimated on average and since the instantaneous realizations of the channel sometimes trigger the delays more clustered. If for system design purposes we were to select and fix a single value of M_1, then based on Fig. C.2, anything in the range from 90 to 150 would seem appropriate. Based on Fig. C.3, however, the optimum value of M_1 seems to appear tightly around 120.

5.3   State-of-the-art Comparison

To get a full picture of the BER performance across a wide SNR-range we have fixed $M_1 = 120$ and conducted another simulation study. We now compare the LMMSE estimator from [2] using Unitary ESPRIT against the robustly designed state-of-the-art channel estimator from [1]. Our comparison is carried out using the dynamical channel with parameters as in the previous section. Figure C.4 reports the outcome, where two selected values for K are shown, namely $K = 1$ and $K = 40$.

In the SNR-range from -10dB to 15dB the state-of-the-art solution is marginally outperformed with $K = 1$. However, when using $K = 40$ the state-of-the-art solution is more notably outperformed and in a slightly wider SNR-range. That is, better or similar performance can be achieved using the LMMSE estimator from [2] together with Unitary ESPRIT. Yet, the state-of-the-art solution operates on lower computational complexity and this fact directly implies a need for complexity reductions in order to comparably gain the performance enhancements suggested in Fig. C.4.

Notice from Fig. C.2, where the static channel model was assumed, that a similar study as reported in Fig. C.4 would conclude that the state-of-the-art solution could be notably outperformed in the entire SNR-range considered, even with $K = 1$. This follows since the BER performance in Fig. C.2 with $K = 1$ and $M_1 = 120$ is almost as good as using known channel frequency responses, both at 10dB and 25dB of SNR. The point here is that the channel model selection can importantly affect the results obtained. In general, validity of the evaluated algorithm performance is achieved through adequate and comprehensive modeling.

6   Conclusion

In this paper we have considered channel estimation techniques for pilot-aided OFDM systems, where the estimation is grounded on a parametric model of the wireless channel. The multipath delay parameters in the channel model have been estimated via the Unitary ESPRIT algorithm and spatial smoothing techniques have been applied to improve the estimation accuracy. Incorporation of the delay estimates in a LMMSE estimator allows for improved performance compared to the robustly designed state-of-the-art solution. That is, the state-of-the-art channel estimator can be outperformed
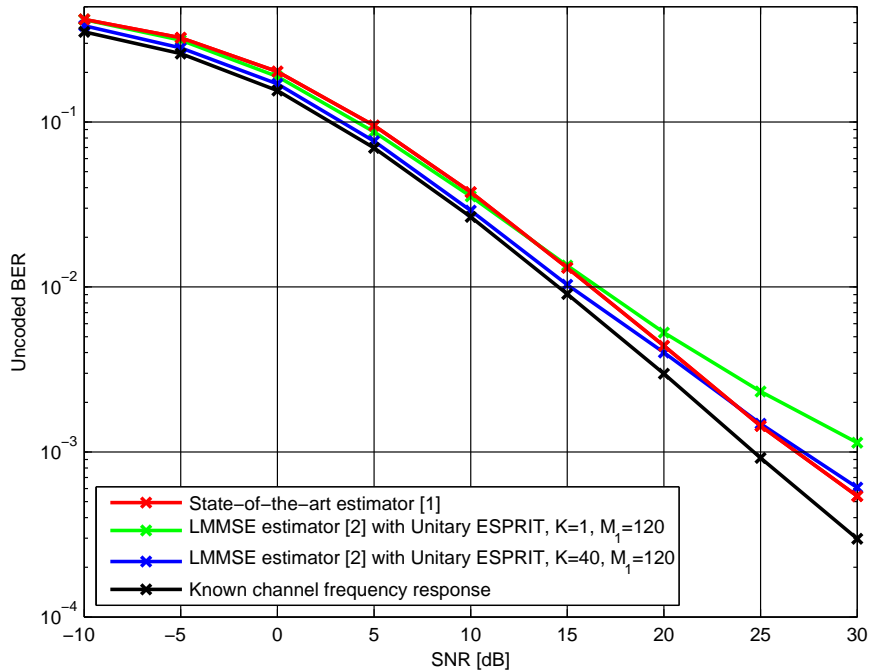
Fig. C.4: BER-performance as a function of average SNR.

over a wide SNR-range. Yet, computational complexity and estimation of the instantaneous number of channel echoes remain critical issues for the opposing channel estimator investigated.

In order to provide a rigorous performance assessment of the opposing channel estimation solution, we have compared state-of-the-art channel modeling against a refined channel model of additional dynamical nature. The main additional features comprise a time-varying number of channel echoes together with fluctuating delay positions, i.e. non-constant inter-delay gaps. From simulations we have analyzed the impact of spatial smoothing techniques when used to improve the multipath delay estimation accuracy. Our results indicate that both estimation accuracy and the optimum smoothing parameters are notably affected with increased dynamical behavior of the channel model assumed.

To conclude, our work shows that the selection of appropriate channel models is crucial when assessing the performance of receiver algorithms. Choosing inadequate models may imply misleading comprehension and could therefore yield improper algorithm selection for practical applications.

Acknowledgment

References

[1] O. Edfors, M. Sandell, J.-J. van de Beek, S. K. Wilson and P. O. Börjesson, "OFDM Channel Estimation by Singular Value Decomposition", *IEEE Transactions on Communications*, Vol. 46, No. 7, 1998.

[2] B. Yang, K. B. Letaief, R. S. Cheng and Z. Cao, "Channel Estimation for OFDM Transmission in Multipath Fading Channels Based on Parametric Channel Modeling", *IEEE Transactions on Communications*, 2001.

[3] J.-J. van de Beek, O. Edfors, M. Sandell, S. K. Wilson and P. O. Börjesson, "On Channel Estimation in OFDM Systems", *In Proceedings of the IEEE Vehicular Technology Conference*, Vol. 2, 1995.

[4] Y. Li, L. J. Cimini Jr. and N. R. Sollenberger, "Robust Channel Estimation for OFDM Systems with Rapid Dispersive Fading Channels", *IEEE Transactions on Communications*, Vol. 46, No. 7, 1998.

[5] "Evolved Universal Terrestrial Radio Access; Base Station Radio Transmission and Reception", *3rd Generation Partnership Project (3GPP) Technical Specification*, TS 36.104 V8.4.0, December 2008.

[6] R. Roy and T. Kailath, "ESPRIT - Estimation of Signal Parameters Via Rotational Invariance Techniques", *IEEE Transactions on Acoustics, Speech and Signal Processing*, Vol. 37, No. 7, 1989.

[7] M. Haardt and J. A. Nossek, "Unitary ESPRIT: How to Obtain Increased Estimation Accuracy with a Reduced Computational Burden", *IEEE Transactions on Signal Processing*, Vol. 43, No. 5, 1995.

[8] P. A. Bello, "Characterization of Randomly Time-Variant Linear Channels", *IEEE Transactions on Communications Systems*, 1963.

[9] A. Goldsmith, "Wireless Communications", *Cambridge University Press*, 2005.

[10] A. Abdi, J. A. Barger and M. Kaveh, "A Parametric Model for the Distribution of the Angle of Arrival and the Associated Correlation Function and Power Spectrum at the Mobile Station", *IEEE Transactions on Vehicular Technonlgy*, Vol. 51, No. 3, 2002.

[11] R. Heddergott, U. P. Bernhard and B. H. Fleury, "Stochastic Radio Channel Model For Advanced Indoor Mobile Communication Systems", *Proceedings of the 8th IEEE International Symposium on Personal, Indoor and Mobile Radio Communications*, Vol. 1, 1997.

[12] P. Stoica and R. Moses, "Spectral Analysis of Signals", *Pearson Prentice Hall*, 2005.

[13] H. Krim and M. Viberg, "Two Decades of Array Signal Processing Research: The Parametric Approach", *IEEE Signal Processing Magazine*, Vol. 13, No. 4, 1996.

References

Appendix/Paper D

Non-Stationary Propagation Model for Scattering Volumes with an Application to the Rural LMS Channel

Frank M. Schubert, Morten L. Jakobsen and Bernard H. Fleury

Abstract

The design of efficient positioning algorithms in navigation satellite systems, like GNSS, operating in land mobile environments demands for detailed models of the radio channel. On the one hand, the models need to accurately describe scattering and shadowing/obstruction caused by vegetation. On the other hand, they have to incorporate the steady change in the propagation constellation due to the receiver displacement. In this paper we propose a model of the non-stationary radio channel in a scenario where a mobile receiver drives past a scattering volume, such as a ball or a cuboid, while the transmitter is elevated, like in satellite positioning applications. Such a volume may represent the canopy of a single tree, the canopies of trees in a grove, or a small forest. Scattering by the volume is characterized by means of multiple point-source scatterers that are assumed to form a marked spatial point process. The system functions of the radio channel are given. An integral form of the time-frequency correlation function of the component in the system functions contributed by the scattering volume is obtained as a direct consequence of Campbell's Theorem. Furthermore, a closed-form approximation of this integral form is derived for time lags corresponding to displacements along the receiver trajectory for which the plane wave assumption holds. The approximation takes into account the steady change in the propagation constellation. The proposed model is validated by means of Monte Carlo simulations and by comparing its prediction capabilities with experimental data in a scenario where a mobile receiver drives past a roadside tree. A good agreement is observed, despite the simplicity of the model.

1   Introduction

Signal scattering, shadowing, and obstruction caused by vegetation and human infrastructures in the surrounding of the mobile receiver of a Global Navigation Satellite System (GNSS) may impair the system performance. The deterioration by such wave propagation effects can be severe if no measure is taken to counterbalance them [1–3]. In rural land-mobile satellite (LMS) environments these propagation effects result mainly from vegetation, like single trees, alleys of trees, groves or forests. Furthermore, for vehicular and pedestrian applications, the steady alteration of the propagation constellation as the receiver moves makes the radio channel non-stationary.

Different models characterizing the propagation effects induced by vegetation, in particular by trees and forests, have been published so far. In the sequel, we briefly review these models and their main features. To do so we categorize the models into narrowband and wideband models, depending on whether they discard or incorporate the specific relative delays of multipath components.

Several narrowband models have been proposed that describe the temporal signal fluctuation experienced by a mobile driving past roadside vegetation. In Loo's LMS

model [4] the complex signal is the sum of a line of sight (LOS) component weighted with a log-normal attenuation factor and a complex Gaussian component accounting for local scattering. The paper [5] presents experimental cumulative signal fade and fade duration statistics obtained in an LMS scenario with roadside trees for both cases with and without shadowing. In [6] the incoherent scattering of a deciduous treetop is derived based on Twersky's multiple scattering theory when the tree is in leaf and defoliated. The same method is applied in an LMS model characterizing the signal fluctuation caused by roadside trees [7]. Radiative transfer models based on the radiative energy theory [8] have also been proposed, which mimic the scattering of trees and vegetation layers, see [9, 10] and the references therein.

Since delay dispersion in the channel has been recognized as one of the most significant effects impairing the ranging ability of GNSS terminals, the attention has focused on wideband characterization and modeling of vegetation. The paper [11] presents results from 2 GHz wideband measurements of scattering by a single tree. In [2] Koh models the GNSS channel in a scenario where the receiver is surrounded by a number of trees: the attenuation through the canopy is modeled using Foldy's approximation, while the scattering is the result of diffraction from finite dielectric cylinders representing tree branches. The investigations in these two papers inherently account for the temporal dispersion caused by individual trees; however, they consider static scenarios.

Time-variant wideband models, which account for the variation of the propagation constellation as the receiver moves, have been published in [12–14]. The LMS model [12] includes a three-state Markov chain which drives the dynamic change of the level of shadowing/obstruction of the LOS component. In the GNSS models presented in [13, 14] shadowing/obstruction of the LOS signal of a satellite is determined by human-made and natural structures, like buildings, trees, etc., randomly selected and placed in a virtual scenery in which the receiver moves. Both models consider multipath propagation as well. The parameters of the multipath components are drawn according to probability distributions estimated from aggregated measurement data. Thus, each generated multipath component conceptually represents the contribution by a virtual scattering object or structure. This scatterer is, however, not linked to any underlying scenery.

Recent experimental investigations of the temporal dispersion by trees in an LMS environment have revealed that the delay spread caused by the geometrical size of trees might be of the same order of magnitude as the inverse signal bandwidth of GNSS, and therefore affects the performance of such systems [15]. Motivated by this observation we present in this paper a model that describes the system functions of the radio channel[1] in a scenario where a mobile receiver drives past a bounded scattering volume, while the transmitter is elevated with respect to the receiver's trajectory and the volume. The

---

[1] We understand as system function any of the four equivalent functions entering in the four integral forms characterizing the input-output relationship of a time-variant linear channel [16]. In this contribution we will focus on the time-variant (temporal or delay) response, the time-variant (frequency) transfer function, and the delay-Doppler spread function of the radio channel.

model belongs to the class of geometric-stochastic channel models (GSCM): it takes into account the geometry of the scenario, i.e. the position of the transmitter, the trajectory of the mobile as well as the location and the size of the scattering volume; the scattering process in the volume is modeled as resulting from random point-source scatterers located in this volume. For simplicity of the presentation, one single scattering volume is considered. The extension to several such volumes is straightforward.

A point-source scatterer is characterized by its position in the volume and its complex scattering coefficient. We model the set of scatterers as a marked spatial point process [17, 18], i.e. the set of scatterer positions is a random point process characterized by a (spatial) intensity function, while the scattering coefficients form the marks of the point process. The statistics of the marks are specified by their conditional first and second moments given the scatterer positions. In particular, given the underlying point configuration, the marks are assumed to be mutually uncorrelated. The advantage of modeling point-source scatterers as a marked point process is manifold. First, this approach includes the traditional method where the number of point-source scatterers is considered fixed, see e.g. [12]. However, the approach also allows for the number of scatterers to be random. Second, the theoretical tools from the theory of point processes can be exploited to compute in a rigorous manner specific functions characterizing the statistical properties of the channel system functions as we will see later[2]. Due to the constant change in the propagation constellation along the trajectory of the moving receiver, the time-variant transfer function of the radio channel is a non-stationary process.

The model provides expressions for the time-variant response and the time-variant transfer function of the radio channel. An integral-form expression for the time-frequency correlation function of the component in the channel system functions that is contributed by the scattering volume is derived by invoking Campbell's Theorem. A closed-form approximation of this correlation function is derived for time lags corresponding to displacements along the trajectory for which the plane wave assumption holds. The model is verified and validated experimentally with wideband measurements and by means of Monte Carlo simulations in a LMS scenario where the volume represents a treetop. Despite its simplicity (no consideration of e.g. the attenuation by leaves, the multiple scattering in the canopy, and diffraction by the trunk) a very good agreement is observed.

This paper is organized as follows. Sec. 2 describes the considered scenario with a mobile driving past a single scattering volume, states the model assumptions, and provides the time-variant response and the time-variant transfer function of the radio channel. The time-frequency correlation function is derived in Sec. 3, together with its

---

[2]The benefit of revisiting traditional approaches for stochastic modeling of the radio channel within the theory of spatial point processes has been recently exemplified with the model by Saleh and Valenzuela [19], see [20–22]. Specific statistical properties and functions of this model, like the rate of occurrence of multipath components on the delay axis and the delay power spectrum, could be derived within this theoretical framework.
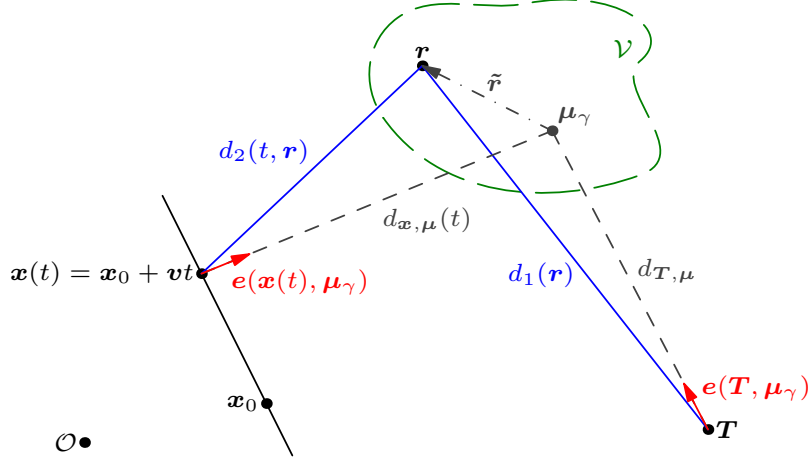
Fig. D.1: Generic LMS scenario with a mobile receiver moving nearby a single scattering volume $\mathcal{V}$: the transmitter is located at position $\boldsymbol{T}$, the receiver moves at constant velocity along the straight trajectory $\boldsymbol{x}(t)$. In the figure, $\mathcal{O}$ denotes the origin of the coordinate system, $\boldsymbol{r}$ is the position of a point-source scatterer in the volume, while $\boldsymbol{x}_0$ and $\boldsymbol{v}$ denote respectively the position at $t = 0$ and the velocity of the receiver. The figure also includes the quantities that appear in the approximations of $d_1(\boldsymbol{r})$ and $d_2(t, \boldsymbol{r})$ introduced in the sequel (see (D.24) and (D.25)).

closed-form approximation. We provide numerical examples in Sec. 4. Sec. 5 concludes with a summary of presented results including their significance and an outlook.

2 Signal Model

In this section we develop a non-stationary GSCM describing the system functions of the radio channel in a scenario where a receiver drives past a scattering volume, while the transmitter is elevated with respect to the volume and the receiver trajectory, see Fig. D.1. An antenna mounted on the top of a vehicle driving along a trajectory $\boldsymbol{x}(t) \in \mathbb{R}^3$ captures the electromagnetic field, which consists of the superposition of the field contributed by the electromagnetic wave impinging directly from the transmitter located at $\boldsymbol{T} \in \mathbb{R}^3$ and the field re-scattered by the volume $\mathcal{V} \subset \mathbb{R}^3$. Here $\mathbb{R}^3$ is used to denote three-dimensional Euclidean space. We assume that the volume is bounded, i.e. $|\mathcal{V}| = \int_{\mathcal{V}} 1 \, d\boldsymbol{r} < \infty$, and that it is sparsely filled with point-source scatterers. For the sake of simplifying the presentation we consider the case with a single volume only. The extension to several scattering volumes is straightforward.

With the scattering volume representing vegetation, like a single tree, a grove, or a forest, and the transmitter being embarked in a satellite, the scenario is typical for LMS applications. Notice that the model is also suitable for representing scattering by other

objects of large dimension such as human infrastructures, like buildings.

2.1   Modeling Assumptions

We group the model assumptions into three categories according to whether they relate to the scattering volume, the geometrical configuration including the vehicle dynamics, or the signals contributed by the electromagnetic waves re-scattered by the volume.

General points in $\mathbb{R}^3$ are denoted by $\boldsymbol{b}$ whereas points corresponding to the point-source scatterers are denoted by $\boldsymbol{r}$.

M1 Scattering volume:

a) The random set of positions of point-source scatterers in the bounded volume $\mathcal{V}$ is a (spatial) point process Π with intensity function $\varrho : \mathcal{V} \to [0, \infty)$. Given the point configuration Π, we assume that a complex-valued scattering coefficient $\beta_{\boldsymbol{r}} \in \mathbb{C}$ is attached to each $\boldsymbol{r} \in \Pi$. Each pair of position and coefficient $(\boldsymbol{r}, \beta_{\boldsymbol{r}})$ describes a point-source scatterer. The collection of all such pairs

$$\{(\boldsymbol{r}, \beta_{\boldsymbol{r}}) : \boldsymbol{r} \in \Pi\} \subset \mathbb{R}^3 \times \mathbb{C} \tag{D.1}$$

forms a so-called *marked* point process [17, 18].

b) Conditioned on Π, the scattering coefficients are mutually uncorrelated, zero-mean random variables such that[3]

$$\mathbb{E}\left\{\beta_{\boldsymbol{r}}^* \beta_{\boldsymbol{r}'} \big| \boldsymbol{r}, \boldsymbol{r}'\right\} = Q(\boldsymbol{r}) \mathbb{1}\left\{\boldsymbol{r} = \boldsymbol{r}'\right\}, \tag{D.2}$$

where $Q : \mathcal{V} \to [0, \infty)$ is a function specifying the conditional power of the scattering coefficient $\beta_{\boldsymbol{r}}$ given its associated location $\boldsymbol{r}$.

c) The product of the intensity function $\varrho(\boldsymbol{r})$ and the power assigning function $Q(\boldsymbol{r})$ is finite on $\mathcal{V}$, i.e. there exists a constant C such that $\varrho(\boldsymbol{b})Q(\boldsymbol{b}) \leq C$ for all $\boldsymbol{b} \in \mathcal{V}$.

d) No multiple scattering occurs in the volume $\mathcal{V}$.

M2 Geometrical configuration and dynamics:

a) The receiver drives past the volume $\mathcal{V}$ along a straight trajectory $\boldsymbol{x}(t)$ with constant velocity vector $\boldsymbol{v}$.

b) The receiver trajectory does not cross $\mathcal{V}$, i.e. $\boldsymbol{x}(t) \notin \mathcal{V}$ for all time instances t. In fact, for consistency in subsequent M3, we assume that the smallest distance from $\boldsymbol{x}(t)$ to $\mathcal{V}$ is always greater than unity.

---

[3]$\mathbb{E}\{\cdot\}$ denotes expectation and $\mathbb{1}\{\cdot\}$ is a generic indicator function.

c) The transmitter's location $\boldsymbol{T}$ as well as the locations of scatterers in Π stay fixed.

d) The transmitter is elevated with respect to $\boldsymbol{x}(t)$ and $\mathcal{V}$. Hence, we consider a three-dimensional model.

M3 Wave propagation:

a) The waves re-scattered by the point-source scatterers in $\mathcal{V}$ are approximated along $\boldsymbol{x}(t)$ as spherical waves.

2.2 Implications and Remarks

The assumptions in M1 provide certain degrees of freedom allowing for some flexibility in the definition of the random cloud of scatterers:

1. The scatterers' locations and the average number of scatterers are governed by the intensity function $\varrho(\boldsymbol{r})$. Specifically, the shape of $\varrho(\boldsymbol{r})$ indicates where points are more likely to occur. The average number of point-source scatterers falling within the volume $\mathcal{V}$ is

$$\mathbb{E}\left\{\sum_{\boldsymbol{r}\in\Pi}\mathbb{1}\left\{\boldsymbol{r}\in\mathcal{V}\right\}\right\}=\int_{\mathcal{V}}\varrho(\boldsymbol{r})\,\mathrm{d}\boldsymbol{r}. \tag{D.3}$$

The identity in (D.3) is a special instance of the famous Campbell Theorem [17, 18]. A location independent intensity appears when $\varrho(\boldsymbol{r})=\varrho_0\mathbb{1}\left\{\boldsymbol{r}\in\mathcal{V}\right\}$. In this case, the positive constant ϱ_0 can be interpreted as the average number of points per unit volume. A non-constant intensity function may be used to model e.g. a treetop with a higher occurrence of scatterers around the center compared to the border.

2. The scatterers' conditional power is determined by the function $Q(\boldsymbol{r})$. In the model we do not specify the statistical properties of the marks $\{\beta_{\boldsymbol{r}} : \boldsymbol{r}\in\Pi\}$ conditioned on the point process beyond their first and second moments. We show later that this will suffice to compute the first- and second-order characteristics of the channel responses. Thus, the conditional probability distributions of the marks are only relevant in that their mean vanishes and their second moments, via $Q(\boldsymbol{r})$, are specified.

3. Location-wise interaction between scatterers can be accounted for via the type of point process assumed for Π, e.g. a Poisson point process, a cluster point process or any other point process on $\mathcal{V}\subset\mathbb{R}^3$ exhibiting desirable properties.

4. Traditional models use a fixed number of scatterers. Such an approach can be seen as a special case of the proposed method when Π is a binomial point process.

Finally, notice that with M3 we assume the receiver trajectory $\boldsymbol{x}(t)$ to be in the far-field region of the volume $\mathcal{V}$.

2.3   Baseband Representation of the Time-Variant Response and the Time-Variant Transfer Function

We model the time-variant response as being the superposition of a LOS component $h_\mathrm{d}(t,\tau)$ due to direct propagation and a component $h_\mathrm{s}(t,\tau)$ contributed by the scatterers $\big\{(\boldsymbol{r},\beta_{\boldsymbol{r}}) : \boldsymbol{r} \in \Pi\big\}$:

$$h(t,\tau) = h_\mathrm{d}(t,\tau) + h_\mathrm{s}(t,\tau). \tag{D.4}$$

The LOS component is given by

$$h_\mathrm{d}(t,\tau) = \exp\left(-j2\pi\frac{d_\mathrm{d}(t)}{\lambda}\right)\delta\big(\tau - \tau_\mathrm{d}(t)\big) \tag{D.5}$$

where λ denotes the wavelength, $d_\mathrm{d}(t) \triangleq \|\boldsymbol{T} - \boldsymbol{x}(t)\|$ is the direct Euclidian distance from $\boldsymbol{T}$ to $\boldsymbol{x}(t)$, and δ is the Dirac delta. The flight time of this direct signal reads

$$\tau_\mathrm{d}(t) \triangleq d_\mathrm{d}(t)/c_0, \tag{D.6}$$

where $c_0 = \lambda f_\mathrm{c}$ is the speed of light and f_c denotes the carrier frequency. Note that the unobstructed LOS signal is normalized to unit amplitude.

In the sequel we focus on the component $h_\mathrm{s}(t,\tau)$ of the channel response solely originating from the scattering volume. According to the set of assumptions M1, $h_\mathrm{s}(t,\tau)$ is the sum of multipath components contributed by the point-source scatterers in $\mathcal{V}$:

$$h_\mathrm{s}(t,\tau) = \sum_{\boldsymbol{r}\in\Pi} \alpha(t,\boldsymbol{r})\delta\big(\tau - \tau_\mathrm{s}(t,\boldsymbol{r})\big). \tag{D.7}$$

Here, $\tau_\mathrm{s}(t,\boldsymbol{r})$ denotes the total signal flight time from the transmitter via a scatterer at location $\boldsymbol{r}$ to the receiver. It can be obtained from the signal's traveled distance from $\boldsymbol{T}$ via $\boldsymbol{r}$ to $\boldsymbol{x}(t)$:

$$d_\mathrm{s}(t,\boldsymbol{r}) \triangleq c_0\tau_\mathrm{s}(t,\boldsymbol{r}) = d_1(\boldsymbol{r}) + d_2(t,\boldsymbol{r}), \tag{D.8}$$

where

$$d_1(\boldsymbol{r}) \triangleq \|\boldsymbol{T} - \boldsymbol{r}\| \tag{D.9}$$

$$d_2(t,\boldsymbol{r}) \triangleq \|\boldsymbol{x}(t) - \boldsymbol{r}\|, \tag{D.10}$$

see Fig. D.1. From assumption M3 the component weight associated with $\boldsymbol{r}$ reads

$$\alpha(t,\boldsymbol{r}) = \frac{\beta_{\boldsymbol{r}}}{d_2(t,\boldsymbol{r})} \exp\left(-j2\pi\frac{d_\mathrm{s}(t,\boldsymbol{r})}{\lambda}\right). \tag{D.11}$$

$$R(f, f', t, t') = \int_{\mathcal{V}} \frac{Q(\boldsymbol{r})\varrho(\boldsymbol{r})}{d_2(t, \boldsymbol{r})d_2(t', \boldsymbol{r})} \exp\left(-j2\pi c_0^{-1}\big[d_1(\boldsymbol{r}), d_2(t, \boldsymbol{r}), d_2(t', \boldsymbol{r})\big] \cdot \bar{\boldsymbol{f}}\right) \mathrm{d}\boldsymbol{r} \tag{D.15}$$

$$R(f, f', t, t') = \Gamma \mathbb{E}_\gamma \left\{ \frac{1}{d_2(t, \boldsymbol{r})d_2(t', \boldsymbol{r})} \exp\left(-j2\pi c_0^{-1}\big[d_1(\boldsymbol{r}), d_2(t, \boldsymbol{r}), d_2(t', \boldsymbol{r})\big] \cdot \bar{\boldsymbol{f}}\right) \right\} \tag{D.20}$$

$$\approx \Gamma \underbrace{\mathbb{E}_\gamma \left\{ \frac{1}{d_2(t, \boldsymbol{r})d_2(t', \boldsymbol{r})} \right\}}_{E_1} \underbrace{\mathbb{E}_\gamma \left\{ \exp\left(-j2\pi c_0^{-1}\big[d_1(\boldsymbol{r}), d_2(t, \boldsymbol{r}), d_2(t', \boldsymbol{r})\big] \cdot \bar{\boldsymbol{f}}\right) \right\}}_{E_2} \tag{D.21}$$

The distance $d_2(t, \boldsymbol{r})$ in the denominator of (D.11) reflects the inverse-square law of power attenuation of spherical waves versus distance. Notice that we always have $d_2(t, \boldsymbol{r}) \geq 1$ due to M2 b). Inserting (D.11) in (D.7) yields

$$h_{\mathrm{s}}(t, \tau) = \sum_{\boldsymbol{r} \in \Pi} \frac{\beta_{\boldsymbol{r}}}{d_2(t, \boldsymbol{r})} \exp\left(-j2\pi \frac{d_{\mathrm{s}}(t, \boldsymbol{r})}{\lambda}\right) \delta\big(\tau - \tau_{\mathrm{s}}(t, \boldsymbol{r})\big). \tag{D.12}$$

The time-variant transfer function is the partial Fourier transform with respect to the delay variable of the time-variant response. As with the time-variant response in (D.4), the time-frequency transfer function can be split into a component due to LOS propagation and a component originating from the scattering volume:

$$H(t, f) = \mathcal{F}\{h(t, \tau)\} = H_{\mathrm{d}}(t, f) + H_{\mathrm{s}}(t, f).$$

The latter component is of main interest. From (D.12) we have

$$H_{\mathrm{s}}(t, f) = \sum_{\boldsymbol{r} \in \Pi} \frac{\beta_{\boldsymbol{r}}}{d_2(t, \boldsymbol{r})} \exp\left(-j2\pi(f_{\mathrm{c}} + f)\frac{d_{\mathrm{s}}(t, \boldsymbol{r})}{c_0}\right). \tag{D.13}$$

$$R(f, f', t, t') \approx \Gamma \frac{1}{d_{\boldsymbol{x},\boldsymbol{\mu}}(t) d_{\boldsymbol{x},\boldsymbol{\mu}}(t')} \left(1 + \frac{\boldsymbol{e}(\boldsymbol{x}(t), \boldsymbol{\mu}_\gamma)^{\mathrm{T}} \boldsymbol{\Sigma}_\gamma \boldsymbol{e}(\boldsymbol{x}(t'), \boldsymbol{\mu}_\gamma)}{d_{\boldsymbol{x},\boldsymbol{\mu}}(t) d_{\boldsymbol{x},\boldsymbol{\mu}}(t')}\right)$$
$$\times \exp\left(-j2\pi c_0^{-1} \big[d_{\boldsymbol{T},\boldsymbol{\mu}}, d_{\boldsymbol{x},\boldsymbol{\mu}}(t), d_{\boldsymbol{x},\boldsymbol{\mu}}(t')\big] \cdot \bar{\boldsymbol{f}}\right) I(\boldsymbol{u}) \qquad \text{(D.30)}$$

3 Time-Frequency Correlation Function of the Component Contributed by the Scattering Volume

The component $H_{\mathrm{s}}(t, f)$ in (D.13) of the time-variant transfer function contributed by the scattering volume $\mathcal{V}$ is a two-dimensional random process, which we seek to characterize in terms of its first and second moments.

We invoke the law of total expectation to intermediately condition on Π and then by use of the assumptions in M1 it can be readily identified that $H_{\mathrm{s}}(t, f)$ is a zero-mean process. The correlation function of $H_{\mathrm{s}}(t, f)$ is defined as

$$R(f, f', t, t') \triangleq \mathbb{E}\left\{H_{\mathrm{s}}^*(t, f) H_{\mathrm{s}}(t', f')\right\}. \qquad \text{(D.14)}$$

We insert (D.13) into (D.14) and condition intermediately on Π followed by repeated application of (D.2). Subsequently, we apply Campbell's Theorem and arrive at (D.15). Notice that our assumptions in M1 and M2 ensure a well-defined integral with an absolute value upper bounded by $C|\mathcal{V}|$. For notational convenience we have introduced the vector

$$\bar{\boldsymbol{f}} \triangleq \bar{\boldsymbol{f}}(f, f') = \begin{pmatrix} f' - f \\ -(f + f_{\mathrm{c}}) \\ f' + f_{\mathrm{c}} \end{pmatrix} \qquad \text{(D.16)}$$

and for any two vectors $\boldsymbol{b}_1, \boldsymbol{b}_2 \in \mathbb{R}^3$ the notation $\boldsymbol{b}_1 \cdot \boldsymbol{b}_2$ represents the usual Euclidean inner product on $\mathbb{R}^3$.

The integral form of the time-frequency correlation in (D.15) is one of our main results. It depends on the underlying marked point process only via the product $Q(\boldsymbol{r})\varrho(\boldsymbol{r})$. Hence, different such processes with the same resulting product will lead to the same correlation function.

The process $H_{\mathrm{s}}(t, f)$ is clearly non-stationary. So, despite the fact that the scattering coefficients are conditionally uncorrelated (resembling Bello's notion of uncorrelated scattering), the contribution by the volume $\mathcal{V}$ to the time-variant transfer function is not stationary. This is due to the steady change of the propagation constellation – in terms of relative delays and incidence directions of the multipath components – as the

mobile receiver moves along its trajectory. Yet, with the selection $t' = t$ we identify by direct inspection of (D.15) that

$$R(f, f', t, t) = \int_{\mathcal{V}} \frac{Q(\boldsymbol{r})\varrho(\boldsymbol{r})}{d_2^2(t, \boldsymbol{r})} \exp\left(-j2\pi \frac{d_{\mathrm{s}}(t, \boldsymbol{r})}{c_0}\Delta f\right)\mathrm{d}\boldsymbol{r} \qquad (\mathrm{D}.17)$$

with $\Delta f \triangleq f' - f$ and $d_{\mathrm{s}}(t, \boldsymbol{r})$ as defined in (D.8). Hence, for any fixed t, the frequency process $H_{\mathrm{s}}(t, f)$ is wide-sense stationary.

Several previous studies have investigated local properties of the channel by restricting attention to time intervals of sufficiently short duration. Within such intervals the receiver moves in the order of few tens of the wavelength. This assumption leads to Bello's WSSUS characterization [16] where the time-frequency correlation function depends only on $\Delta t \triangleq t' - t$ and Δf. Basically, the time interval should be short enough to ensure a fixed propagation constellation. Our general result in (D.15) can as well be simplified to this local setup by assuming in (D.12) only the phase term $-2\pi\lambda^{-1}d_{\mathrm{s}}(t, \boldsymbol{r})$ to dependent on t. The two other time dependent terms in (D.12) are assumed to remain constant since they vary only marginally within any sufficiently short time interval. Without loss of generality we assume this interval to be centered around zero. Then, for every scatterer position $\boldsymbol{r} \in \Pi$ we introduce a Doppler shift $\nu_{\boldsymbol{r}} = \lambda^{-1}\|\boldsymbol{v}\|\cos(\psi_{\boldsymbol{r}})$ via the first-order Taylor approximation

$$\frac{d_{\mathrm{s}}(t, \boldsymbol{r})}{\lambda} \approx \frac{d_{\mathrm{s}}(0, \boldsymbol{r})}{\lambda} + \nu_{\boldsymbol{r}}t \qquad (\mathrm{D}.18)$$

where $\psi_{\boldsymbol{r}}$ is the angle between the receiver velocity vector $\boldsymbol{v}$ and the vector $\boldsymbol{x}_0 - \boldsymbol{r}$ (recall Fig. D.1, but notice that $\psi_{\boldsymbol{r}}$ is not depicted). The time-frequency correlation function resulting from these assumptions reads

$$\int_{\mathcal{V}} \frac{Q(\boldsymbol{r})\varrho(\boldsymbol{r})}{d_2^2(0, \boldsymbol{r})} \exp\left(-j2\pi\nu_{\boldsymbol{r}}\Delta t - j2\pi\frac{d_{\mathrm{s}}(0, \boldsymbol{r})}{c_0}\Delta f\right)\mathrm{d}\boldsymbol{r}, \qquad (\mathrm{D}.19)$$

which is a function only of Δt and Δf. Thus, at least locally, the time-variant transfer function appears wide-sense stationary in both variables.

3.1 Simplifications and Approximations

The core assumption leading to the expression (D.19) is restrictive in the sense that the time interval considered must be short enough to ensure essentially a fixed incidence constellation. On the other hand the expression in (D.15) is the most general one available but the integral involved is not easily handled. Consequently, we now impose a set of assumptions giving rise to a closed-form expression which approximates (D.15) for time lags corresponding to displacements along the trajectory for which the plane wave assumption holds. Specifically, the closed-form approximation derived in the sequel

takes into account the fact that the incidence constellation changes with the movement of the receiver (and so can be seen as a tractable intermediate between (D.15) and (D.19)).

Initially, we define the probability density function (pdf) $\gamma(\boldsymbol{r}) \triangleq \Gamma^{-1}Q(\boldsymbol{r})\varrho(\boldsymbol{r})$ where $\Gamma \triangleq \int Q(\boldsymbol{r})\varrho(\boldsymbol{r})\,\mathrm{d}\boldsymbol{r}$ is finite due to our assumptions in M1. We call $\gamma(\boldsymbol{r})$ the (normalized) power spatial density of the scattering volume $\mathcal{V}$. This terminology is self-explanatory. The advantage of introducing the pdf $\gamma(\boldsymbol{r})$ is that it allows us to interpret a generic element from Π and its associated weight via a random vector in three-dimensional space. With the above definition of $\gamma(\boldsymbol{r})$, (D.15) can be recast as the expectation given in (D.20). Then, we approximate this expectation by the product of two expectations and finally we arrive at (D.21). This approximation relies on the fact that, in (D.20), the slowly changing term of inverse distances and the rapidly changing complex exponential term are virtually uncorrelated. We will see later in Sec. 4 that this approximation is reasonably accurate.

We now proceed with invoking the plane wave assumption to further simplify (D.21). If the scatterers are sufficiently far away from the receiver trajectory, the re-radiated spherical waves (Assumption M3) can be approximated as plane waves. First, we introduce the first and second moments of $\gamma(\boldsymbol{r})$:[4]

$$\boldsymbol{\mu}_\gamma \triangleq \mathbb{E}_\gamma\{\boldsymbol{r}\} \tag{D.22}$$

$$\boldsymbol{\Sigma}_\gamma \triangleq \mathbb{E}_\gamma\left\{(\boldsymbol{r}-\boldsymbol{\mu}_\gamma)(\boldsymbol{r}-\boldsymbol{\mu}_\gamma)^\mathrm{T}\right\}. \tag{D.23}$$

Both quantities exist since the support set of $\gamma(\boldsymbol{r})$ is bounded. The plane wave representation results from the first-order approximations (see Fig. D.1)

$$d_1(\boldsymbol{r}) \approx d_{\boldsymbol{T},\boldsymbol{\mu}} + \boldsymbol{e}(\boldsymbol{T},\boldsymbol{\mu}_\gamma)\cdot\tilde{\boldsymbol{r}}, \tag{D.24}$$

$$d_2(t,\boldsymbol{r}) \approx d_{\boldsymbol{x},\boldsymbol{\mu}}(t) + \boldsymbol{e}(\boldsymbol{x}(t),\boldsymbol{\mu}_\gamma)\cdot\tilde{\boldsymbol{r}} \tag{D.25}$$

with the definitions

$$\tilde{\boldsymbol{r}} \triangleq \boldsymbol{r} - \boldsymbol{\mu}_\gamma \tag{D.26}$$

$$d_{\boldsymbol{T},\boldsymbol{\mu}} \triangleq \|\boldsymbol{T} - \boldsymbol{\mu}_\gamma\| \tag{D.27}$$

$$d_{\boldsymbol{x},\boldsymbol{\mu}}(t) \triangleq \|\boldsymbol{x}(t) - \boldsymbol{\mu}_\gamma\| \tag{D.28}$$

$$\boldsymbol{e}(\boldsymbol{b}_1,\boldsymbol{b}_2) \triangleq \frac{\boldsymbol{b}_2 - \boldsymbol{b}_1}{\|\boldsymbol{b}_2 - \boldsymbol{b}_1\|}. \tag{D.29}$$

Note that $\boldsymbol{e}(\boldsymbol{b}_1,\boldsymbol{b}_2)$ returns the unit vector from $\boldsymbol{b}_1$ towards $\boldsymbol{b}_2$. We insert the approximations (D.24) and (D.25) into (D.21). Then, closed-form approximations of E_1 and E_2 in (D.21) can be computed (see Appendices 5 and 5, respectively). We obtain (D.30)

---

[4]The notation $(\cdot)^\mathrm{T}$ indicates the usual matrix-vector transpose operation.

with the definitions

$$\boldsymbol{u} \triangleq \boldsymbol{u}(t, t', f, f') = -\frac{1}{c_0} \left[\boldsymbol{e}(\boldsymbol{T}, \boldsymbol{\mu}_\gamma) \quad \boldsymbol{e}(\boldsymbol{x}(t), \boldsymbol{\mu}_\gamma) \quad \boldsymbol{e}(\boldsymbol{x}(t'), \boldsymbol{\mu}_\gamma) \right] \bar{\boldsymbol{f}} \qquad (D.31)$$

and

$$I(\boldsymbol{u}) \triangleq \mathbb{E}_\gamma \left\{ \exp\left(j2\pi \tilde{\boldsymbol{r}} \cdot \boldsymbol{u} \right) \right\}. \qquad (D.32)$$

Note that $I(\boldsymbol{u})$ is the characteristic function of a centered version of the pdf $\gamma(\boldsymbol{r})$. We see immediately from (D.30) that the scattering volume affects the approximation of $R(f, f', t, t')$ via $\gamma(\boldsymbol{r})$ in several ways. Specifically, $\gamma(\boldsymbol{r})$ determines $\boldsymbol{\mu}_\gamma$, $\boldsymbol{\Sigma}_\gamma$, and $I(\boldsymbol{u})$.

3.2   Example Power Spatial Densities

In the following, a few simple examples are given to demonstrate the easy evaluation and general use of (D.30). We acknowledge the assumptions given in M1 and consider different tractable forms of the power spatial density $\gamma(\boldsymbol{r})$. It is important to realize that with e.g. $\gamma(\boldsymbol{r}) \propto \mathbb{1}\left\{ \boldsymbol{r} \in \mathcal{V} \right\}$, we cannot conclude that the scatterers' locations in Π appear uniform on $\mathcal{V}$. When $\gamma(\boldsymbol{r})$ is uniform on $\mathcal{V}$ it merely means that, on average, equally much power is re-radiated from every single location in $\mathcal{V}$.

Uniform Power Spatial Density on a Cuboid

The power spatial density is of the form

$$\gamma(\tilde{\boldsymbol{r}}) = \frac{\mathbb{1}\left\{ \tilde{\boldsymbol{r}} \in [-w_1, w_1] \times [-w_2, w_2] \times [-w_3, w_3] \right\}}{2w_1 2w_2 2w_3}. \qquad (D.33)$$

The set in (D.33) represents a cuboid centered at $\boldsymbol{\mu}_\gamma$ and oriented along the axes of the coordinate system. Inserting (D.33) in (D.32) yields

$$I(\boldsymbol{u}) = I\left([u_1, u_2, u_3]\right) = \prod_{i=1}^{3} \operatorname{sinc}\left(2w_i u_i\right). \qquad (D.34)$$

Insertion of (D.34) and $\boldsymbol{\Sigma}_\gamma = \frac{1}{3}\operatorname{diag}\left(w_1^2, w_2^2, w_3^2\right)$ into (D.30) yields the approximation of $R(f, f', t, t')$ for the case when equally much power is re-radiated from everywhere in the cuboid.

Isotropic Power Spatial Density

The power spatial density is such that

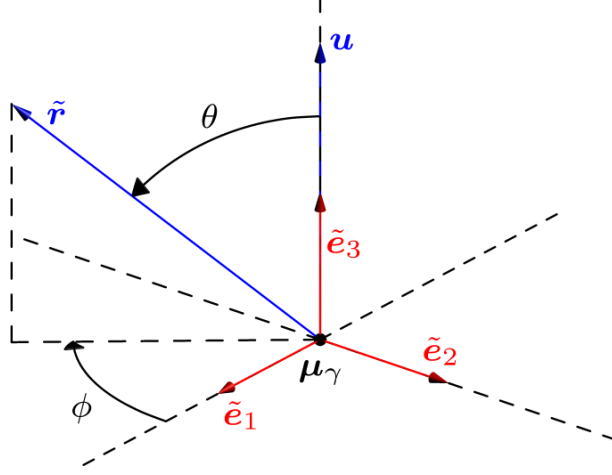$$\gamma(\tilde{\boldsymbol{r}}) = f(\|\tilde{\boldsymbol{r}}\|), \qquad (D.35)$$

Fig. D.2: Spherical coordinates used to derive $I(\boldsymbol{u})$ for $\gamma(\boldsymbol{r})$ isotropic.

corresponding to an isotropic distribution in a coordinate system with $\boldsymbol{\mu}_\gamma$ as origin. To ease the computation of $I(\boldsymbol{u})$ for fixed $\boldsymbol{u} \neq \boldsymbol{0}$, we select the coordinate system $\left(\boldsymbol{\mu}_\gamma, (\tilde{\boldsymbol{e}}_1, \tilde{\boldsymbol{e}}_2, \tilde{\boldsymbol{e}}_3)\right)$ using an orthonormal basis such that

$$\tilde{\boldsymbol{e}}_3 \triangleq \boldsymbol{e}(\boldsymbol{0}, \boldsymbol{u}) \qquad \text{and} \qquad \tilde{\boldsymbol{e}}_1 \perp \tilde{\boldsymbol{e}}_2 \perp \tilde{\boldsymbol{e}}_3, \tag{D.36}$$

see Fig. D.2. Subsequently, we proceed by changing to spherical coordinates. Then with $r \triangleq \|\tilde{\boldsymbol{r}}\|$ the vector $\tilde{\boldsymbol{r}}$ has coordinates

$$\tilde{\boldsymbol{r}} = \begin{pmatrix} \tilde{r}_1 \\ \tilde{r}_2 \\ \tilde{r}_3 \end{pmatrix} = \begin{pmatrix} r \sin\theta \cos\phi \\ r \sin\theta \sin\phi \\ r \cos\theta \end{pmatrix} \tag{D.37}$$

and by (D.36) and (D.37) we have $\tilde{\boldsymbol{r}} \cdot \boldsymbol{u} = r\|\boldsymbol{u}\| \cos\theta$. Accordingly, our change to spherical coordinates allows for the expectation in (D.32) to be recast as (still, assuming that $\boldsymbol{u} \neq \boldsymbol{0}$)

$$\begin{aligned} I(\boldsymbol{u}) &= \iiint \exp\left(j2\pi r\|\boldsymbol{u}\| \cos\theta\right) f(r) r^2 \sin\theta \, \mathrm{d}r \, \mathrm{d}\theta \, \mathrm{d}\phi \\ &= 2\pi \int_0^\infty \left[\int_0^\pi \exp\left(j2\pi\|\boldsymbol{u}\|r \cos\theta\right) \sin\theta \, \mathrm{d}\theta\right] r^2 f(r) \, \mathrm{d}r \\ &= \frac{2}{\|\boldsymbol{u}\|} \int_0^\infty \sin\left(2\pi\|\boldsymbol{u}\|r\right) r f(r) \, \mathrm{d}r. \end{aligned} \tag{D.38}$$

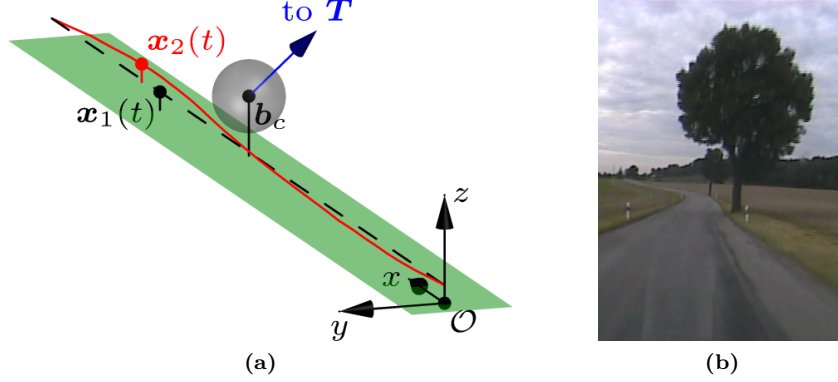**(a)**   **(b)**

Fig. D.3: (a) Representation of the real LMS scenario considered with a vehicle passing by a tree. The tree canopy is represented as a spherical volume (in gray). The red curve $\boldsymbol{x}_2(t)$ denotes the real trajectory driven by the vehicle, while the dashed curve $\boldsymbol{x}_1(t)$ represents a straight-line approximation with constant velocity of $\boldsymbol{x}_2(t)$. (b) Photograph of the scenario taken from the vehicle's front camera.

As expected, the isotropy condition (D.35) implies that $I(\boldsymbol{u})$ only depends on the norm of $\boldsymbol{u}$.

We now consider the special case of a uniform power spatial density on a ball. Specifically, we assume that $\gamma(\boldsymbol{r})$ is defined as in (D.35) with

$$f\big(\|\tilde{\boldsymbol{r}}\|\big) = f(r) = \frac{3}{4\pi\zeta^3}\mathbb{1}\left\{0 \leq r \leq \zeta\right\}. \tag{D.39}$$

By substituting (D.39) directly in (D.38) and solving we obtain

$$I(\boldsymbol{u}) = 3\left[\frac{\sin\big(2\pi\|\boldsymbol{u}\|\zeta\big)}{\big(2\pi\|\boldsymbol{u}\|\zeta\big)^3} - \frac{\cos\big(2\pi\|\boldsymbol{u}\|\zeta\big)}{\big(2\pi\|\boldsymbol{u}\|\zeta\big)^2}\right], \tag{D.40}$$

which inserted in (D.30) together with $\boldsymbol{\Sigma}_\gamma = \frac{1}{5}\zeta^2\boldsymbol{I}$ yields the approximation of $R(f, f', t, t')$ for the case when (on average) equally much power is re-radiated from everywhere in a ball with radius ζ.

4   Numerical Results

In this section we verify the proposed channel model by applying it to a common LMS scenario where a vehicle equipped with a GNSS receiver drives past a roadside tree with almost constant velocity vector. This situation is typical for ranging to one satellite of a GNSS in rural environments. Such a scenario was experimentally investigated in a

Table D.1: Parameter setting used in the measurement campaign

Parameter	Value
Carrier frequency [GHz]	1.51
Bandwidth [Mhz]	100
Receiver antenna pattern	Hemispherical
Signal transmission power [W EIRP]	10
Polarization	RHCP
Delay resolution [ns]	10
Channel resp. update rate f_{CR} [Hz]	$1/3.072 \approx 325.5$
Transmitter's approx. location $\boldsymbol{T}$ [m]	$(-618.6, -603.3, 912.7)^{\mathrm{T}}$
Transmitter's elevation	$\approx 46.5°$

measurement campaign. It is sketched in Fig. D.3a with a photo shown in Fig. D.3b. Subsection 4.1 outlines the measurement campaign. Subsection 4.2 describes the parameter setting characterizing the scenario.

We report three different investigations in the considered scenario. Firstly, in Subsection 4.3 the proposed model is used to investigate the dynamic change of the component contributed by the tree canopy in the time-variant response and the time-variant transfer function of the channel when the mobile drives past the tree. Secondly, in Subsection 4.4 the model is experimentally validated by contrasting the synthetically generated time-variant response and delay-Doppler spread function with estimates of these functions obtained from the measurement data. Finally, in Subsection 4.5 the closed-form approximation (D.30) of the time-frequency correlation function of the component in the system response contributed by the tree is validated by comparing it with an estimate computed by means of Monte Carlo simulations.

4.1 Measurement Campaign

In 2002, DLR conducted channel sounding measurements in a rural area approximately 30 km south-west of Munich, Germany. The transmitter of the channel sounder was mounted on a Zeppelin and the receiver was installed in a van with its antenna assembled on the vehicle's roof. This configuration allowed for reproducing realistic LMS radio channel conditions for varying transmitter elevations.

Tab. D.1 summarizes the parameter setting used in the measurement campaign that is relevant to the subsequent investigations. The transmitter was hovering at a height of approximately 912 m, around 618 m south and 603 m east of the starting point of the

Table D.2: Parameter setting used for the simulated scenario

Parameter	Value
Transmitter location $\boldsymbol{T}$	as in Tab. D.1
Estimated van trajectory	$\boldsymbol{x}_2(t)$
Straight-line approximation	$\boldsymbol{x}_1(t) = (0, 0, 2.5)^{\mathrm{T}} + t(\|\boldsymbol{v}\|, 0, 0)^{\mathrm{T}}$
Receiver speed $\|\boldsymbol{v}\|$ [m/s]	18
Scattering volume $\mathcal{V}$	$\left\{ \boldsymbol{b} \in \mathbb{R}^3 : \|\boldsymbol{b} - \boldsymbol{b}_{\mathrm{c}}\| \leq \zeta \right\}$
Center and radius of $\mathcal{V}$ [m]	$(\boldsymbol{b}_{\mathrm{c}}, \zeta) = \left((90.67, -2.76, 8.25)^{\mathrm{T}}, 5 \right)$
Intensity height ϱ_0	0.038
Per-scatterer power Q_0	0.19

vehicle's trajectory. The elevation angle was thus approximately 46.5°. Notice that the measurement set-up was equipped with right-hand circularly polarized (RHCP) transmit and receive antennas, as used in satellite navigation applications. Further information on the measurement campaign is given in [15].

4.2   Modeling Details and Simulation Setup

As indicated in Fig. D.3a we employ a spherical scattering volume $\mathcal{V}$ to represent the treetop in Fig. D.3b. For simplicity, we assume the point-source scatterers to be uniformly distributed in $\mathcal{V}$ with location independent average power contributions from the associated scattering coefficients. In the terminology of Section 2 we thus have $\varrho(\boldsymbol{r}) = \varrho_0 \mathbb{1} \left\{ \boldsymbol{r} \in \mathcal{V} \right\}$ and $Q(\boldsymbol{r}) = Q_0$. Tab. D.2 lists the setting of the parameters used for the simulations.

Two different trajectories are considered in the numerical investigations: the estimated trajectory $\boldsymbol{x}_2(t)$ that the measurement vehicle actually drove and a straight-line approximation $\boldsymbol{x}_1(t)$ of it, see Tab. D.2. As depicted in Fig. D.3b the real vehicle's trajectory leads very close to the tree. It deviates slightly from a straight line since the road is bent a little. The receive antenna is 2.5 m above the driven trajectory, see Fig. D.3a.

We consider a generic bandlimited system that mimics actual GNSS receivers. The bandwidth limitation leads to a smearing of the Dirac impulses in (D.7) in the delay domain. We imitate this behavior by employing the HANN function

$$w_{\mathrm{hann}}(t; B) = \frac{1}{2} \left[1 + \cos(2\pi Bt) \right] \mathbb{1} \left\{ |t| < \frac{1}{2B} \right\} \tag{D.41}$$
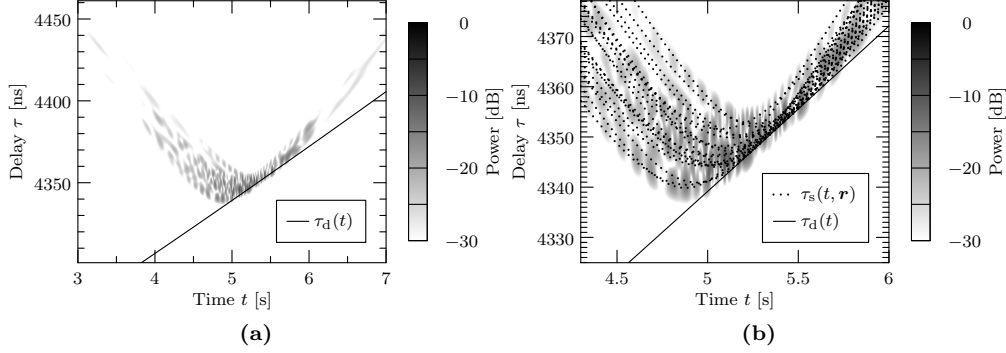
Fig. D.4: Amplitude of the filtered version of an example realization of $h_\mathrm{s}(t,\tau)$ in (D.12). The solid line shows the signal flight time of the direct component $\tau_\mathrm{d}(t)$. Fig. D.4b is a zoom of Fig. D.4a to the time interval $4.4\,\mathrm{s} \le t \le 6\,\mathrm{s}$ (Phase II). The trajectory of the delays of the multipath components contributed by the 20 point-source scatterers in $\mathcal{V}$ are shown as dotted lines.

as the impulse response of the system. Modern GNSSs use bandwidths ranging from $1\,\mathrm{MHz}$ up to $60\,\mathrm{MHz}$. We compute an approximation of the time-variant response of the concatenated system made of the radio channel and the generic band-limited system by convolving $h_\mathrm{s}(t,\tau)$ for any t (considered fixed) with the HANN function. Since $h_\mathrm{s}(t,\tau)$ changes slowly with time with respect to the extent of its support in delay, this approximation is almost indistinguishable from the true concatenated response. In the sequel we refer to this approximation as the filtered version of $h_\mathrm{s}(t,\tau)$. We choose the same bandwidth $B = 100\,\mathrm{MHz}$ as used in the measurement campaign.

4.3 Dynamic Change of the Component in the System Functions Contributed by the Tree Canopy

In this investigation we use the proposed channel model to generate a realization of the contribution by the tree canopy to the time-variant response and the time-frequency transfer function of the radio channel, i.e. $h_\mathrm{s}(t,\tau)$ in (D.12) and $H_\mathrm{s}(t,f)$ in (D.13). We consider the straight-line trajectory $\boldsymbol{x}_1(t)$. Since only one realization is generated, we choose Π as a binomial point process with 20 points in $\mathcal{V}$. Hence, $\varrho_0|\mathcal{V}| = 20$. Furthermore, the associated scattering coefficients (the marks) have identical deterministic amplitude and random independent phases. More specifically $\beta_{\boldsymbol{r}} = \sqrt{Q_0}\exp(j\theta_{\boldsymbol{r}})$, where each $\theta_{\boldsymbol{r}}$ is uniformly distributed on the interval $[0, 2\pi)$.

Fig. D.4 depicts the amplitude of the filtered version of a realization of $h_\mathrm{s}(t,\tau)$ for two different time intervals. The solid line in the figure represents the direct signal flight time from transmitter to receiver $\tau_\mathrm{d}(t)$ in (D.6). It is remarkable that, although all scattering coefficients have the same modulus, a high level of interference can be
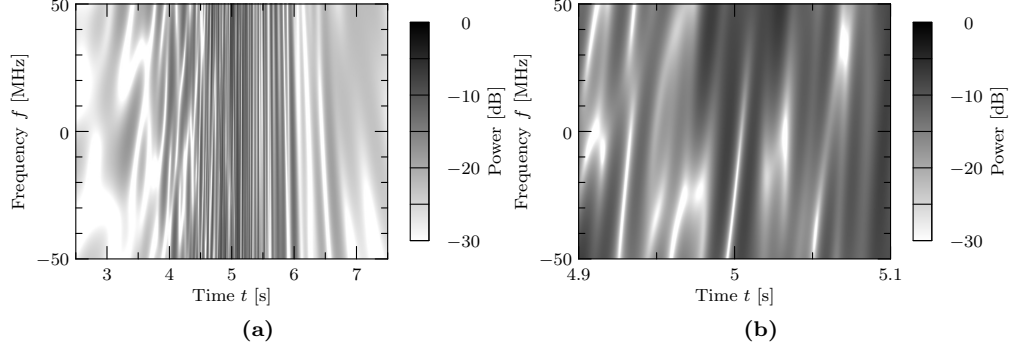
Fig. D.5: Amplitude of an example realization of $H_s(t, f)$ in (D.13). Fig. D.5b is a zoom of Fig. D.5a to the time interval $4.9 \leq t \leq 5.1$ (Phase II).

observed in Fig. D.4. This is due to the individual phase changes of the weights caused by the receiver's relative movement, recall (D.11) and (D.12). The effect of the variation of the time-dispersion in $h_s(t, \tau)$ has also a direct impact on the frequency selectivity of $H_s(t, f)$. The amplitude of the latter function is reported in Fig. D.5.

As evidenced in Fig. D.4a and Fig. D.5a, three dominant phases can be distinguished as the vehicle moves along the trajectory $\boldsymbol{x}_1(t)$:

- Phase I: The vehicle approaches $\mathcal{V}$ ($t < 4.5\,\text{s}$):
  We observe that $h_s(t, \tau)$ exhibits a large delay spread yet varies relatively slowly. Accordingly, $H_s(t, f)$ is slowly-varying versus time but exhibits a relatively high frequency selectivity which can be seen as the bright notch-like structures in Fig. D.5a.

- Phase II: The vehicle drives alongside $\mathcal{V}$ ($4.5\,\text{s} < t < 5.5\,\text{s}$):
  We observe that the delay spread of $h_s(t, \tau)$ becomes smaller. As a result $H_s(t, f)$ is almost flat with respect to frequency but its variations over time become more pronounced as can be seen in Fig. D.5b.

- Phase III: The vehicle drives away from $\mathcal{V}$ ($t > 5.5\,\text{s}$):
  The delays of the scatterers are all close to $\tau_d(t)$ resulting in a smaller delay spread and a weaker frequency selectivity as compared to that observed in Phase I.

4.4   Experimental Validation of the Channel Model

In this example the system functions estimated from the measurement data are contrasted with those generated using the proposed channel model with the parameter
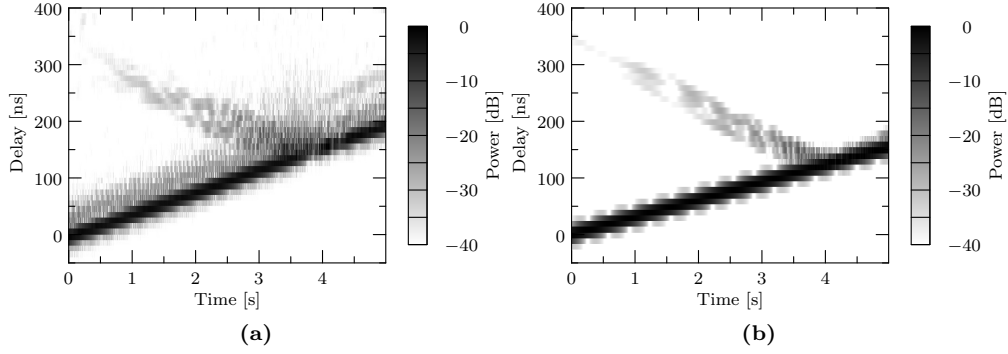
Fig. D.6: Amplitude of the filtered version of the time-variant channel response: (a) estimated; (b) simulated.
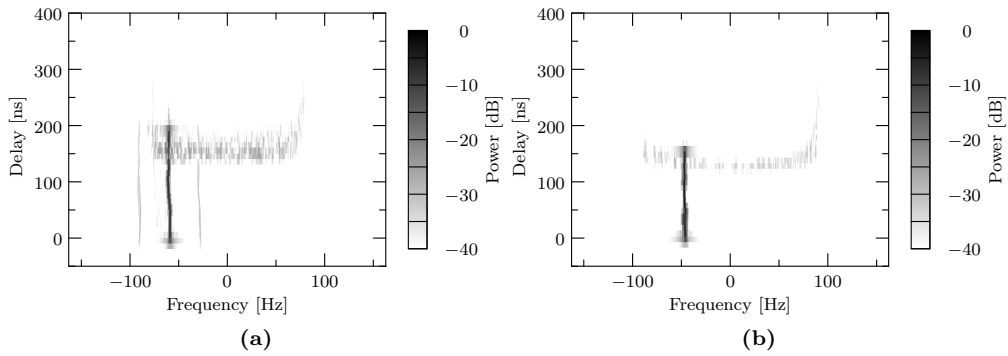

Fig. D.7: Amplitude of the delay-Doppler spread function: (a) estimated; (b) simulated.

setting in Tab. D.2. The real trajectory driven by the receiving mobile, i.e. $\boldsymbol{x}_2(t)$, is used in these investigations, see also Fig. D.3a.

The recorded time-variant response is filtered as already described using the HANN function with $B = 100\,\text{MHz}$. The result is pictured in Fig. D.6a. The estimated delay-Doppler spread function is shown in Fig. D.7a. It is computed as the discrete Fourier transform (DFT) of the recorded channel response with respect to the time variable t. The vertical axes of all figures are in decibels. Since the vehicle is driving away from the transmitter, the strong LOS component in Fig. D.7a has a negative Doppler frequency of approximately $-50\,\text{Hz}$. We can easily relate the shape of the estimated delay-Doppler spread function to the three distinct phases identified in Subsection 4.3. In Phase I, when the vehicle is approaching the tree, the electromagnetic waves scattered by the
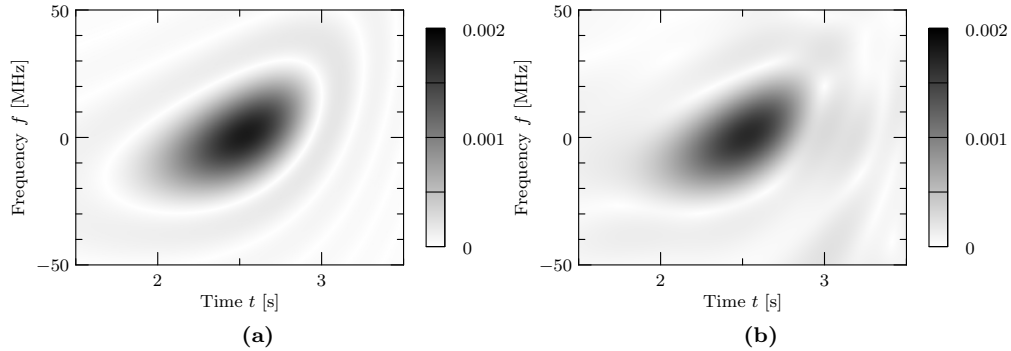
Fig. D.8: Comparison of the amplitudes of (a) the approximate correlation function (D.30) and (b) the approximation (D.42) computed from $K = 1000$ channel realizations; the amplitudes are depicted versus t and f with t' and f' fixed to 2.5 s and 0 Hz, respectively.

tree are impinging at the receiver's antenna from the front with respect to the vehicle's velocity vector. Their positive Doppler frequencies have values around 80 Hz. This can be seen in Fig. D.7a for delays larger than 200 ns. In Phase II, when the vehicle drives alongside the tree, the waves' Doppler frequencies are spread from −80 Hz to 80 Hz. Finally, in Phase III, when the vehicle drives away from the tree, the Doppler frequencies lie around −80 Hz.

We verify the proposed channel model by applying it with the geometric setting in Tab. D.2 to generate a realization of the time-variant response and the delay-Doppler spread function. The point-source scatterers in the tree are modeled again as a binomial point process with 20 points but this time the scattering coefficients are drawn independently according to the complex normal distribution $\mathcal{CN}(0, Q_0)$. We calibrate the model by setting the number of scatterers and the parameter Q_0 so that a good agreement between simulation and measurement can be observed. The filtered realization of the time-variant response is depicted in Fig. D.6b, while Fig. D.7b shows the delay-Doppler spread function. By visual inspection of the plots in Fig. D.6 and in Fig. D.7 we observe a remarkable similarity between the simulated and estimated results.

4.5 Validation of the Closed-Form Approximation (D.30)

In this investigation we compare the closed-form approximation (D.30) of $R(f, f', t, t')$ with a numerical approximation computed by means of Monte Carlo simulations.

We choose Π to be a Poisson point process. For each $\boldsymbol{r} \in \Pi$ we let $\beta_{\boldsymbol{r}} \sim \mathcal{CN}(0, Q_0)$ as in the previous example. With the parameter setting in Tab. D.2 we get $\Gamma = \varrho_0 Q_0 |\mathcal{V}| \approx 3.78$ and $\boldsymbol{\Sigma}_\gamma = \frac{1}{5}\zeta^2 \boldsymbol{I} = 5\boldsymbol{I}$. The characteristic function $I(\boldsymbol{u})$ is evaluated using (D.40) since $\mathcal{V}$ is spherical with a uniform average power re-radiation. Note that since Π is a
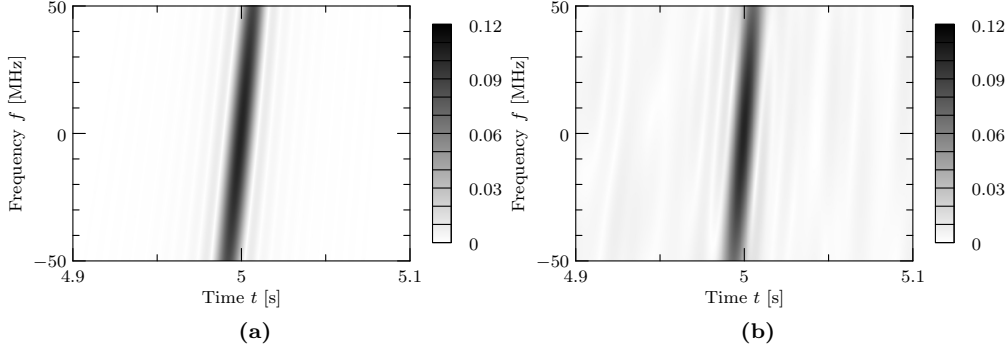
Fig. D.9: Comparison of the amplitudes of (a) the approximate correlation function (D.30) and (b) the approximation (D.42) computed from $K = 1000$ channel realizations; the amplitudes are depicted versus t and f with t' and f' fixed to $5\,\mathrm{s}$ and $0\,\mathrm{Hz}$, respectively.

Poisson point process, the number of point-source scatterers in the spherical volume $\mathcal{V}$ changes from realization to realization with an average of $\varrho_0\,|\mathcal{V}| = 20$ points per realization. We have now all the elements to evaluate (D.30). The amplitude of this expression is reported versus (f, t) in Fig. D.8a and Fig. D.9a for (f', t') fixed to $(0\,\mathrm{Hz}, 2.5\,\mathrm{s})$ and $(0\,\mathrm{Hz}, 5\,\mathrm{s})$ respectively.

We use Monte Carlo simulations to compute an approximation of the integral expression in (D.15): K independent realizations of the time-variant transfer function, denoted by $H_{\mathrm{s},k}(t, f)$, $k = 1, 2, ..., K$, are generated; the approximation of the right-hand side in (D.15) is computed from these K realizations as

$$\hat{R}(f, f', t, t') = \frac{1}{K} \sum_{k=0}^{K-1} H_{\mathrm{s},k}^*(t, f) H_{\mathrm{s},k}(t', f'). \tag{D.42}$$

The amplitude of the approximation obtained with $K = 1000$ realizations is depicted in Fig. D.8b and Fig. D.9b.

By visual inspection of Fig. D.8 and Fig. D.9 we observe a very good visual agreement between the amplitudes of the closed-form approximation (D.30) and the Monte Carlo approximation. To provide a quantitative analysis of the accuracy of the approximation, we report in Fig. D.10 the approximation and the estimated correlation function versus the frequency f with the other arguments set to $f' = 0\,\mathrm{Hz}$, $t = t' = 2.5\,\mathrm{s}$ (a) and $t = t' = 5\,\mathrm{s}$ (b). Overall, we observe a good agreement. As expected, the fit is better when the vehicle is far away from the canopy (Phase I). We also observe that the depicted curves are in accordance with the wide-sense stationarity property (D.17), namely, they are symmetric around $f = 0$.
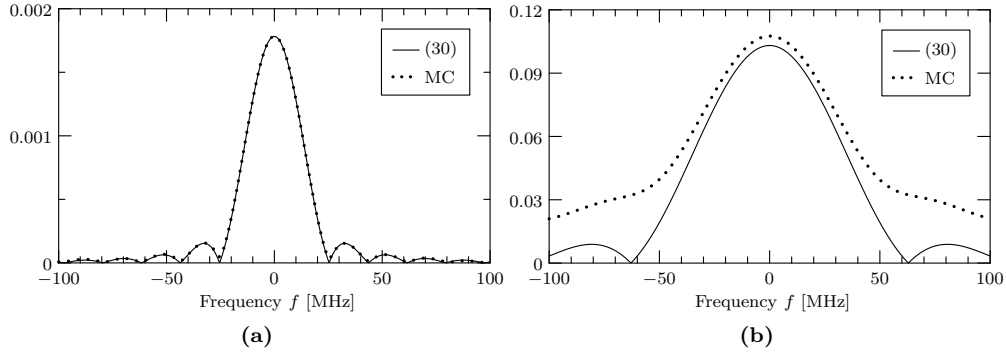
Fig. D.10: Comparison between the amplitudes of the closed-form approximation (D.30) and the Monte Carlo (MC) estimation (D.42) of the correlation function (D.15) versus the frequency f with the other arguments kept fixed to $f' = 0\,\mathrm{Hz}$, $t = t' = 2.5\,\mathrm{s}$ (a) and $t = t' = 5\,\mathrm{s}$ (b). The Monte Carlo approximations are computed from $K = 100000$ channel realizations.

5   Conclusions and Outlook

In this contribution we presented a non-stationary model describing the system functions of the radio channel that result in a scenario with an elevated transmitter and a mobile receiver moving nearby a scattering volume. The model is generic in the sense that it can be applied to many scenarios with a receiver moving past a scattering object by appropriately setting the parameters describing the geometry and the scattering property of this object. An LMS application is considered where the object is a tree, or more specifically, a treetop.

The virtue of the model is threefold:

- It includes the delay and Doppler dispersion induced by the volume due to its geometric extent and the receiver's movement.

- It incorporates the non-stationary behavior due to the steady change of the propagation constellation as the receiver moves.

- Scattering by the tree canopy is described by point-source scatterers that form a marked spatial point process.

Three different phases were evidenced where the system functions exhibit distinct behaviors when the receiving vehicle drives past an isolated tree: approaching, passing by, and departing the tree. An integral-form of the time-frequency correlation function of the component in the system response scattered by the tree was derived by invoking Campbell's Theorem. A tractable approximation of this function, for time lags corresponding to displacements along the trajectory for which the plane wave assumption

holds, was derived and validated by means of Monte Carlo simulations. The model was also validated by means of experimental results. Overall, visual inspections of the results show a very good agreement, despite the simplifying assumptions underlying the model derivation.

Future work will comprise the determination of the attenuation caused by the canopy. Additional wideband measurements of individual trees will be evaluated to accomplish this task. Additionally, the scattered power by treetops will be quantified based on these measurement data.

Appendix A: Approximation for E_1

We derive the approximation for E_1 as defined in (D.21). Initially, by using the approximation (D.25) we get

$$
\begin{aligned}
E_1 &\triangleq \mathbb{E}_\gamma \left\{ \frac{1}{d_2(t,\boldsymbol{r})d_2(t',\boldsymbol{r})} \right\} \\
&\approx \frac{1}{d_{\boldsymbol{x},\boldsymbol{\mu}}(t)d_{\boldsymbol{x},\boldsymbol{\mu}}(t')} \mathbb{E}_\gamma \left\{ \left[1 + \frac{\boldsymbol{e}(\boldsymbol{x}(t),\boldsymbol{\mu}_\gamma)\cdot\tilde{\boldsymbol{r}}}{d_{\boldsymbol{x},\boldsymbol{\mu}}(t)} \right]^{-1} \left[1 + \frac{\boldsymbol{e}(\boldsymbol{x}(t'),\boldsymbol{\mu}_\gamma)\cdot\tilde{\boldsymbol{r}}}{d_{\boldsymbol{x},\boldsymbol{\mu}}(t')} \right]^{-1} \right\}.
\end{aligned}
$$

With x in the vicinity of zero we apply $(1+x)^n \approx 1+nx$ to both terms within the above expectation and get

$$
E_1 \approx \frac{1}{d_{\boldsymbol{x},\boldsymbol{\mu}}(t)d_{\boldsymbol{x},\boldsymbol{\mu}}(t')} \mathbb{E}_\gamma \left\{ \left(1 - \frac{\boldsymbol{e}(\boldsymbol{x}(t),\boldsymbol{\mu}_\gamma)\cdot\tilde{\boldsymbol{r}}}{d_{\boldsymbol{x},\boldsymbol{\mu}}(t)} \right) \left(1 - \frac{\boldsymbol{e}(\boldsymbol{x}(t'),\boldsymbol{\mu}_\gamma)\cdot\tilde{\boldsymbol{r}}}{d_{\boldsymbol{x},\boldsymbol{\mu}}(t')} \right) \right\}.
$$

Next, we expand the product in the expectation and apply the expectation operator. Using that $\mathbb{E}_\gamma\{\tilde{\boldsymbol{r}}\} = \boldsymbol{0}$, since $\boldsymbol{\mu}_\gamma$ is the center of gravity of the pdf $\gamma(\boldsymbol{r})$, we get

$$
E_1 \approx \frac{1}{d_{\boldsymbol{x},\boldsymbol{\mu}}(t)d_{\boldsymbol{x},\boldsymbol{\mu}}(t')} \left[1 + \frac{\boldsymbol{e}(\boldsymbol{x}(t),\boldsymbol{\mu}_\gamma)^{\mathrm{T}}\boldsymbol{\Sigma}_\gamma\boldsymbol{e}(\boldsymbol{x}(t'),\boldsymbol{\mu}_\gamma)}{d_{\boldsymbol{x},\boldsymbol{\mu}}(t)d_{\boldsymbol{x},\boldsymbol{\mu}}(t')} \right],
$$

with $\boldsymbol{\Sigma}_\gamma = \mathbb{E}_\gamma\{\tilde{\boldsymbol{r}}\tilde{\boldsymbol{r}}^{\mathrm{T}}\}$ as defined in (D.23) in Section 3.

Appendix B: Approximation for E_2

We seek the approximation for E_2 as defined in (D.21). Initially, we approximate the distances $d_1(\boldsymbol{r})$, $d_2(t,\boldsymbol{r})$ and $d_2(t',\boldsymbol{r})$ via (D.24) and (D.25). From these approximate distances we straightforwardly approximate the inner product

$$
\left[d_1(\boldsymbol{r}), d_2(t,\boldsymbol{r}), d_2(t',\boldsymbol{r}) \right] \cdot \bar{\boldsymbol{f}} \tag{D.43}
$$

as a sum of two inner products, namely

$$\left[d_{\boldsymbol{T},\boldsymbol{\mu}}, d_{\boldsymbol{x},\boldsymbol{\mu}}(t), d_{\boldsymbol{x},\boldsymbol{\mu}}(t') \right] \cdot \bar{\boldsymbol{f}} - c_0 \tilde{\boldsymbol{r}} \cdot \boldsymbol{u} \tag{D.44}$$

with $\boldsymbol{u} = \boldsymbol{u}(t, t', f, f')$ as defined in (D.31). Note that the first term in (D.44) is not random. Replacing (D.43) by (D.44) in the expression for E_2 yields the approximation

$$E_2 \triangleq \mathbb{E}_\gamma \left\{ \exp \left(-j2\pi c_0^{-1} \left[d_1(\boldsymbol{r}), d_2(t, \boldsymbol{r}), d_2(t', \boldsymbol{r}) \right] \cdot \bar{\boldsymbol{f}} \right) \right\}$$
$$\approx \exp \left(-j2\pi c_0^{-1} \left[d_{\boldsymbol{T},\boldsymbol{\mu}}, d_{\boldsymbol{x},\boldsymbol{\mu}}(t), d_{\boldsymbol{x},\boldsymbol{\mu}}(t') \right] \cdot \bar{\boldsymbol{f}} \right) I(\boldsymbol{u}),$$

with $I(\boldsymbol{u}) = \mathbb{E}_\gamma \left\{ \exp \left(j2\pi \tilde{\boldsymbol{r}} \cdot \boldsymbol{u} \right) \right\}$ as defined in (D.32).

Acknowledgments

References

[1] G. Lachapelle, "Seasonal effect of tree foliage on GPS signal availability and accuracy for vehicular navigation," in *Proceedings of the 7th International Technical Meeting of the Satellite Division of the Institute of Navigation (ION GPS)*, Salt Lake City, Utah, USA, 1994.

[2] I.-S. Koh and K. Sarabandi, "Polarimetric channel characterization of foliage for performance assessment of GPS receivers under tree canopies," *IEEE Trans. Antennas Propag.*, vol. 50, no. 5, pp. 713–726, May 2002.

[3] F. M. Schubert, B. H. Fleury, P. Robertson, R. Prieto-Cerdeira, A. Steingass, and A. Lehner, "Modeling of multipath propagation components caused by trees and forests," in *Antennas and Propagation (EuCAP), 2010 Proceedings of the Fourth European Conference on*, Apr. 2010, pp. 1–5.

[4] C. Loo and J. Butterworth, "Land mobile satellite channel measurements and modeling," *Proceedings of the IEEE*, vol. 86, no. 7, pp. 1442–1463, Jul. 1998.

[5] J. Goldhirsh and W. Vogel, "Mobile satellite system fade statistics for shadowing and multipath from roadside trees at UHF and L-band," *IEEE Trans. Antennas Propag.*, vol. 37, no. 4, pp. 489–498, Apr. 1989.

[6] Y. de Jong and M. Herben, "A tree-scattering model for improved propagation prediction in urban microcells," *IEEE Trans. Veh. Technol.*, vol. 53, no. 2, pp. 503–513, Mar. 2004.

[7] M. Cheffena and F. Pérez-Fontán, "Land mobile satellite channel simulator along roadside trees," *Antennas and Wireless Propagation Letters, IEEE*, vol. 9, pp. 748 –751, 2010.

[8] A. Ishimaru, *Wave Propagation and Scattering in Random Media, Volume I: Single scattering and transport theory.* Academic Press, New York, 1978.

[9] K. McDonald, M. Dobson, and F. Ulaby, "Using MIMICS to model L-band multi-angle and multitemporal backscatter from a walnut orchard," *IEEE Trans. Geosci. Remote Sens.*, vol. 28, no. 4, pp. 477–491, Jul. 1990.

[10] R. F. S. Caldeirinha, "Radio characterization of single trees at micro- and millimetre wave frequencies," Ph.D. dissertation, University of Glamorgan, 2001.

[11] R. Caldeirinha and M. Al-Nuaimi, "Wideband characterisation of the dispersive effects on isolated mature trees for 2-GHz band urban microcells," in *Proceedings of the URSI General Assembly*, Maastricht, The Netherlands, Aug. 2002.

[12] F. Pérez-Fontán, M. Vázquez-Castro, C. Cabado, J. García, and E. Kubista, "Statistical modeling of the LMS channel," *IEEE Trans. Veh. Technol.*, vol. 50, no. 6, pp. 1549–1567, 2001.

[13] A. Lehner and A. Steingass, "A novel channel model for land mobile satellite navigation," in *Proceedings of the 18th International Technical Meeting of the Institute of Navigation Satellite Division*, Long Beach, California, USA, 2005.

[14] A. Steingass and A. Lehner, "Navigation in multipath environments for suburban applications," in *Proceedings of the 20th International Technical Meeting of the Satellite Division of the Institute of Navigation*, Fort Worth, Texas, USA, 2007.

[15] A. Lehner, "Multipath channel modelling for satellite navigation systems," Ph.D. dissertation, Universität Erlangen-Nürnberg, Germany, 2007.

[16] P. Bello, "Characterization of randomly time-variant linear channels," *IEEE Trans. Commun. Syst.*, vol. 11, no. 4, pp. 360–393, Dec. 1963.

[17] J. F. C. Kingman, *Poisson Processes.* Oxford University Press, 1993.

[18] J. Møller and R. P. Waagepetersen, *Statistical Inference and Simulation for Spatial Point Processes.* Chapman & Hall/CRC, 2004.

[19] A. Saleh and R. Valenzuela, "A statistical model for indoor multipath propagation," *IEEE J. Sel. Areas Commun.*, vol. 5, no. 2, pp. 128–137, Feb. 1987.

[20] A. Ridolfi, "Power spectra of random spikes and related complex signals," Ph.D. dissertation, École polytechnique fédérale de Lausanne, Lausanne, Switzerland, 2004.

[21] K. Hao, "Modeling and statistical analysis of ultra-wideband (UWB) channels and systems: A point-process approach," Ph.D. dissertation, University of Wisconsin-Madison, Wisconsin, USA, 2006.

[22] M. L. Jakobsen, T. Pedersen, and B. H. Fleury, "Analysis of the stochastic channel model by Saleh & Valenzuela via the theory of point processes," in *International Zurich Seminar on Communications*, Zurich, Switzerland, Mar. 2012, pp. 1–4.

Appendix E

Study Note: Point Processes in 2D

Morten Lomholt Jakobsen

This study note has been created to be part of the reading material used by master students in the course "Stochastic Processes" at Department of Electronic Systems.

In this study note we introduce the concept of a two-dimensional (2D) *point process*. We cover only the simplest classes of point processes, namely *binomial point processes* and *Poisson point processes*. If you are interested in getting to know about other classes of point processes (or perhaps point processes in more than 2D), then browse the literature listed at the end of this note or ask the lecturer for recommendations on books, papers, tutorials, etc.

1   Observing "random" point patterns

Assume that yesterday's weather was horrible with lots of rain, strong winds and lightning (fair assumption in Denmark!). Meteorologists have equipment for monitoring and recording the exact locations of individual lightning strikes. A certain meteorologist creates a map with the locations of all lightning strikes recorded yesterday within some fixed geographical region (rectangular, 10km by 5km). The complete map is shown in Figure E.1.
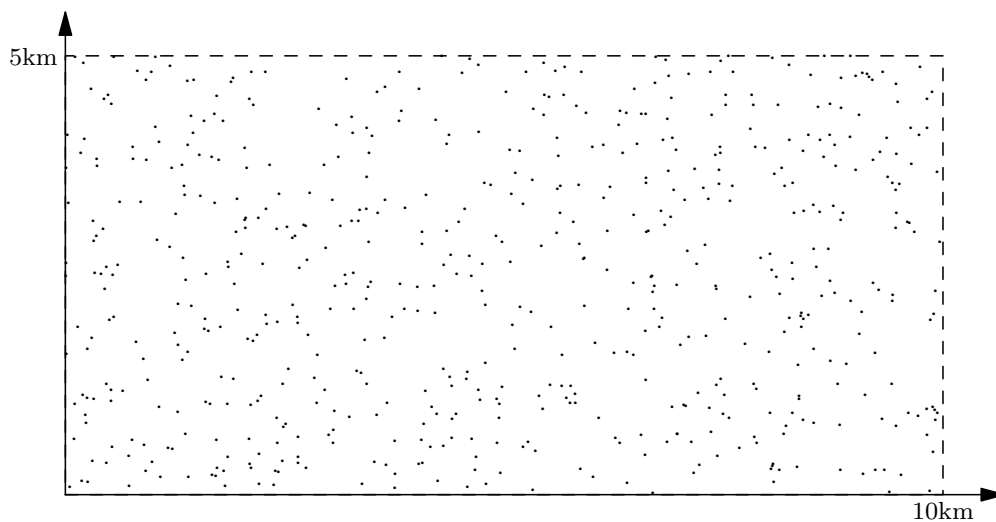

Fig. E.1: Locations of lightning strikes within a fifty square kilometer region. A total of 613 lightning strikes were recorded.

The meteorologist wonders if it makes sense to think of this particular point pattern as being random. More precisely, he wonders if the observed point pattern in Figure E.1 can be thought of as a *realization* of some random mechanism.

Exercise 1. What do you think, is the meteorologist on the right track? Assume that in two months from now the weather will turn out similar as yesterday (i.e. rain, wind,

and lightning). What will happen if the meteorologist creates a new map for the same rectangular region? Where will lightning strike exactly? How many strikes in total?

The meteorologist is particularly interested in the following type of questions: Do the locations of lightning strikes tend to cluster or do they spread out regularly? Are certain regions more likely to be hit than others (e.g. if a region contains tall metallic obstacles or hills)? How likely is it that some single square kilometer sub-region is not going to be hit at all?

Now, replace the meteorologist with a biologist and replace the locations of lightning strikes with locations of trees of some particular type. The biologist is similarly interested in knowing if the locations of trees tend to cluster (local seed spreading) or if there is some kind of repulsion going on (survival of the fittest). Are there certain pronounced regions which do not contain any trees at all? If so, why could that be?

Finally, replace the biologist with a telephone network operator and replace the locations of trees with the locations of active mobile users within some fixed communication cell.

Exercise 2. What kind of questions do you think a network operator would like to ask? Think in terms of system operability, connectivity, coverage, throughput rates, interference levels, user quality of service, etc. Next, think of examples of random point patterns which you would be likely to encounter within your own field of study. What questions would you be interested in being able to answer?

Point patterns show up everywhere and so far we have mentioned three examples. In most applications the observer of such point patterns is not directly interested in the exact point locations themselves. The observer is more likely to be interested in what can be inferred from these locations about some underlying mechanism that governs where the points occur. In a nutshell, this has to do with statistical estimation theory. However, in order to apply such statistical tools we need a mathematical modeling framework for random point patterns. In fact, as we shall see in Section 8, stochastic models of point patterns are very important in their own right. In particular, they can be used as building blocks for generating ordinary random processes (our goal in this note).

2 Mathematical framework for point processes

We desire a simple and convenient mathematical theory for our random point patterns. To achieve this we restrict ourselves along the way. For example, we cannot handle if there are so many points that we can no longer count them. Moreover, the theory is simpler if points cannot fall directly on top of each other.

Definition 1. A two-dimensional (2D) *point process* is a random countable collection of points in the cartesian plane $\mathbb{R}^2$.

After having read the above definition we would probably like to ask the following questions. What does it really mean that a collection is *random* and what does it mean that a collection is *countable*?

Example 1. The collection of *natural numbers* $\mathbb{N} = \{1, 2, 3, \ldots\}$ is countable. An arbitrary collection is countable if each of its members can be associated uniquely with a number in $\mathbb{N}$. The idea is that the members of a countable collection can be counted one at a time. The counting procedure is allowed to never end but every member must eventually be associated with a natural number. $\qquad\qquad\square$

Exercise 3. Is $\mathbb{Z} = \{\ldots, -2, -1, 0, 1, 2, \ldots\}$ a countable collection? What about the closed interval $[0, 1] \subset \mathbb{R}$, is this a countable collection?

Exercise 4. Consider a collection of points obtained by drawing 75 points uniformly in the square $[-5, 5] \times [-5, 5]$. Is it a random collection? Is it countable? Think about how to simulate such collections and write a (Matlab) script for this purpose.

Exercise 5. Now, consider a collection of points constructed as follows. First draw a Poisson distributed random number L with mean 75. Given L, then draw L points uniformly in the square $[-5, 5] \times [-5, 5]$. Is this a random collection? Is it countable? Think about what happens from one realization to another. Compare with the construction from the previous exercise.

Historically, one-dimensional (1D) point processes were the first to be considered. The 1D space was almost exclusively used to represent *time*, e.g. the entire real line $\mathbb{R}$ or the set of positive reals $[0, \infty)$.

Exercise 6. Qualitatively, how does a 1D point process realization look like? Is there something very special about the 1D case, something that is not really possible in 2D? Sketch a few figures with your own example realizations of 1D point processes. Discuss where such a 1D random point pattern could happen to emerge in practice. What do you think a 1D point process could be used to represent? Occurrences of earthquakes for instance?

3 Convenient restrictions and notation

From a mathematical point of view it is convenient to add a few restrictions to Definition 1 on page 143. Specifically, we limit ourselves to consider only point processes which are *locally finite* and *simple*. These two conditions are of technical kind and by default we assume that they are fulfilled with probability one. That a point process is locally finite means that only a *finite* number of points are falling in every *bounded* region of $\mathbb{R}^2$. That a point process is simple means that no two points of the process coincide.

Example 2. The square region $[-1, 1] \times [-1, 1] \subset \mathbb{R}^2$ is bounded. The first quadrant $[0, \infty) \times [0, \infty) \subset \mathbb{R}^2$ is an unbounded region. The diagonal $\{(x_1, x_2) : x_1 = x_2\} \subset \mathbb{R}^2$ is also not bounded. $\square$

Example 3. The collection $\left\{ \left(\frac{\cos(n)}{\sqrt{n}}, \frac{\sin(n)}{\sqrt{n}} \right) : n \in \mathbb{N} \right\} \subset \mathbb{R}^2$ is countable but indeed not random. However, it is not locally finite either. Do you see why? If not, try drawing it. $\square$

In the rest of this chapter we use X to denote a locally finite and simple point process defined on a space $S \subseteq \mathbb{R}^2$. Do not confuse X with a random variable or a random process. Now, X is a random countable collection of points in S. The 2D space S could be the whole $\mathbb{R}^2$, the unbounded subset $\mathbb{R} \times [0, \infty)$ or perhaps the bounded rectangle $[a, b] \times [c, d]$. Since the point process X is assumed to be simple it follows that X has no repetitions of points. Accordingly, the individual realizations of X can be seen as countable *sets* of points

$$\{\boldsymbol{x}_1, \boldsymbol{x}_2, \boldsymbol{x}_3, \dots\} \qquad \boldsymbol{x}_i \in S. \tag{E.1}$$

In (E.1) we use boldface notation for the individual points to stress the fact that each point $\boldsymbol{x}_i$ is a 2D vector. The set in (E.1) can be either finite or countably infinite. The dummy index i is used only to distinguish points and to indicate countability. *We emphasize that the dummy index i is not used to indicate any ordering of the points.* Notice also that we now make use of the term "set" instead of collection. If X had not been a simple point process the set notation in (E.1) would be useless and misleading since occurrences of multiple points would be disregarded. For example, the set $\{4, 1, 1, 2, 1, 3, 3\}$ is the same as the set $\{1, 2, 3, 4\}$. Right?

4   Region counts

A natural and intuitively appealing way of exploring the properties of a point process X is to count the number of points falling in different regions. Accordingly, for any set $B \subseteq S$ consider the *region count*

$$N_X(B) = \text{"the number of points from } X \text{ falling in } B\text{"} \tag{E.2}$$

$$= |X \cap B| \tag{E.3}$$

$$= \sum_{\boldsymbol{x} \in X} \mathbb{1}[\boldsymbol{x} \in B], \tag{E.4}$$

where $|\cdot|$ in (E.3) denotes *set cardinality* (not absolute value) and where $\mathbb{1}[\cdot]$ in (E.4) denotes an ordinary *indicator function*. For *fixed* and *bounded* $B \subseteq S$, the region count $N_X(B)$ is a discrete random variable with range $\{0, 1, 2, 3, \dots\}$. This property is due to our default assumption of X being locally finite. The interplay between X and N_X is illustrated in Figure E.2.
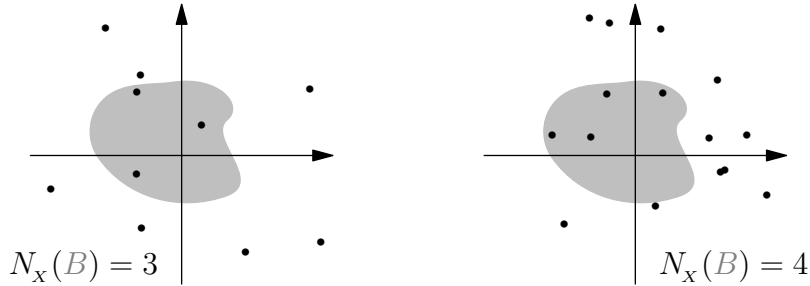
Fig. E.2: Two realizations of a point process X inducing different values of the associated region count $N_X(B)$. Here, B is a fixed potato-shaped region.

The probability distribution of $N_X(B)$ depends on the region B via its overall area, its location, its orientation, and so on. The region B can be very complicated but certain general properties of the region counts are easily established.

Exercise 7. Let X be a point process on $S \subseteq \mathbb{R}^2$. Show that $N_X(\emptyset) = 0$ where $\emptyset$ denotes the empty set. Furthermore, show that if $A, B \subseteq S$ are *disjoint* then $N_X(A \cup B) = N_X(A) + N_X(B)$. *Hint:* Make a drawing at first and use your intuition to argue for the two properties of N_X. Afterwards, show that the properties are satisfied by direct use of (E.4).

In general, various complicated regions can be build up by simpler ones by use of set operations for which the behavior of N_X is well-understood.

5   Intensity measures and intensity functions

We have just learned that for any fixed and bounded region $B \subseteq S$, the region count $N_X(B)$ is a non-negative integer-valued random variable. By forming the expected value of this random variable we get a deterministic function of the region B (i.e. a function which takes as input a set and outputs a number).

Definition 2. The *intensity measure* μ_X of X is defined as

$$\mu_X(B) := \mathbb{E}\big[N_X(B)\big] = \mathbb{E}\left[\sum_{\boldsymbol{x} \in X} \mathbb{1}[\boldsymbol{x} \in B] \right], \qquad B \subseteq S. \tag{E.5}$$

Using the definition of expected values, the intensity measure in (E.5) can "in principle" be computed as

$$\mu_X(B) = \mathbb{E}\big[N_X(B)\big] = \sum_{n=0}^{\infty} n \Pr\big(N_X(B) = n\big).$$

The snag is just that this approach is often not possible. In most cases we simply don't know the probability distribution of $N_X(B)$. Luckily, the intensity measure $\mu_X(B)$ can nearly always be expressed in terms of integrating another non-negative function across the region B.

Definition 3. If the intensity measure μ_X in (E.5) can be written as

$$\mu_X(B) = \int_B \varrho_X(\boldsymbol{x})\mathrm{d}\boldsymbol{x}, \qquad B \subseteq S, \tag{E.6}$$

for some *locally integrable* function $\varrho_X : S \to [0, \infty)$, then ϱ_X is called the *intensity function* of X.

Definition 4. If the intensity function ϱ_X is constant across the entire space S, then X is called a *homogeneous* point process. If ϱ_X is not constant on S, then X is said to be *inhomogeneous.*

By now we have introduced something called the intensity measure as well as the intensity function of a point process. Do not confuse these two quantities with one another, the former is simply obtained by integrating the latter. *The shape of the intensity function ϱ_X indicates where points from X are more likely to occur.* The integral of ϱ_X across some region $B \subseteq S$ gives the expected number of points from X falling within B, i.e. the intensity function specifies the mean value structure of the region count $N_X(B)$. If X is a homogeneous point process such that $\varrho_X(\boldsymbol{x}) = \varrho_0$ for all $\boldsymbol{x} \in S$, then the non-negative constant ϱ_0 has a plain and simple interpretation: The average number of points per unit area.

Exercise 8. As mentioned above, the shape of the intensity function ϱ_X indicates where points from X are more likely to occur. This is very similar to the interpretation of an ordinary probability density function (pdf) of a random variable. Apart from a shift in notation, does (E.6) look familiar to you? Discuss the similarities as well as the distinctions between the intensity function of a point process and the pdf of an ordinary random variable.

6   The binomial point process

Definition 5. Let f be a pdf on $S \subseteq \mathbb{R}^2$ and fix an integer $k \in \mathbb{N}$. A point process X consisting of k points drawn i.i.d. according to f is called a *binomial point process.* We denote this by writing $X \sim \mathtt{binomialPP}\big(S, k, f\big)$.

Let's start out by looking at a simple example.

Example 4. Let S be the bounded rectangle $[a, b] \times [c, d]$ and let f be the uniform density on S, i.e. $f(\boldsymbol{x}) = \frac{1}{(b-a)(d-c)}$ for every $\boldsymbol{x} \in S$. We fix $k = 75$ and plot two different example realizations in Figure E.3. We have used the parameters $a = c = -5$ and $b = d = 5$. Does the construction seem familiar? Recall Exercise 4 on page 144. □

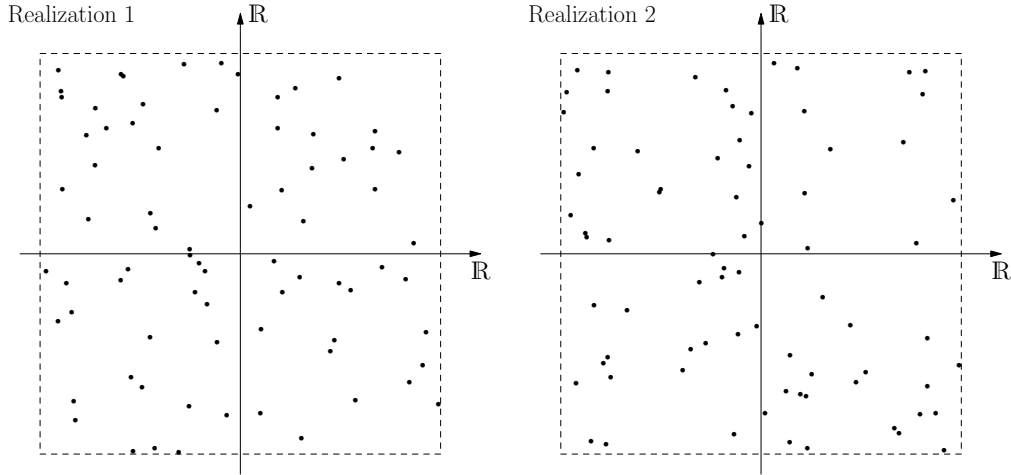**Fig. E.3:** Two example realizations of $X \sim \texttt{binomialPP}\left([-5, 5]^2, 75, \frac{1}{100}\right)$.

At a first glance, one may wonder why the construction in Definition 5 is called a binomial point process. The answer has to do with the probability distribution of an arbitrary region count.

Exercise 9. Let $X \sim \texttt{binomialPP}(S, k, f)$ where $S \subseteq \mathbb{R}^2$ and f is some arbitrary pdf on S. Argue that the region count $N_X(B)$, $B \subseteq S$, has a binomial distribution (think of a coin tossing experiment) and identify the two parameters of this discrete probability distribution. Does it make sense that the *success probability* depends on B?

Exercise 10. Determine the intensity function ϱ_X for a general binomial point process $X \sim \texttt{binomialPP}(S, k, f)$. *Hint:* Recall and make use of (E.5) and (E.6).

Exercise 11. Let $X \sim \texttt{binomialPP}(S, k, f)$ and let $B \subset S$ be some fixed region. Argue whether or not the two region counts $N_X(B)$ and $N_X(S \backslash B)$ are independent random variables (draw it). Intuitively, are $N_X(B)$ and $N_X(S \backslash B)$ positively correlated, negatively correlated or uncorrelated?

7   The Poisson point process

In the following, the binomial point process enters directly in a two-step definition of the Poisson point process. This two-step definition is convenient since it gives a direct procedure for simulation of Poisson point processes, e.g. in Matlab.

Definition 6. A point process X on $S \subseteq \mathbb{R}^2$ is called a *Poisson point process* with intensity function ϱ_X if:

i) For any region $B \subseteq S$ with $\mu_X(B) = \int_B \varrho_X(s)\mathrm{d}s < \infty$ the associated region count $N_X(B)$ has a Poisson distribution with parameter $\mu_X(B)$, i.e.

$$\Pr\big(N_X(B) = k\big) = \exp\big(-\mu_X(B)\big) \frac{\big(\mu_X(B)\big)^k}{k!}, \qquad k = 0, 1, 2, \ldots$$

ii) Given that $N_X(B) = k \in \mathbb{N}$, then these k points form a binomial point process on B such that

$$X \cap B \sim \texttt{binomialPP}\big(B, k, f_B\big), \qquad f_B(\boldsymbol{x}) = \mathbb{1}[\boldsymbol{x} \in B] \frac{\varrho_X(\boldsymbol{x})}{\mu_X(B)}.$$

We denote this by writing $X \sim \texttt{PoissonPP}\big(S, \varrho_X\big)$.

For a Poisson point process the individual region counts are Poisson distributed random variables. Hence the name of the process. An important property of the Poisson point process is that if $B_1, B_2, \ldots, B_n \subset S$ are fixed disjoint regions, then the corresponding region counts $N_X(B_1), N_X(B_2), \ldots, N_X(B_n)$ are mutually independent random variables. This property could as well have been used instead of part *ii)* in Definition 6, but the definition would then not directly tell us how to simulate the Poisson point process.

Example 5. Recall Exercise 5 on page 144. This construction is in fact a homogeneous Poisson point process X on $S = [-5, 5] \times [-5, 5]$ with $\varrho_X(\boldsymbol{x}) = \varrho_0 = \frac{3}{4}$. With our notation from above we have $X \sim \texttt{PoissonPP}\big([-5, 5] \times [-5, 5], \frac{3}{4}\big)$. $\qquad\square$

Exercise 12. Consider part *i)* in Definition 6. What happens with the region count $N_X(B)$ if $\mu_X(B) = 0$? Will it affect part *ii)* and how?

Exercise 13. Let $X \sim \texttt{PoissonPP}\big([0, 2] \times [0, 1], \varrho_0\big)$ for some constant $\varrho_0 > 0$. That is, X is a homogeneous Poisson point process on the bounded rectangle $S = [0, 2] \times [0, 1]$. What is the expected number of points from X falling in the region $B = [0, 1] \times [0, 1]$? What is the probability that X has no points in S at all?

Exercise 14. Let's think in terms of computer simulation. In principle, what steps do you need to carry out if you want to simulate the point process $X \sim \texttt{PoissonPP}\big(\mathbb{R}^2, 1\big)$? What is $\mu_X(S)$ in this case?

8 Applications of point processes

In this section we show how point process models such as those from the previous two sections can be used as building blocks for generating ordinary random processes. Numerous text books on probability theory and random processes cover topics like *the Poisson counting process* and *queuing theory*. In the following we cover these topics as well but our treatment is most likely different from what you will find in standard text books.

The Poisson counting process

Let $Y \sim \texttt{PoissonPP}\big([0,\infty), \varrho_0\big)$ be a one-dimensional (1D) homogeneous Poisson point process. We use the symbol Y to stress the fact that we are now dealing with a 1D point process. Then, consider an ordinary random process $Z(\cdot)$ defined as

$$Z(t) := \sum_{y \in Y} \mathbb{1}[y \leq t], \qquad t \geq 0. \tag{E.7}$$

By definition, $Z(\cdot)$ is a continuous-time staircase alike random process with jumps at every point of Y. It is often referred to as a Poisson counting process. When writing $Z(\cdot)$ we mean the entire random process and when writing $Z(t)$ it means that time t is considered fixed. Hence, $Z(t)$ is a random variable.

Exercise 15. Sketch a few different example realizations of the 1D point process Y. Sketch the corresponding realizations of $Z(\cdot)$, e.g. in the range $t \in [0, 20]$. Explain what will happen if ϱ_0 is selected larger. Express $Z(t)$ as a certain region count $N_Y(B_t)$ for some suitably chosen region B_t and argue that $Z(t)$ is Poisson distributed with mean parameter $\varrho_0 t$. Is $Z(\cdot)$ a wide-sense stationary (WSS) process?

Queuing theory

Queuing theory deals with arrival times of customers and service times at counters, e.g. humans at checkout lines in supermarkets. Stochastic models of queues are widely used for analyzing the behavior of time-shared computer and communication systems.

Exercise 16. What kind of questions do you think are typically sought to be answered in applications involving queues? *Hint:* Think of concepts such as queue lengths and customer waiting times.

Denote by p the pdf of some non-negative continuous random variable (exponential, gamma, Weibull, chi-square, etc.). Then, consider the 2D inhomogeneous Poisson point process $X \sim \texttt{PoissonPP}\big(\mathbb{R} \times [0,\infty), \varrho_X\big)$ where the intensity function has the form

$$\varrho_X(\boldsymbol{x}) = \varrho_X(x_1, x_2) = \lambda p(x_2), \qquad (x_1, x_2) \in \mathbb{R} \times [0,\infty).$$

Each random point $\boldsymbol{x} = (x_1, x_2) \in X$ has two components and the interpretation of each component is as follows:

$$x_1 = \text{the random time instance where a new customer enters}$$
$$x_2 = \text{the random service time needed to process this customer.}$$

Notice that the intensity function ϱ_X is such that it does not vary with its first argument x_1. This means that customers keep arriving with constant intensity λ all day long. On the other hand, ϱ_X has a functional dependency on its second argument x_2 such that the average service time of any customer is given by the expected value associated with the pdf p.

Exercise 17. For each random point $\boldsymbol{x} = (x_1, x_2) \in X$, what is the interpretation of the random time instance $x_1 + x_2$?

We now use the 2D point process X to form a random process similar to the one in (E.7). Specifically, our construction now reads

$$Z(t) := \sum_{\boldsymbol{x} \in X} \mathbb{1}[x_1 \leq t, \ x_1 + x_2 > t], \qquad t \in \mathbb{R}. \tag{E.8}$$

and this continuous-time random process is jumping both up and down. It models the behavior of the so-called $M/G/\infty$ queue. The random variable $Z(t)$ gives the instantaneous queue length at time t (do you see why?). Thus, $\mathbb{E}[Z(t)]$ is the average queue length at time t.

Exercise 18. Sketch one example realization of the 2D point process X. Sketch the corresponding realization of $Z(t)$, e.g. in the range $t \in [-20, 20]$. Look carefully at (E.8) and express $Z(t)$ as a certain region count $N_X(B_t)$ for some[1] appropriately chosen region $B_t \subset \mathbb{R} \times [0, \infty)$. Recall Definition 6 and argue that $Z(t)$ is a Poisson distributed random variable. Finally, try to calculate

$$\mathbb{E}[Z(t)] = \mathbb{E}[N_X(B_t)] = \mu_X(B_t) = \int_{B_t} \varrho_X(\boldsymbol{x}) \mathrm{d}\boldsymbol{x} = \iint_{B_t} \lambda p(x_2) \mathrm{d}x_1 \mathrm{d}x_2,$$

and discuss whether you find it reasonable that this mean function does not depend on time t.

Final remark: It can be shown that the random process $Z(\cdot)$ in (E.8) is in fact strict-sense stationary (SSS).

---

[1] The correct region B_t has an unbounded triangular shape.

9   Final remark: 1D versus 2D

In section 2 we mentioned that 1D point processes were the first to be considered (historically). Indeed, the 1D approach may at first glance appear more attractive and simpler compared to our 2D approach (and compared to higher dimensional generalizations as well). However, there is one very peculiar feature of $\mathbb{R}$ which has no straightforward analogue in $\mathbb{R}^2$, $\mathbb{R}^3$ and $\mathbb{R}^d$ in general. *The real line has a natural ordering of its members.* For this single reason it is highly recommended to always think of (and relate to) the 2D case when dealing with point processes. Despite the peculiar ordering feature in 1D, it is crucial to keep in mind that this setup comprises a very important special case. However, the general theory of point processes is easier to comprehend if we initially develop it without relying on features which are valid only for the 1D case. *This is the very reason why we have chosen the 2D case as our reference approach.*

10   Further reading

- David R. Cox and Valerie Isham, "Point Processes", Chapman & Hall, 1980.
- John F. C. Kingman, "Poisson Processes", Oxford University Press, 1993.
- Adrian J. Baddeley, "Spatial Point Processes and their Applications" (in "Stochastic Geometry - Lecture Notes in Mathematics"), Springer, 2007.